Technische Universität Wien
Vienna University of Technology

Examination of ionic diffusion permeability of polymer thin films

Diploma thesis of Adrian Strasser BSc.

Executed from: 04.12.2018 – 13.12.2019

Supervised by:

Univ.Prof. Dipl.-Ing. Dr.techn.Andreas Limbeck

Ao.Univ.Prof. Dipl.-Ing. Dr.techn.Günter Fafilek

Acknowledgments

At this point I would like to thank the ladies and gentlemen, who have supported me executing this thesis.

First, I would like to thank my thesis-supervisor of the electrochemistry research group, Lars Varain, who accompanied me on my way from the beginning. He not only encouraged me in accomplishing the electrochemical part, but also ensured with his natural cheerful and serene appearance a pleasant working environment. Especially I want to thank for the many discussions with him, most of them buttressed the scientific fundament of this entire thesis.

Special thank also goes to my main-supervisor Andreas Limbeck. Since I had already accomplished my bachelor thesis and also several lectures, seminars and laboratory exercises under his guidance, it was a great pleasure to know that I was allowed to write my diploma thesis, supervised by him. His knowledge and expertise were a conceptual linchpin for this thesis and so made an important contribution for this thesis.

Thank goes to the entire electrochemistry and surface, - and trace element research group for their support.

Additionally, I want to thank special people, who aided me executing my thesis in scientific way, but also by several conversations, my fellow students and friends Sarah Fleissner, Maximilian Weiss, Christopher Roberts and Roman Poberezhny.

I thank my family for their encouragement, my sisters, my father and my mother and, at last, I want to thank Jennifer Linzner, who was always there for me and lifted me up when I was on the ground.

Table of contents

1 Statutory declaration

I declare that I have developed and written the enclosed Master thesis completely by myself and have not used sources or means without declaration in the text.

Any thoughts from others or literal quotations are clearly marked.

The Master Thesis was not used in the same or in a similar version to achieve an academic grading or is being published elsewhere.

Strasser Adrian BSc.

2 Abstract

Materials based on polyimide show a wide range of use in electrical engineering, for example as isolation and protection medium. Nevertheless, ions can penetrate such layers, which leads to corrosion and to deterioration of the system. Consequently, it is important to understand the interaction between ions and polymer layers.

In this project, polyimide layers were produced, and their thicknesses determined. Subsequently, these layers were integrated into a diffusion cell. In this cell, the polymer was used as a separator for two different concentrated salt solutions. The diffusion leaded to a reduction of potential difference, which can be measured. Furthermore, a Laser Ablation Induced Coupled Plasma Mass Spectrometer (LA ICP MS) was used to examine diffusion profiles and elemental distributions on the surface of these layers.

During this project, a new method for determining layer thicknesses and for producing more homogeneous polyimide layers were implemented. Also, Nafion® membranes were used to examine the difference when switching from a ionic highly impervious barrier to a more permeable one and to identify the osmotic impact on layers. Using polyimide P84® layers, no reproducible diffusion trend curves were obtained, despite of several optimisations. Nevertheless, most of the sources of error could be located for further improvement measures. By using LA ICP MS, conclusions about diffusion and their inhomogeneous localities were evaluated.

In conclusion, several statements and propositions about mechanics of ionic diffusion using Nafion® and polyimide layers were made. For higher quality, used polyimide layer should be produced industrially. Additionally, a new method should be implemented, to fix penetrated layers on a substrate for the ablation process.

The obtained results can be used for comparison with diffusion simulations and further analyses for determining diffusion mechanics in polymers.

3 Introduction

In modern times, polymeric materials are becoming increasingly important. Because of their high variability of their characteristics, a wide range of applications in global industry exists, from the production of a simple polyethylene drinking bottle to high-performance polymer for the semiconductor industry.

In this thesis, the focus lies in the development of a method to investigate the ion diffusion in polymers, which are used in electric and electronic industry especially. For example, polyimide is used as isolating material or electronic devices. Polyimide benefits from its natural dielectric properties as well as from its low weight and flexibility compared to many inorganic isolators, like mica, glass, or ceramic isolators, but also from its heat resistance and chemical stability. For example, a polyimide isolator has a higher electric resistance by two orders of magnitude and is stable against phosphoric or fluoric acid compared to zirconium.[1] These characteristics make polyimide an important material for semiconductor applications.

Despite the many advantages, polyimide and other polymers have the same weak point, the ionic penetrability: The main task of such materials for electronic devices is to isolate the electric components and to protect it from harmful environmental influences, which could cause corrosion phenomena on the surface. However, polymer isolators, which are penetrated by ions, have increased conductivity, this can lead to corrosion in form of anodic metal dissolution, then the ions can form dendrites between electrodes and therewith lead to short circuits. These lead to a loss of expected quality and therefore deterioration of the complete electric and electronic system.[2] Corrosion is an ubiquitous issues, a electrochemical process, which cannot be eliminated, but at least reduced to an absolute minimum by using high performance materials, but also by understanding how this process is evolved and interacts. Consequently, it is of high interest, to determine the diffusion permeability and the ionic diffusion profile of penetrated layers.

For this thesis, diffusion processes are observed in polyimide and Nafion® layers via diffusion cell and concentration dependent potential difference instrument. After observing diffusion trend, the used polymer layer represents ionic penetrated protection medium, which could cause corrosion on the semiconductor, for instance, underneath. The diffusion profile of the ionic contaminated polymer is examined using a Laser Ablation-Inductively Coupled Plasma-Mass Spectrometer. The focus lies on recording potential difference trend by diffusion in layer samples and matching trends with diffusion profiles by elemental analysis, as well as creating methods for artificially penetrating sample layers and determining the ionic profile.

---

[1] [19] Top Seiko Co.,LTD. "Guide to Materials ", S.: 5
[2] [23] John Osenbach, Semiconductor Science and Technology · January 1999 "Corrosion-induced degradation of microelectronic devices", S: 159

4 Theoretical basics

4.1 Ionic conductivity

"Ions are defined as particles that carry electrical charges. They may exist in gaseous phases as individual ions, but in condensed phases (solids and liquids), they exist as electrically neutral combinations of cations and anions, and in solutions they exist as electrolytes, the ions of which may be bound or relatively free to migrate."[3]

In this thesis, potassium chloride is the selected ionic diffusion medium. This salt benefits from its physicochemical and molecular characteristic. It dissociates easily in deionised water into one simple positive charged potassium cation and one simple negative charged chloride anion, which have nearly the same electrochemical mobility in free, aqueous solution [10]. Furthermore, the molar conductivities of both ions are nearly equal, shown in table 1. [22].

Table 1: Characteristics of potassium and chloride ion

Property	Potassium ion K^+	Chloride ion Cl^-
Transference number []	0.495	0.505
Molar conductivity [$S * cm^2 * mol^{-1}$]	73.5	76.4

This characteristic simplifies diffusion related calculations and evaluations, which will be discussed in further chapters.

4.2 Diffusion in general

"The tendency of matter to migrate in such a way as to eliminate spatial variations in composition, thereby approaching a uniform equilibrium state, is well known. Such behaviour, which is a universal property of matter at all temperatures above absolute zero, is called diffusion and is simply a manifestation of the tendency towards maximum entropy or maximum randomness." [4]

Diffusion flow rate and diffusion coefficient can be calculated by using Fick's first law, presented in equation (11). [11]

$$J = \frac{dm_A}{dt * A} = D * \frac{dc}{dx} \qquad (11)$$

Fick's first law is the most common and simplified equation for explaining diffusion processes and diffusion dependent concentration changes. Further diffusion related explanations and mathematical background will be shown in chapter "Diffusion and diffusion coefficient determination".

---

[3] [24] Yizhak Marcus: "Ions In solutIon and theIr solvation"; S. 10

[4] [22] Jörg Kärger,Douglas M.Ruthven,and DorosN.Theodorou: „Diffusion in Nanoporous MaterialsVolume 1"; S.3

4.3 Nernst potential and Diffusion potential

For understanding ionic transport mechanism in liquid and solid media and the interaction with the phase boundary, it is important to explain the physical, chemical and mathematical fundamental basics of such processes. For this, the terminus "diffusion potential" must be explained:

> "*Cause for the formation of diffusion potentials are the different chemical potentials of mobile charge carriers in two adjacent phases. The calculation of the diffusion potential is based on the consideration of the particle currents of positive and negative ions generated by the driving forces of the gradient of the chemical potential and the electrical potential through the phase boundary and their mutual influence.*" [5]

A galvanic element with reversible, electrical continuity is considered. For electromotive force (EMK) equation (1) is applied [10]

$$E_0 = -\frac{\Delta G}{n * F} \tag{1}$$

If $d\mu_i$ (I) is the change in the chemical potential of the i-type of ion via an infinitesimal liquid layer belonging to the diffusion layer, then the change in the free enthalpy occurring over this liquid layer applies to the free enthalpy. (2) (3) [10]

$$d\Delta G = \sum_i \nu_i \, d\mu_i \rightarrow \text{Integration over entire diffusion layer } (\mu_i(I) > \mu_i(II)): \tag{2}$$

$$\Delta G_{\text{Diffusion}} = \int_{\mu_i(II)}^{\mu_i(I)} \sum_i \nu_i \, d\mu_i \tag{3}$$

The complete change of the free reaction enthalpy in the cell bases on equation (4).

$$\Delta G_{\text{total}} = \Delta G_{\text{Cell reaction}} + \Delta G_{\text{Diffusion}} \tag{4}$$

On the base of these equation, two electrodes, attached on each side of the diffusion layer, will measure following potential difference: (5) [10]

$$E_{0,\text{total}} = E_0 + \Delta\varphi_{\text{Diffusion}} = -\frac{\Delta G_{\text{Cell reaction}}}{n * F} + \left(-\frac{\Delta G_{\text{Diffusion}}}{n * F}\right) \tag{5}$$

So, measured potential difference is a summation of the concentration dependent difference of both ionic solutions, which are surrounding the diffusion layer, and of the "diffusion potential" $\Delta\varphi_{\text{Diffusion}}$ (= $\Delta\varphi_{\text{diff}}$), which describes the mutual interference of two different particle flows. For determining $\Delta\varphi_{\text{diff}}$, or ΔG_{diff}, it must be assumed, that during current flow the charge transport is distributed into individual transference numbers t_i of the individual ion sorts. When one Faraday n fully penetrates the liquid / liquid phase boundary, n * (t_i / z_i) mole

---

[5] [10] Carl H.Hartmann, Wolf Vielstich: „Elektrochemie", 4., vollständig überarbeitete und aktualisierte Auflage; S. 105

of ion i wanders. $n * (t_i / z_i)$ can be equate with the stoichiometric coefficient v, resulting in following equations (6) (7): [10]

$$\Delta G_{Diffusion} = \Delta G_{diff} = \int_{\mu_i(II)}^{\mu_i(I)} n \sum_i \frac{t_i}{z_i} \, d\mu_i$$

$$\rightarrow \quad -\frac{\Delta G_{diff}}{n * F} = \Delta\varphi_{diff} = - \int_{\mu_i(II)}^{\mu_i(I)} \sum_i \frac{t_i}{z_i * F} \, d\mu_i \tag{6}$$

$$\mu_i = \mu_i^0 + R * T * \ln(a_i) \rightarrow \Delta\varphi_{diff} = -\frac{R * T}{F} \int_{a_i(II)}^{a_i(I)} \sum_i \frac{t_i}{z_i} \, da_i \tag{7}$$

Based on these equations the final equation for determining diffusion potential can be formed (8). [15]

$$\Delta\varphi_{diff} = -\frac{R * T}{z * F} \int_{a_i(II)}^{a_i(I)} (t^+ - t^-) \, da_i = -\frac{R * T}{z * F} (t^+ - t^-) * \ln\frac{a(I)}{a(II)} \tag{8}$$

From equation (5), (7) and (8) equation (9) is made. [10] Equation (9) is used to calculate from the measured potential difference by the instrumental setup and the calculated Nernst potential into the Diffusion potential.

$$U_{ges} = U_{Nernst} + \Delta\varphi_{Diff} = \left(\frac{R * T}{z * F} * \ln\frac{c_1}{c_2} - \frac{R * T}{z * F} * (t^+ - t^-) * \ln\frac{c_1}{c_2}\right) \tag{9}$$

Using equation (9), transference numbers are determinable. These transference numbers are unique for each transported ion type. For a common binary system, there is a transference number for the cation and anion of the salt solution, t^+ and t^-. Measured, total voltage can only be higher than Nernst voltage, if transference numbers are not equal.

> "The transference number of an electrolyte is defined as that fraction of the total current through the ion conductor that is carried by the cations or anions. [...] The higher the transfer coefficient of an ion, the greater its conductivity contribution."[6]

Furthermore, following equation is valid. (10) [10]

$$(t^+ + t^- = 1) \tag{10}$$

Using the total measured potential difference, the transference numbers are determinable to realise the influence of the polymeric matrix on the individual ion types.

---

[6] [10] Carl H.Hartmann, Wolf Vielstich: „Elektrochemie", 4., vollständig überarbeitete und aktualisierte Auflage, S. 26

4.4 Concentration cell

In this thesis diffusion can be observed indirectly by measuring potential difference. To achieve this, a certain instrumentation is constructed, a diffusion cell for thin film layers. The functionality of this system is represented schematically in figure 1.
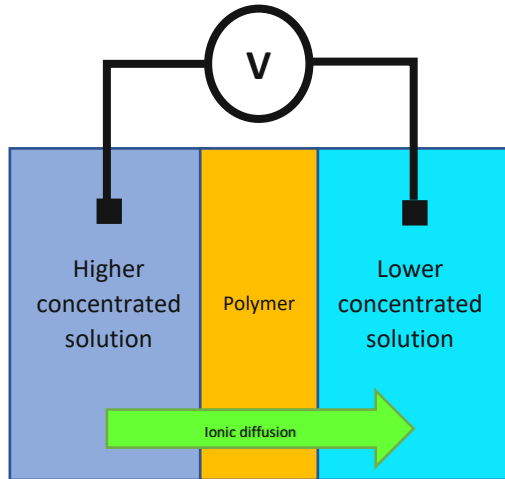
Figure 1: Scheme of the concentration cell

For this purpose, a system is used in which the examined polymer separates two ionic liquids of different concentrations with inserted electrodes. The electrodes are connected to a multimeter for electric potential measurement, but not connected to each other, so potential measurement is electroless. Measured potential of each electrode side is depending on the concentration of the chamber fluid, the Nernst potential. With increasing time, ions will diffuse through the polymer from the higher concentrated region to the lower concentrated region until the concentrations are balanced, which can be observed by the equalisation of the potentials. Using this system, not only a graphic presentation of diffusive resistance of the sample layer can be produced, but also a controlled penetrated contamination can be achieved, so the layer can be used for element analytical issues.

For the electric potential measurement, it is necessary to integrate electrodes into the diffusion cell. The materials of the used electrodes are silver (Ag) and silver chloride (AgCl). These electrodes are designated as electrodes of "type 2". A highly insoluble salt (AgCl) surrounds a cation corresponding metal (Ag). Potential dependent is the oxidation of silver to silver chloride.

$$Ag + Cl^- \rightarrow AgCl + e^- \tag{11}$$

According to reaction equation (11), the corresponding Nernst equation is showed in (12).

$$E = E^0 + \frac{R * T}{e * F} * \ln a_{Ag^+} \tag{12}$$

Due to the high insolubility of the silver chloride salt, activity of the silver ions (a_{Ag+}) and chloride ions (a_{Cl-}) in equilibrium is directly proportional to the solubility product. (13)

$$K = a_{equ,Ag^+} * a_{equ,Cl^-} \tag{13}$$

Consequently, equation (12) and (13) can be combined to equation (14), which shows, that Nernst potential is depending on chloride activity.

$$E = E^0 + \frac{R * T}{e * F} * \ln\frac{K}{a_{Cl^-}} \tag{14}$$

The diffusion cell represents a special form of galvanic element, a concentration cell. It consists of two half cells, filled with the same electrolyte elemental type, but with different ionic concentrations. Consequently, Nernst voltage is depending on the concentrations of both half cells, according to equation (15).

$$dE = \frac{R * T}{e * F} * \ln\frac{a_1}{a_2} \xrightarrow{for\ KCl\ and\ 278.15\ [K]} 0.059\ [V] * \log\frac{c_{1,KCl}}{c_{2,KCl}} \tag{15}$$

In equation (15), a_1 is the electrolyte concentration with lower ionic activity than a_2. So, $\ln\frac{a_1}{a_2}$ is the concentration depending terminus of the Nernst equation for a concentration cell. In this thesis, only KCl will be used as electrolyte, so the concentration of aqueous potassium chloride solution of each half cell $c_{1,\ KCl}$ and $c_{2,\ KCl}$. Furthermore, temperature is a constant parameter of 278.15 [K], so $\frac{R*T}{e*F}$ is reduced for KCl to 0.059 [V] and logarithm to the base of e (ln) is changed into logarithm of the base of 10 (log). (15) is used for determining Nernst potential and diffusion potential for calculating transference numbers.

5   Methods and Materials

5.1   Diffusion cell and potential difference measuring device

In chapter "Diffusion in general" and "Nernst potential and Diffusion potential" the mathematical basics about diffusion and concentration dependent electric potentials are given, in chapter "Concentration cell" the theoretical, schematic realisation is shown. Now, the following chapters describe the instrumental setup for such diffusion examinations, concerning the concentration cell, also described as "diffusion cell", and the instrument for measuring potential differences within the diffusion cell.

5.1.1   Diffusion cell construction

Table 2 shows a list of all required components.

Table 2: Diffusion cell components

Component	Quantity
Sealing ring for membrane	4x
Sealing ring for polyamide screws	6x
Unmodified polyamide screws	2x
Electrode polyamide screws	2x
Polyamide screws with an inner bore	2x
Glass rod	2x
Polycarbonate cover plate	2x
Polycarbonate inner plate	2x
M6 steel screw with plain washes and nut	2x

5.1.1.1 Assembling the basic body of the diffusion cell

This cell consists of four pre-tempered, 5.5 cm x 5.5 cm x 1 cm, polycarbonate plates, which ensue a two-chamber-fluid system when they are stacked

Diffusion cell assembling starts with inserting each of the four big sealing rings into the circular cavity of the plates. Then M6 steel screws are put in one polycarbonate cover plate. On this element one inner plate with is mounted. On the top of this construction should be a big sealing ring. Now, the polymer membrane of interest must be applied. Using a tweezer, this membrane is isolated from the soaking cell and washed with deionised water. Then the membrane is put on the centre of the big sealing ring. The last two plates must be placed congruently with the others. It means that the plate with the bores is put on first, then the cover plate. The construct is fixed by inserting the plain washes and the nuts. When tightening, to avoid unnecessary tension, it is important to turn each nut slightly and often change position. Figure 3 shows a complete assembled basic body with integrated sample.

Figure 2: Basic body of the diffusion cell

5.1.1.2 Production of the electrodes

In this chapter the production of the electrodes for the diffusion cell in chapter "Concentration cell" is explained. AgCl will be produced in galvanic way. Figure 4 shows the scheme of this galvanic cell. [1]
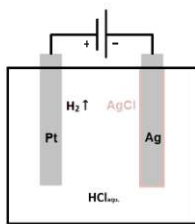
Figure 3: Scheme of galvanic Ag/AgCl electrode production

A silver wire (Ag) is electronically connected to a platinum wire (Pt) via a voltage source. Both metal components are submerged into a liquid medium, which provides a source of chloride ions. For such galvanic process aqueous hydrochloric acid (HCl$_{aqu.}$) is used commonly, as chloride is easily dissociated. Nevertheless, in this thesis, aqueous potassium chloride solution is used, as remaining hydrochloric residues could harm the functionality of the diffusion cell. [1]. If voltage is applied, the silver electrode forms the anode. Potassium chloride molecules are existent as protons with stabilised chloride anions in hydrophile medium such as water. Silver will be oxidised by chloride ions, while two protons form a diatomic hydrogen molecule, consequently this ensues hydrogen gas emission. To avoid increasing gas pressure, the system must not be self-contained. The following equations show the occurred reactions.

Dissociative, electrolytic reaction: $KCl \rightarrow K^+ + Cl^- ; H_2O \rightarrow H^+ + OH^-$

Anodic reaction: $Ag + Cl^- \rightarrow AgCl + e^-$

Kathodic reaction: $2H^+ + 2e^- \rightarrow H_2$

Charge Equilibrium reaction: $K^+ + OH^- \rightarrow KOH$

5.1.1.3 Filling and sealing of the cell

In this thesis, any diffusion related solutions are made by the operator. Any used chemicals, including deionised water, is provided by the research group electrochemical methods and corrosion of the institute of chemical technologies and analytics. Salt of the examined ions, potassium chloride, must be solved in deionised water. Then the salt solution will be degassed in an ultra-sonic bath. To avoid any contamination or evaporating during degassing, this procedure takes two hours with a five-minute break every thirty minutes to reduce thermal impacts.

Continuing preparation the diffusion cell, the filling process, can be enabled. To reduce carry-over effects, filling starts always with the lower concentrated salt solution. The filling process is executed with 5 ml-syringe with injection needles.

Figure 6 shows a completely assembled diffusion cell.

Figure 4: Fully assembled diffusion cell

5.1.1.4 Conductivity measurement cell (CMC)

For determining conductivity of the chamber solutions of the diffusion cell after proceeded diffusion examination, a setup for measuring electric conductivity is established, called conductivity determination device, CMC. The setup is a TU-internal product, so construction is explained.

After finishing diffusion recording, chamber solutions are extracted via scaled syringe, with using a cannula. A volumetric determination is possible. The solution is transferred into another syringe, which is modified with platinum plates with certain size and distance. The platinum plates are connected to silver wires to apply conductivity meter to determine ohmic resistance of the solution. A TU in-house product is preferred, as various commercially available systems require a much higher sample solution and ionic liquid of interest is limited to chamber volume, excluding sample lost due to transfer. The conductivity measurement syringe has a minimum limitation of sample volume of about 0.5 ml, which is sufficient for this issue. A cell correction factor of 4 m^{-1} is calculated for this setup.

Additionally, conductivity is calculated into concentration by establishing a calibration for the used salt solution. Figure 7 shows the calibration line for CMC measurements, referenced to potassium chloride solution.
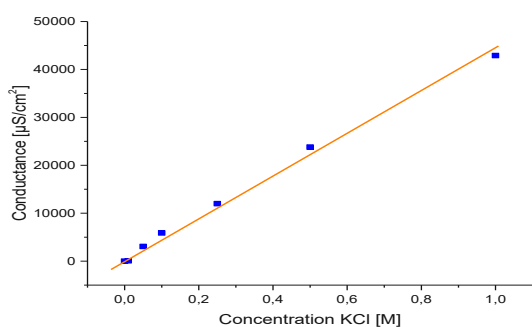
Figure 5: Calibration curve for conductivity examination

Using this it is possible to determine chamber concentration after diffusion.

5.1.2 Potential difference measuring device (PDMD)

The potential difference measuring device, short PDMD, is a TU-internal instrument, subsequently there is neither an external producer, nor a model number. Technically PDMD is not a self-consistent measuring instrument as such, but a measurement setup.

Nevertheless, in further chapters it will described as instrument, as measuring device, for convenient reasons.

Figure 8 shows a photographic picture of the PDMD with marks. These marks classify different sections of this instrument and are described in table 4.

Figure 6: PDMD with section marks

Table 3: PDMD mark description

Mark	Description
a	Junction for electrodes (crocodile clip)
b	Instrumentation amplifier
c	Agilent 34970A data acquisition / switch unit
d	Computer for data recording
e	Grounded shielding

The electrodes of an assembled diffusion cell are connected to the crocodile clips, which are connected to an instrumentation amplifier, with an input impedance of 10^{13} Ω. This input resistance enables measuring membranes with a high internal impedance. The amplifier is connected to a voltage source and to a data acquisition device. With this set-up, the potentials of the different solution are measurable, and data is transmitted to a computer, to record the time resolved potential difference change. To avoid static potential charging, the diffusion cells and the amplifier is surrounded by grounded shielding.

5.1.2.1 Recording diffusion

After assembling and filling the diffusion cell with ionic solutions, as explained in chapter "Diffusion cell construction", it must be connected to the multimeter potential difference measuring device, PDMD, as quickly as possible due to the already running diffusion. The longer the time until the diffusion cell is fully connected to the instrument and the measurement is started, the more information is lost. The cell is placed on a measuring position and the wires of the electrode screws are connected to the crocodile clamps. Thus, the measurement can be started via computer after setting the desired data acquisition frequency.

After diffusion, or more precisely after desired, manually abortion, the cell can be removed from the PDMD. For conductivity determination chamber solution can be extracted, this is discussed more in detail in chapter "Conductivity measurement cell(CCD)". The four M6

screws are removed to exposure the sample layer. Using tweezers, the layer is cleaned with deionised water to remove salt particles as much as possible. Then the layer is dried using fibre and dust-free tissues.

5.2 Spin coater

A spin coater is used to bring liquid polyimide solution into layer shape by using centrifugal force. Figure 10 shows the used spin coater with marked instrumental sections. The explanations of the marks are listed in table 5.

Figure 10: Spin coater with section marks

Table 4: Spin coater mark descripton

Mark	Description
a	Spin coater
b	Rotation plane with chuck
c	Membrane pump
d	Rotation speed / frequency meter

The membrane pump is connected with the rotation plane of the spin coater, so that the vacuum flow goes from the centre of the plane, through an organic solvent vapor condenser, to the pump. A wafer can be put on top of the rotation plane and is held by depression. To achieve an efficient sealing, a polysiloxane plane with a bore hole for the vacuum flow lies between sample and rotation plane. The rotation number is measured by coupled frequency meter. Table 6 shows device specific parameters.

Table 5: Spin coater specific parameters

Smallest adjustable rotation number	150 rpm
Highest adjustable rotation number	3500 rpm
Smallest useable wafer size	1 cm x 1 cm
Programming possibility	None
Rotation number settability	Manual via potentiometer
Arithmetic mean of rotation time after disconnecting from voltage source	2.74 sec
Arithmetic mean of time needed to reach set rotation number (examined for 2000 rpm)	1.35 sec

5.3 Profilometer

For surface specific analyses a "Stylius DekTak XT profilometer", manufactured by Bruker, is used. In this thesis, it is used to determine the layer thickness of the self spinned polyimide layers. A cantilever needle gauges the sample surface. Differences in highness and local structures have an impact on the needle and the applied force on the cantilever is apprehended by a force measuring cell. The collected data is referenced to certain base points, to achieve depth/height resolution depending on lateral area, which is the scan route of the cantilever. Figure 11 shows a schematic profilometer, figure 12 shows the used one.
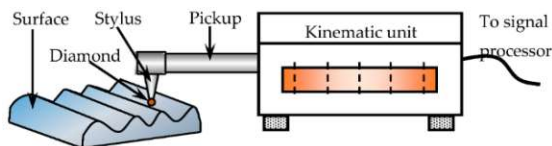
Figure 11: Schematic profilometer

Figure 12: Stylius DekTak XT

Table 7 shows technical details of Stylius DekTak XT.

Table 6: Stylius DekTak XT technical details [20]

Measurement technique	Stylus profilometry (contact measurement)
Measurement capability	2D surface profile measurements; Optional 3D measurement/analyses
Scan length range	55 mm
Maximal sample thickness	50 mm
Vertical resolution	1Å

5.3.1 Determination of layer thickness of produced polyimide samples

For characterisation of the produced polyimide layers it is necessary to determine the thickness of these, while finding correct reference points is decisive. To achieve this, two methods are used, "Cratering" and "Total profile". During execution of this thesis, it has turned out, that "Total profile" method has showed more precise and accurate characterisation

14

information, whereas "Cratering" falsifies layer thicknesses results. However, in this chapter both methods are explained, as both are executed. The results of the confirmation, that "Cratering" is not advisable for polymer layer thickness determination are shown in chapter "Verification of layer thickness determination method".

5.3.1.1 Cratering method

The theoretical basic of this determination method is to generate definite crater in the polyimide layer, which are as deep as the complete polymeric material, analytically determined by using silicon wafer as marker. This can be achieved by ablating stepwise with single laser shots. Via mass spectrometer, the elemental composition can be determined. The ablation takes as long as there is no silicon signal detected.

A polyimide layer sample on silicon wafer is inserted into the laser ablation chamber and the cell is purged with helium. Then, the laser power supply and the plasma torch of the mass spectrometer is initiated, and both are preheated over 15 minutes. Table 8 shows the set LA-ICP-MS parameters.

Table 7: LA-ICP-MS parameter for cratering

Output	50 [%]
Spot size	100 [µm]
Frequency	1 [Hz]
Dwell time for preliminary examination-crater	30 [sec]

For cratering, the laser is set with "frequency" to fire every second. The shot number could be adjusted with the parameter "dwell time". The parameter in table 8 is set for 30 shots. Ablating pure polyimide layer is visible by a high intense carbon peak in the mass spectrum. When the laser reaches the silicon surface, a silicon peak is observable. Figure 13 shows a representation of ideal cratering.
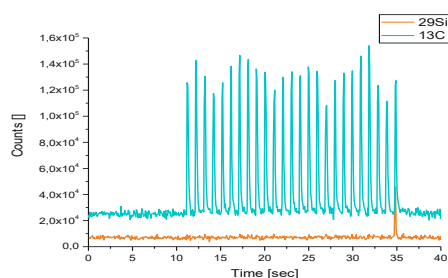
Figure 13: ICP-MS Spectrum of ideal crater production

In figure 13 two trends are observable. The cyan line represents the carbon signal. Every peak is generated by a single shot on the sample surface. The silicon signal, marked as an orange line, does not show any significant changes in trend until the breaking point of the polymer is reached, when the laser ablates polymeric material and material from the wafer surface. This point observable, when the first significant silicon peak arises. The depth of the generated craters can be measured via profilometer.

Using a profilometer, a diamond tip moves across the sample surface in contact mode. In this scanning mode passes the crater hole. Figure 14 shows an exemplary crater, which is scanned by the used profilometer.
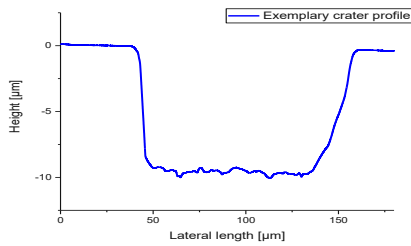
Figure 14: Profilometer result of exemplary crater

For data processing the polyimide surface, which is not ablated by the laser, is set as a reference baseline. From this baseline it is possible to calculate an average difference between the bottom of the laser crater and the polyimide surface.

5.3.1.2 Total profile method

The "Total profile" method is a layer thickness examination method developed by the operator. Instead of determining the layer thickness indirectly by profiling craters, an entire polyimide coated wafer is scanned by the profilometer. The difficulty with this method lies in setting the reference points. Using the crater method, the polyimide, which is unscathed by the laser, is used as reference point. Using cratering method, the from the laser unscathed polyimide around a crater is set as reference point. Scanning the entire layer requires, that the reference points must be beside of the layer, which makes the reference to the silicon wafer substrate suitable.

Using the wafer surface beside the layer as reference for thickness determination is possible, by taking advantage of a phenomenon that occurs during spin coating. After spinning, the polyimide must be heated out, to remove organic solvents from the polymer. During this process, the highly viscous sample liquid at the peripheral zone withdraws itself towards the wafer centre. Subsequently, the polymer leaves the peripheral zone free of residues and expose a clean silicon surface. This effect is effective at 20 to 40 µm from every wafer edge and is visible by using microscopes. So, the layer is surrounded by a small silicon plane and this is useable for reference points for profilometry.

5.4 LA-ICP-MS

The instrumental coupling of a laser ablation (LA) and an inductively coupled plasma torch mass spectrometer (ICP MS) forms the basis of the elemental specific examination. Figure 15 shows the used laser ablation, a "New Wave ESI 213", the spectrometer a "Thermo Scientific™iCAP™Q ICP-MS" is shown in figure 16.

Figure 15: Laser ablation "New Wave ESI 213™"

Figure 16: ICP MS "Thermo Scientific™iCAP™Q ICP-MS"

5.4.1 Ablation and ionisation

The laser ablation is an efficient method for sampling solid surfaces. The laser is a Nd-YAG (Neodymium doped Yttrium Aluminium Garnet) with a wavelength of 213 nm, so it operates in the close UV region of the electromagnetic spectrum. Using this solid-state laser, a laser beam fires in pulsed mode onto a sample surface. The photon energy is transferred to the electrons and further this results in vibration on atomic level, chemical bondings will be broken. A helium gas flow transports the produced aerosol from the ablation into the ionisation source of the coupled mass spectrometer. [34] [31] [38]

The ICP is the ionisation source of the mass spectrometer. The torch consists of three concentrically arranged tubes. The inner one is the injector. The ablated sample enters the second tube, transported by a helium gas flow, where it is mixed with argon. An electric spark is generated at the torch head and a silver coated, water cooled copper coil accelerates the electron at about 27 MHz. When an electron hits an argon atom, it splits off an electron inevitably and the atom is simply positively charged. This gas, which contains charged particles, Ar^+, other ions and electrons, represents the plasma, and has temperatures of 6000 to 8000 Kelvin and is able to ionises incoming sample atoms. Another argon stream tangentially surrounds the plasma and cools the flare in the outer zone to protect the surrounding quartz mantle from the plasma heat.

A quadrupole analyser is used as mass analyser. This consists of four electrode rods arranged in parallel and surrounded by an electric field. When a charged, accelerated particle passes through the gap in the middle of the four rods, it is deflected from its trajectory to varying degrees, depending on its mass to charge (m/z) ratio. After this the ions enter the detector, which consists of a combination of a secondary electron multiplier (SEV) and a Faraday cup.

5.4.2 Selection of masses [14]

For using this quadrupole, it is required to pre-select wanted ions before starting measurement. For this thesis following ions are measured: 39K, 13C, 29Si, 35Cl and 37Cl. Although 13C isotope only occurs with a probability of 1.1 %, carbon with the mass number 12 will not be measured directly. The reason for this is, that 13C Signal Intensity is two orders of magnitude less than intensity of 12C Signals. As polymer matrix is measured mainly in this project, amount of measured 12C would be so high, that this would overload and overstrain the detector. On the one hand precision could not be guaranteed at such high signals, on the other hand persistence of the detector would be reduced due to this endurance stress. It is important to measure carbon amount, to use it for normalisation issues. Additionally, mass spectrum shows eventual laser fluctuation or simple inhomogeneous ablation, as these are reflecting in carbon intensity and signal trend over ablation trend. 29Si is chosen for the same reason. Although 28Si is the isotope with highest probability, it is enough to select isotope with only 4.67 %. Silicon must be checked during ablation, not for direct elemental analysis within the polymer, but silicon signal intensity gives information when polyimide is fully ablated and silicon substrate is hit. 39K, 35Cl and 37Cl are selected for diffusion related issues. As only potassium chloride salt is used for diffusion no other elements are needed to analyse. However, even these two elements are sufficient to generate great analytical obstacles and issues due to their characteristics. For this table 9 shows the isotopic ratio of these. [7] [39]

Table 8: Isotopic ratio of potassium and chloride

Element	Potassium			Chloride		
Isotope	39K	40K	41K	35Cl	36Cl	37Cl
Isotopic ratio / percentage [%]	93.26	0.01	6.73	75.77	$7 * 10^{-11}$	24.23

The main isotopes of potassium are 39K and 41K, while 40K, and other, is not considerable due to its low probability of existence. 41K would be a useful isotope, as polymer samples after diffusion are penetrated and so highly contaminated with potassium and with an isotopic ratio of 6.73 % it would be sufficient for determination without overloading detector. Nevertheless, 41K is not possible to measure without spectral interferences. Although ICP-MS has a significant detection limit and precision for various elements, spectral interferences are a ubiquitous issue due to equal masses of isotopic variations. Ion source of ICP-MS is an argon supplied plasma torch. So, sample aerosol with transport gas helium from ablation cell is mixed with plasma gas argon and is ionised. Due to high temperature and other physicochemical properties semi-stable polyatomic bonds and adducts are formable, especially with argon isotopes. So, before isotopic and elemental selection for determination, it should be analysed which spectral interferences can occur. For 41K, a polyatomic adduction consisting 40Ar and one proton has a high change to form for these experimental conditions, $40ArH^+$ [7]. 40Ar is with 99.6 % the most stable form of all its isotopes und hydrogen is an ubiquitous element. A single hydrogen examination would be not possible with ICP-MS anyway. Other probable interferences, which resulted in the same, approximate mass and has a high, absolute abundance (over 75%), are 14N+27Al, 1H+40Ca and 16O+1H+24Mg. All these polyatomic interferences has the same theoretical origins. The non-metal component, nitrogen, oxygen and hydrogen come from laboratory air residues within the ablation cell and

from ablated matrix polymer material. The metal component, aluminium, calcium and magnesium come from contaminations within the polymer and on its surface due to non-ideal pure basic substances and external influences like dust depositions. In summary, 41K based examination would suffer from these spectral interferences. Consequently, 39K must be selected. This resulted in very intensive signals. On the one hand this increased precision, but on the other hand other isotopic / elemental specific signals could be suppressed or simply overload the detector. The used ICP-MS instrument is equipped with a dual detector system, combining a photomultiplier with a faraday-cup. Which one is used, is depending on signal intensity. Even signal is measured analogously by faraday-cup, without any amplification, average measured counts per second for potassium with used ablation conditions is within 10^6 to 10^8 region, close to overloading limitation from detector. Nevertheless, absolute spectral interferences of 39K exist indeed, but are less problematic for examination. For 39K the polyatomic $38ArH^+$ is interfering [7]. However, isotopic ratio of 38Ar is only about 0.063 %. This fact made 39K the only selectable isotope.

For chloride examination 35Cl and 37Cl are selectable isotopes, which exist in typical ratio of 3:1 approximately. Thus, for chloride evaluation and for quantification, 35Cl is chosen primarily. On the one hand, abundance of 35Cl is three times higher than 37Cl isotope. In general, for chloride determination via laser ablation inductively coupled mass spectrometry low intense signals are expected due to the lower ionisation yield of 37Cl. [28] So, contrary to potassium determination, proceeding with high expected isotopic abundance for chloride is required. Additionally, known spectral interferences are $16O+18O+1H$ and $34SH^+$ [7]. Indeed, these elements are common to fin within this experimental application, however, 16O and 34S has both a very low probability to exist. Equal-mass interference of 37Cl is $36ArH^+$ mainly. Indeed, 36Ar has an abundance of about 0.336 %, both elements exist in extreme surplus, which increased probability of absolute number of polyatomic formations. The influence of spectral interference is observable when measuring simultaneously 35Cl and 37Cl, insofar as typical expected isotopic ratio between both isotopes is not kept constant over sampling time but is subjected to fluctuations.

To understand this assumption better, figure 9 shows the determined 35Cl / 37Cl ration of three different spiked calibration standards. There, the spike level or pattern number is irrelevant, only the absolute ratio of individual examinations and compared ones to each other should be visualised.
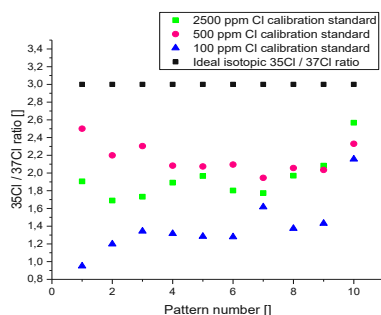

Figure 7: 35Cl / 37Cl ratio of various pattern numbers = penetration depths

In black colour the ideal isotopic ratio, so multiplicative factor of 37Cl, is given (1:3). Nevertheless, all calculated sample ratio points are below the expected ratio. It can be assumed, that counts of 37Cl is increased by interferences, for example by $36Ar^1H^+$ compounds. [28] Consequently, the typical isotopic ratio of chloride is not useable and only 35Cl is used for quantification and qualification.

29Si is chosen for two reasons. It has a typical abundance of 4.7 %, so probability to overload detector of mass spectrometer is lower than using 28Si with 92.2 %. Second reason concerns spectral interferences. 28Si is interfered with N_2, which is an ubiquitous contamination due to laboratory air. Additionally, 30Si interferes with several multi atomic combinations of carbon, oxygen and nitrogen.

5.4.3 Sampling and evaluation

The execution of element specific analyses via LA-ICP-MS starts with fixing the penetrated sample layer on a silicon wafer with 1 x 2 mm adhesive strips. This is done, as surface specific examinations require a planar target and to provide a sample substrate for the ablation chamber. It must be ensured, that the sample surface, especially the diffusion region, is as planar as possible on the silicon without any deformations. (more information about "diffusion region" is located in chapter " Polyimide layer production method, proposed by the supervisor " When sample is attached to the wafer, it is ready for ablation.

For sampling via laser ablation, a specialised ablation and evaluation mode is created. In contrary to common liquid sampling, it is difficult for solid sampling to obtain high reproducibility and precession due to several side effect during this process, like surficial inhomogeneity and structural effects. In this thesis the only used matrix material is based on polymers. Advantageously, organic polymers have a reduced thermal conductivity coefficient as metals, which why typical melting, solidification and consequently stratification on the peripheral zones of layer target cross sections due to the thermic impact of the laser pulse shock waves are not expected. Nevertheless, peripheral zone effects also exist using polymeric matrices.

Single spot laser measurement mode leads to various problems like crater depth depending diameter reduction, superficial excavation and artifacts and the relatively small analytical surface are used for analysis. Because of this, sampling method contains lateral laser movement resulting in ablation patters. If the laser makes a line tape move during shooting, ablation depending side effect of peripheral zones are eliminated along the laser direction. Nevertheless, peripheral zones still have effects due to the edges parallel to the movement direction. Subsequently, an entire ablation area raster is created for every examined sample: During measurement, laser moves along a set line for a certain length. After reaching the end of the line, shooting stops. The laser instrument moves back to origin position, but this time beneath the ablated line, where next line is set with exact same alignment and laser parameter. Laser starts shooting and moving again. This process is repeated until last set line is reached. Now, first ablation area raster is complete. Now instrument moves back to origin position of the first line and entire process is repeated to achieve layer penetration.

At the end of the line, ablation area is bigger than set laser spot size. This comes from the fact, that, when end is reached, following command to shut down laser delayed comparing with laser pulses. So, although order is proceeding, laser keeps on shooting at this single point. Penetration depth at this position is much bigger than at other locations. This effect intensifies with increasing number of penetration layers. Beside of laser bore hole depth, lateral effects are also visible by increasing ablation diameter. Intensified vertical but also lateral ablation leads to another problem. With continued penetration, so repeated laser lines over previous lines, substrate is reached faster than at other locations as well as the higher ablated region initialises abrasion into opposite scan direction and crack extension into every side of the matrix.

Consequently, despite of improved ablation sampling, evaluation has to be reduced to correct ablated regions. The first and the last line is not evaluated, as both suffered from one-sided peripheral effects. Depending on set laser scan lateral length, pulse frequency and laser output, beginning and ending ablation zones are also not evaluated. About three to four times of set spot size is eliminated for evaluation to successfully reduce these effects. So, evaluation pattern is a reduced ablation pattern.

5.4.4 Normalisation procedure

As mentioned before, precisions and reproducibility of LA-ICP-MS measurements are limited by sometimes insufficient sample homogeneity but also artefacts in the ablation process. Nevertheless, using normalisation technic, it is possible to correct this sampling errors. The theory is based on correcting every elemental signal in mass spectrum read out after measurement by referring to simultaneously recorded carbon signal. If the amount of ablated material is reduced, by changing lateral position for example, not only the measured elemental density but also the total carbon content will decrease. Consequently, read out counts of the element "x" per second from the mass spectrometer, is calculated into counts of the element "x" per second divided by counts of measured carbon per second. Normalisation procedure is executed before any averaging or other mathematical or statistical calculations, so raw data is always normalised first.

5.4.5 Determination of pattern depth

Raw data of ablated samples is given in signal or counts per seconds per ablated pattern. However, element specific analyses is of higher information, if pattern is calculated into a metric depth, which will be discussed in this chapter.

First, polymer layers without any spike level or other additives are produced. Then laser ablation parameters correspond to potassium and chloride quantification are set. (more details about set parameters in chapter "Element specific quantification") A line with lateral length between 1.0 and 1.5 mm is set. Then a copy of this line is set parallel to the previous one, but with a minimum distance of twice the spot size. Directly, coextensively on this line a second one is set. So, this region is "two lines deep". These processes are repeated until the number of duplicates on the last line is the number of all executed patterns on sample or quantification measure for one examination. Consequently, a raster on the polyimide is applied with every line corresponding to a certain pattern depth. After ablation is executed,

21

wafer is inserted into DekTak profilometer (see chapter 5.3 "Profilometer"). Perpendicular to the LA scan lines, DekTak scan lines are set. Now, obtained profilometric result shows multiple cavities, which are getting deeper with each additional pattern line. An exemplary ablation profile is shown in figure 10.
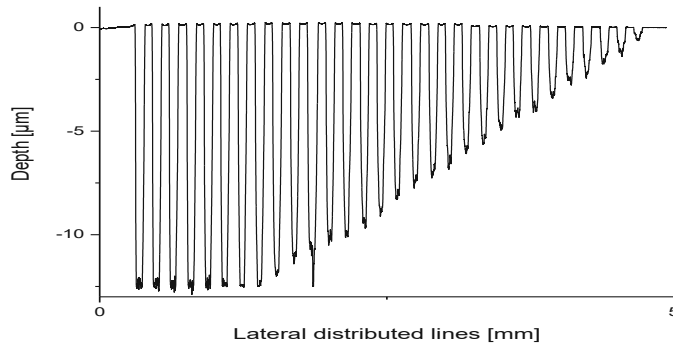

Figure 8: Profilometer result of laser line cavities for pattern depth determination for polyimide layer

By setting a correct reference point, using silicon edges already mentioned in chapter "Total profile method", line depth is determinable. In figure 11 the stepwise pattern depth increasing is observable. After breaking through polymeric matrix, no intensive depth increase is observable, as adjusted laser power and pulse rate is too less intensive to ablate silicon substrate significantly.

After measuring, the difference of all pattern depth is calculated and averaged. Consequently, a value for average penetration depth is obtained. This is executed for potassium and chloride measurements separately using the corresponding ablation parameters. It must be mentioned that there are two ablation modes for potassium and chloride, the two main diffusive transported elements in the polymer, to achieve quantification, which will be explained in chapter "Element specific quantification"

Table 9: Average penetration per pattern for certain ablation modes

Element (specific ablation mode)	Ablation parameters		Average penetration depth [µm / pattern] [µm / line]
Chloride	Laser energy [%]*	60	2.2 +/- 0.2
	Pulse rate [Hz]	20	
	Spot size [µm]	200	
	Plasma power [W]	1550	
	Scan speed [µm/sec]	400	
Potassium	Laser energy [%]	35	0.4 +/- 0.1
	Pulse rate [Hz]	10	
	Spot size [µm]	80	
	Plasma power [W]	1400	
	Scan speed [µm/sec]	240	

The dimension for laser energy is [%]. This is the settable parameter for ablation experiments. Laser fluence is calculated by laser ablation instrument software while firing and is not

constant during process, whereas [%] is adjustable by the operator before starting measurement.

5.4.6 "Great Line" method

Within the diffusion cell, interaction area (=diffusion region) has a diameter of about 1.1 mm. For molecule and ion scale this region is a spacious area, where ions can penetrate. However, due to non-ideal surface form and bulk and electrostatic charged localisations it is possible, that ions penetrate the layer not homogeneously over the entire area. This assumption will be confirmed in chapter "Element specific analyses of penetrated samples". Consequently, sampling by pattern ablation of randomly selected sample areas would be error-prone due to local-depending concentrations. To confirm this assumption an ablation method for determining this effect is established, called "Great line" method.

"Great line" method is a diversification of common ablation pattern. Instead of setting a rectangular pattern within the diffusion cell, number of executed lines is reduced while increasing lateral length immensely. Additionally, another pattern is set with perpendicular direction. So, both patterns represent a cross, over the layer diffusion region. In figure 11 schematic and photographic presentation of polymer layer on silicon matrix with marked laser patterns for "Great line" method is shown.
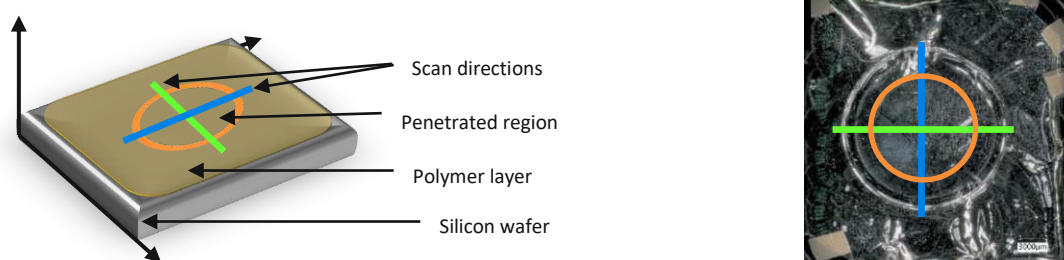
Figure 9: Schematic and photographic presentation of a polymer layer with marked lines for Great line method

5.4.7 "Imaging" method

As explained in chapter "Great line" method", diffusion indicated ionic penetration does not proceed ideal homogeneously over entire diffusion region. However, using "Great line" method, only concentration distribution along set vertical and homogeneous scan lines, but not over entire sample surface, is examinable.

"Imaging" method is a well-established technic to gain an insight into element specific concentration distribution within a definite area. First, via microscope entire sample layer is recorded with lowest possible magnification. Then sample is ablated with definite parameters. It must be guaranteed, that an entire raster is ablated completely without sample residues after line scan. So intensive ablation conditions are needed. Nevertheless, ablation intensity must not be too high, so that surrounding material of set spot is not destroyed before reaching it. Entire ablation raster must be recorded by ICP-MS, so detection, in one file, contrary to common sample examination. After that, scan is exported into imaging software program "ImageLab". This software calculates distribution images on the base of counts/time data and ablation rate parameters. But evaluation method is explained: Imported sample scan is cleaned from measurement idle times, like laser instrument moving or warming up times, and

wanted signals are corrected to an internal standard, which is 13C concentration. At last, element specific signal image, described as hyperspectral image is overlapped and matched with microscoped record of the sample.

Table 10: Ablation parameter for "Imaging"

Laser energy [%]	65
Pulse rate [Hz]	20
Spot size [µm]	100
Plasma power [W]	1400
Scan speed [µm/sec]	300
Overlap [µm]	0
Average number of set scan lines []	Depending on sample size
Average number of evaluated scan lines []	= Average number of set scan lines
Average lateral line length [mm]	Depending on sample size
Average evaluated line length [mm]	= Average lateral line length

5.5 Membrane materials

The following sub-chapters contain information about the used polymers membranes in this thesis.

5.5.1 Nafion® membranes

Nafion®, in further discussing simply described as Nafion, is a perfluorinated polyethylene with ether linked side chains, terminated with sulfonated groups. It is built up on a Teflon® backbone to provide high chemical stability but is modified with these ether chains. By using ether bridges, chains deviate from linear structure and so higher flexibility is provided. The side chains are terminated with sulfonacid groups. Contrary to the lipophile backbone and sidechains, this sulfonated groups show high hydrophilicity. So, this material is able to take up water reversibly. After soaking in water or aqueous media, inner, water filled nano channels are formed by interacting with the sulfonated groups. Furthermore, the material becomes high conductive (for cations). The Teflon® backbone keeps stability. With these structural properties, ions of different size are possible to use these nano channels for transport, enhanced by the protonation and deprotonation equilibrium of the sulfonated groups. Figure 13 shows a scheme of such a nano channel after water soaking. [3]
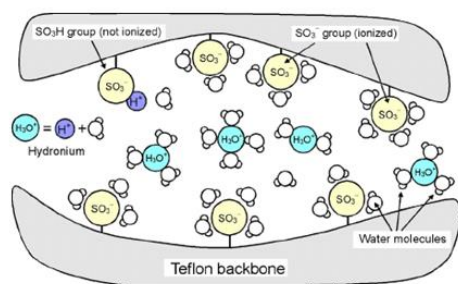

Figure 10: Scheme of Nafion nano channel

The scheme shows the proton conductively and the water-hydronium equilibrium, where protonation and deprotonation on the acidic proton of the sulfonic group occurs. So, if an electric propulsion is given, protons, but also other positive ions cannot only move through these channels, but also get a higher electromobility. Movement by anions are not promoted by this effect. This function is the fundamental basis of the Nafion examinations of this thesis. Additional properties of this material are elaborated in the following chapters, where such information is needed.

The used Nafion membranes are classified as 25.4 µm thick NR-211® membranes. All used membranes are prepared from the same material sheet, so they are still described simply as "Nafion". Before using Nafion membranes, these must be soaked in water or aqueous medium first. The pre-set method for soaking is executed as follows: Nafion membrane is cut from the material sheet in 3 x 3 cm piece size. The sheet is protected with a two-sided PE foil, a backing film a cover sheet. Using two adhesive tapes, preferably insulation tape, the covering sheets can be removed, represented in figure 14 [I]
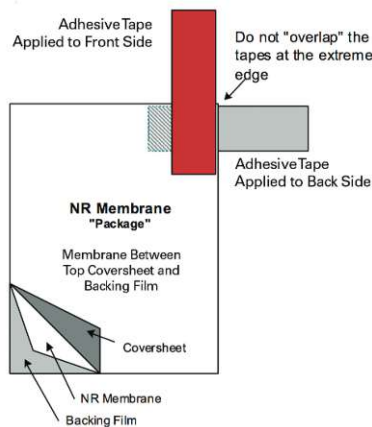
Figure 11: Scheme for removing cover sheets from Nafion membranes [I]

Nafion membranes are used as model membrane. Nafion channel interaction with positive charged ions are well known, furthermore used NR-211® membranes has got definite layer thickness and sufficient planar surface for interaction with both fluid media. These membranes are used to determine reproducibility of using diffusion cell and PDMD and examine impacts on potential difference observation, like sample layer preparations.

5.5.2 P84® membranes

5.5.2.1 P84® layer properties

In comparison to Nafion®, P84® (P84, polyimide or PI) shows different properties, which are listed.

- Less water uptake characteristics (Polyimide: 1-2%; Nafion®: 50.0 ± 5.0% [III])
- No ionic functional characteristics or additives
- Higher Young's elasticity module (Polyimide: 5.5 GPa [21]; Nafion®: 280 MPa [III])
- Less planarity and surface homogeneity
- Less layer thicknesses

25

- Different macroscopic properties (e.g. colour)

After production, a polyimide layer is assumed as an agglomeration of P84® particles with residues of organic solvent. There are no nano channels like in Nafion or hydrophilic functions, which support water soaking. Consequently, PI layer shows less water uptake condition. Due to low liquid medium within the bulk, diffusion coefficient is reduced for ionic mobility. P84 has also no ionic active substituents. There is no opportunity to enhance ionic movement trough the layer bulk, so for ionic diffusion only the ionic permeability of the membrane material is the speed limited parameter, excluding other layer properties. Furthermore, cations are not bonded by acidic or other negative charged locations, so the concentration of potassium and chloride in the membrane should be lower than in Nafion layers after diffusion. A major disadvantage of using polyimide layers are surface relating planarity errors due to the production, which cause several impacts on diffusion mechanism, like non-ideal interaction surface diffusive gradients and coefficients caused by local evaginations and invaginations. Additionally, also the bulk of a polyimide layer represents an obstacle. While Nafion is produced industrially with including quality assurance measures and guidelines, polyimide is still an in-house product. Therefore, different physicochemical interaction could occur, for example gravity induced material sedimentation and layer by layer solvent evaporation. However, these effects will be discussed in "Results and Discussion". Another difference to Nafion is the layer thickness. Polyimide layers show an average thickness of nearly 9 – 10 µm, instead of 25.4 µm. There are also other macroscopic differences, such as colour. While Nafion membranes are clear and colourless, polyimide layers are slightly dull, yellowish. This property had no impact on potential difference change observation, but on surface and elemental analytical issues, as material with higher contrast to the background are easier to work with, for example when adjusting camera of the laser ablation instrument for optimal zoom.

5.5.2.2 Production of the polyimide stock solution

For this thesis, the liquid precursor stock solution for polyimide layer are produced by the operator. A 50 ml polypropylene screw cap eprouvette is tared and pale-yellow P84 powder is weighed in. For this thesis, a limitation of deviation while weighing polyimide is defined, which interval width is +/- 50 mg.

Now, the polyimide powder must be dissolved. To reach this, the organic solvent N-methyl-2-pyrrolidone, NMP, is used. Details about this chemical product can be read in chapter "List of used chemicals and materials". The most important properties are on the one hand the noxious and carcinogenic characteristic, why work in an extractor hood is done as often as possible, and on the other hand, the hydroscopic characteristics of this substance. Due to water absorption, the liquid should not be unnecessarily long exposed to the air. Otherwise the consequence is an uncertain amount of absorbed water molecules, which can deteriorate the production of the polyimide layers.

For this thesis, the produced stock solution is a mixture of 20 w% polyimide and N-methyl-2-pyrrolidone, PI-NMP, proposed by the supervisor. Originally the liquid NMP is diaphanous and colourless. After combining the powder with the solution, the colourisation changes into yellow-dark brown and become nearly intransparent. Nevertheless, the solvation of PI powder

does not happen abruptly. Indeed, in local areas, where NMP comes in contact with the powder fill, it comes to the formation of a very viscous, gel-like suspension. Now, the former suspended material blocks unsaturated NMP from. To achieve a homogeneous and complete solvation, filled eprouvette is shaken manually with high frequency and power for three minutes to provide capacious interphases. Then, the eprouvette is put into an ultra-sonic bath for 30 minutes. This process enables an intensive mixing, so that inner cavities with this high viscous mantle break up, as well as increases temperature in the eprouvette. After this, the warm mixture is shaken again manually with the same intensity and time. To avoid local phase separation, the eprouvette is placed on a horizontal shaker and is set in motion with 600 to 700 rpm until use.

Table 11: Stepwise description of PI-NMP mixture production

Weighing in polyimide powder P84 (limitation of deviation: +/- 50mg)
Adding N-methyl-2-pyrrolidone to achieve 20 w% PI-NMP mixture
Shaking eprouvette for three minutes manually
Ultra-sonic treatment for 30 minutes
Shaking eprouvette for three minutes manually
Continuous shaking on horizontal shaker with 600 until use

5.5.2.3 Production of the polyimide layers

The sample polyimide layers, used for diffusion experiments, are produced by a spinning process via spin coater. Precleaned with acetone, silicon wafer with a 3 x 3 cm surface are used as layer substrate. The inner surface of the spin coater is covered with commercially available aluminium sheets. Sample material, which is thrown away from the wafer by spinning, lands on the aluminium and can be removed easily when cleaning the spin coater. Before inserting the wafer, a polysiloxane added on the rotating plate of the spin coater. This pad is 1.5 mm thick with a 1 x 1 cm surface and a hole in its centre. This pad is placed between spinning plate and wafer, so that both holes coincide with each other. If vacuum is applied, the wafer will be pressed on the chuck in centre of the rotatable plate and the pad seals the entire system, so wafer will not shift during the spinning process due to adhesion power of the elastic polysiloxane. Without using the pad, the wafer could change its position and so the effective range of the centrifugal force, which lead to different layer profiles.

When the wafer is applied, the rotary vane pump is activated to generate the vacuum. The complete wafer will be bespattered with acetone until the solvent covers the complete surface for cleaning. Then, the cover plate of the spin coater is closed, and the spin coater is turned on for 5 seconds with 2000 rpm. The rotation number is reduced to 200 rpm and the cover plate is opened. Nitrogen is used to remove the remaining acetone from the wafer. If the waver is free from acetone and solid particles, the rotation is stopped, and the wafer is ready for use.

Using a polypropylene 10 ml-syringe polymer solution is superimposed, evenly distributed over the substrate dropwise. After superimposition, the cover plate is closed, and the spin

coater is activated. When spinning is complete, the wafer must be removed from the spin coater and from the polysiloxane pad. Now, the polyimide must be hardened to achieve the final, solid form and to preserve the layer profile. The polyimide coated wafer is placed on a heating plate. Then the wafer is coated with a solid polyimide layer.

The parameter of the spinning process is optimised intensely to achieve satisfactory results. Therefore, the method, proposed by the supervisor, the optimisation process and comparison between proposed and optimised method are shown in chapter "Polyimide layer production examination" in the appendix. The following table 13 contains the parameters for the optimised and used layer spinning. Table 14 shows a stepwise description of the entire production process.

Table 12: Parameters for optimised layer spinning process

Number of different spinning modes []		2
Pre-spinning phase	Spinning time [sec]	240
	Rotation number [rpm]	200
Fast-spinning phase	Spinning time [sec]	10
	Rotation number [rpm]	2000
Resting-phase [sec]		120
Volume of superimposed sample solution [ml]		0.8
Number of different heating modes []		2
Solidification phase	Temperature [°C]	90
	Heating time [min]	15
Hardening phase	Temperature [°C]	180
	Heating time [h]	15

Table 13: Stepwise description of polyimide layer production

Position siloxane pad on chuck of the rotation plate
Position silicon wafer on siloxane pad and activate vacuum membrane pump
Cover silicon wafer with acetone and rotate it off with 2000 rpm
Remove acetone residues with nitrogen from the wafer while rotating with 200 rpm
Superimpose 0.8 ml PI-NMP solution dropwise
Initiate spinning sequence
Isolate covered wafer from the spin coater and place it on the preheated heating plate
Initiate hardening sequence

5.5.2.4 Preparation of the polymer layer for diffusion

Polyimide samples are produced on silicon substrate. For diffusion examinations polymer membranes must be isolated from the substrate by soaking process.

The silicon wafer with the sample on it is inserted into a 100 ml wide-neck bottle with screw cap. Before closing the bottle, a polyethylene grid is put in. The reason for using a grid is, if the polymer layer comes off, it will float on the surface of the deionised water, if it is not soaked completely. As a result, one side of the layer will stay in contact with the water, but the other

will be exposed to the air. Consequently, the soaking process is not ideal on every area of the layer. The grid prevents the sample from reaching the surface. Additionally, the bottle is fixed on a horizontal shaker. During the soaking process, the bottle moves with 600 rpm. Due to the artificially generated dynamics of the water, the layer removes itself from the wafer, much faster than in hydrostatic matrix.

6 Measurements

6.1 Examination of layer thickness determination method

For this thesis, "Cratering" is chosen by the supervisor as default method for layer thickness determination for polyimide layers. However, the repeatability and reproducibility of thickness determination results must be examined to determine, if "Cratering" is an adequate method for these layers or if the method must be changed. For this method examination, the theoretical and practical background of sampling is explained.

"Cratering" method is destructive. Using laser ablation, sample material must be destroyed to create the carbon signal and laser bombardment is repeated until the layer is penetrated completely. Consequently, it is not expedient, to examine the section, where the diffusion will take place, as a penetrated PI region would make diffusion analyses meaningless. In further explanations this zone will also be described as "forbidden zone" or "forbidden area". So, layer thickness determination is indirect, as it must be assumed, that the thickness around the diffusion region is the same as inside. Thus, different located, ablation points are defined to examine the reproducibility of this method. Figure 16 shows a scheme of a produced polyimide layer on silicon substrate.
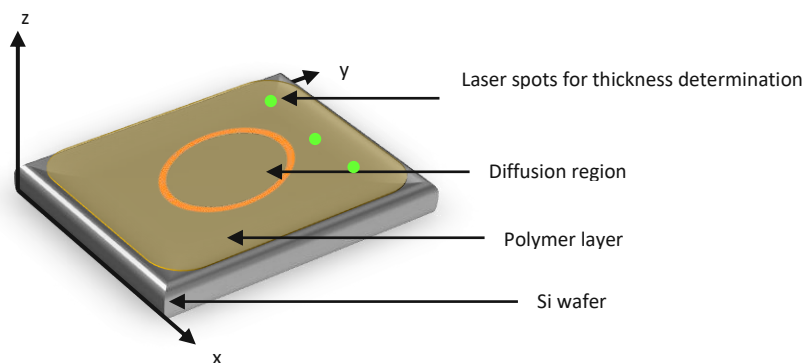
Figure 12: Scheme of laser spot location for cratering method

The scheme shows examples for laser spot locations to determine the thickness of the layer. On the layer the diffusion region is marked in orange. This section cannot be used for thickness examination. Another non-expedient zone is the domain around the diffusion zone. There the sealing ring of the diffusion cell is located, consequently penetration by laser shots will harm the entire system seal. Additionally, to reduce the impact by surface irregularities on layer beam cross section, measuring peripheral zones is avoided. In summary, measure points for layer thickness determination lies between peripheral and diffusion region, without coming to close to these regions, represented exemplary as green points in the scheme.

The created craters are measured profilometric and the results compared to determine the deviation of the measured thicknesses.

6.2 Observation of potential difference change due to diffusion

This chapter contains the potential difference observation examinations, using Nafion and P84 membranes. The basic goal of all membrane specific examinations is to confirm the attainableness of reproducibility. This criterium predicates, that measuring different samples of the same material source, (Nafion® sheet charge LOT, P84® membranes with the same production condition) should lead to the same results approximately, realised by recording the same potential difference change observation trend. Repeatability is not a possible analytical issue, as an already penetrated sample layer cannot be measured again.

6.2.1 Nafion® membranes

6.2.1.1 Reproducibility determination

Table 15 shows the parameters of the diffusion observation for Nafion reproducibility examination.

Table 14: Parameters for Nafion reproducibility examination

Type of membrane	Nafion® NR-211
Soaking medium	$KCl_{aqu.}$ solution
Soaking medium concentration [M KCl]	0.05
Soaking medium volume [ml]	250
Salt solution for diffusion chambers	$KCl_{aqu.}$ solution
Concentration difference for diffusion [M]	0.05 : 0.5
Additional cell modifications	none
Recording frequency [sec/datapoint]	10
Number of measured sample layers	7
Number of evaluated sample layers	7

In the beginning of the execution, a concentration difference between 3 M and 0.01 M is proposed by the supervisor, however experimental results shows that this ratio must be changed due to several reasons: 3M KCl solution is so close to saturation limit, that even the lowest over-concentration zones will lead to crystallisation effects, while 0.01 M harmed the electrode stability. Furthermore, such a high concentration difference increases osmotic deformation, which will be discussed later in chapter "Osmotic impact on diffusion observation".

6.2.1.2 Osmotic impact on diffusion observation

Nafion acts an ion exchange membrane as soon as it is soaked in water by forming water filled nano channels, which provides ionic exchange. But by allowing liquids exchanging ions by this

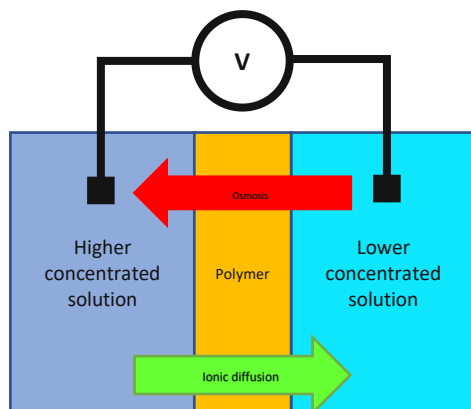membrane, channels can also be used for transporting molecules, for example water, shown in figure 17.

Figure 13: Scheme of ionic diffusion and osmosis in diffusion cell

Ions of the higher concentrated solution, irrespective to the ion and its charge, moves to the lower concentrated liquid to reach equilibrium. Simultaneously, the osmotic effect tries to transport water into the higher concentrated liquid to adjust the chemical potential. Consequently, both mechanism act in opposite direction. Now, there are two different processes, which promote concentration balance adjustment. This additional mechanism is not separable by potential difference measurements, as PDMD only records absolute changes in voltage and as a result, this effect sophisticates a too fast ionic diffusion.

For this thesis, the consequence of osmotic impact will be discussed in chapter "Results and Discussion", but also a method for reducing the structural impact due to the osmosis on sample layer is established, explained as follows:

Diffusion cell is modified by integrating a barrier. This barrier is a close meshed (7µm) PET network. An adequate size of the network is cut out, then the network lattice is closed with elastic polysiloxane glue with exception of a round area in the centre for diffusion region. The hardened "osmosis barrier" is placed between polymer membrane and sealing ring of the polycarbonate chamber part for lower concentrated solution. The theoretical consideration of this assembling is as follows: When the polyimide membrane is getting deformed by increasing hydrostatic pressure of transferred water, the membrane starts pressing against the stable, unmoveable PET network. Due to the close meshing, polymer membrane is not able to press trough these lattice openings. Consequently, the resulting back pressure would reduce further deformation and reduce further water transferring as soon as backpressure is higher than osmose pressure.

For reproducibility determination, seven Nafion samples are prepared and measured using osmotic barriers. Table 16 shows the parameters for diffusion observation.

Table 15: Parameters for Nafion reproducibility examination

Type of membrane	Nafion® NR-211
Soaking medium	KCl$_{aqu.}$ solution
Soaking medium concentration [M KCl]	0.05
Soaking medium volume [ml]	250
Salt solution for diffusion chambers	KCl$_{aqu.}$ solution
Concentration difference for diffusion [M]	0.05 : 0.5
Additional cell modifications	PET-barrier modification
Recording frequency [sec/datapoint]	5
Number of measured sample layers	7
Number of evaluated sample layers	5

6.2.1.3 Soaking impact on diffusion observation

Another reproducibility determination is executed with pure water soaked Nafion membranes. The reason for this is to observe the effect of using a Nafion membrane transport matrix with fully protonated sulfonated groups and with potassium contaminated and occupied places. Table 17 shows the parameters for reproducibility determination using water soaked Nafion membranes.

Table 16: Parameters for Nafion soaking impact observation

Type of membrane	Nafion NR-211®
Soaking medium	Deionisied water
Soaking medium volume [ml]	250
Salt solution for diffusion chambers	KCl$_{aqu.}$ solution
Concentration difference for diffusion [M]	0.05 : 0.5
Additional cell modifications	none
Recording frequency [sec/datapoint]	5
Number of measured sample layers	5
Number of evaluated sample layers	5

6.2.1.4 Layer thickness influence on diffusion observation

All analyses concerning Nafion, mentioned in previous chapters, are proceeded with NR-211 membranes with a layer thickness of 25.4 µm. To examine the impact of using layers with other thicknesses, another Nafion batch sheet is used, described as "N-117". The membranes, cut out from this sheet, have a layer thickness of 185 µm. Reproducibility examination is proceeded to determine the effect of increased layer thickness, parameters are shown in table 18.

Table 17: Parameters for Nafion N-117® reproducibility determination

Type of membrane	Nafion N-117®

Soaking medium	KCl$_{aqu.}$ solution
Soaking medium concentration [M KCl]	0.05
Soaking medium volume [ml]	250
Salt solution for diffusion chambers	KCl$_{aqu.}$ solution
Concentration difference for diffusion [M]	0.05 : 0.5
Additional cell modifications	none
Recording frequency [sec/datapoint]	10
Number of measured sample layers	4
Number of evaluated sample layers	4

6.2.1.5 Examination of proton exchange with potassium of Nafion membrane soaking

Already mentioned soaking medium and soaking time has an important impact on osmotic interaction and recorded potential difference change trend for Nafion membranes. It can be concluded that the results are based on the amount and homogeneity of exchanged protons from the sulfonated groups of the membrane bulk with the potassium ions of the soaking medium. During soaking process, water molecules and ions from the medium diffuse into Nafion membrane. The cations from the solution removes protons from their acidic places. The high electrochemical mobile hydrogen moves, to reduce its own chemical potential referring surrounding atoms, out of the layer into the soaking medium. To prove this statement, pH-value of soaking solution is measured via pH-electrode.

This examination contains an evidence analysis for real proton exchange and a method establishment for guaranteeing optimised soaking process.

6.2.2 P84® membranes

6.2.2.1 "Jump" examination

In first weeks, responding characteristics of PDMD are determined. For this, a modification of diffusion cell is made, seen in figure 18.
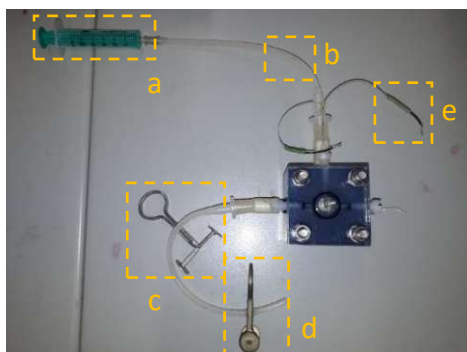

Figure 14: Modification of diffusion cell for first examination

Table 18: Description for marks in figure 19

Mark	Description
a	Syringe for source of diffusion solution supply

b	Tube for passing liquid into chamber
c	First clamp for closing outlet tube
d	Second clamp for closing inlet tube
e	Conductivity measuring cannula

This modification has two functions. One chamber is modified by inserted tubes, one connected to a syringe, another with two clamps. Instead of filling the diffusion chambers with two different concentrated solutions, both liquids are the same. As both liquids have the same ionic concentration, they have the same electric potential, and as a result the measured potential difference will be the normal electrode voltage. The syringe is filled with 5 ml of higher concentrated liquid. While recording, the clamps are opened, the solution from the syringe is pressed trough the tube into one chamber slowly removing the previous chamber solution into the outlet tubes. After this, clamps are used to close the system again. Now, one chamber is filled with higher concentrated solution, directed diffusion gradient is established.

So, with this method the reaction of the electrodes and of the entire PDMD system is measurable. The recorded trend should show a nearly constant potential difference during first minutes with an average deviation referring to normal electrode voltage. As soon as solution is pushed through the cell and substituted the low concentration, a saltational increase of potential difference is visible. After reaching maximum, the expected decreasing trend should be observable. This experiment is called "Jump". Table 20 shows parameters for "Jump" examination.

Table 19: Parameters for "Jump" examination

Type of membrane	P84® polyimide
Production method for layers	Supervisor production method (Chapter: Polyimide layer production method, proposed by the supervisor)
Soaking medium	Deionised water
Soaking medium volume [ml]	250
Salt solution for diffusion chambers	$KCl_{aqu.}$ solution
Concentration difference for diffusion before injection [M]	0.01 : 0.01
Concentration difference for diffusion after injection [M]	3 : 0.01
Additional cell modifications	"Jump" modification
Recording frequency [sec/datapoint]	5
Number of measured sample layers []	8
Number of evaluated sample layers []	0

6.2.2.2 Reproducibility determination

Table 21 shows the parameters for the diffusion observation for in-house produced, P84 layer reproducibility examination.

Table 20: Parameters for P84 reproducibility examination

Type of membrane	P84® polyimide
Production method for layers	Optimised production method (Chapter: [Production of the polyimide layers](#))
Soaking medium	Deionised water
Soaking medium volume [ml]	250
Salt solution for diffusion chambers	KCl$_{aqu.}$ solution
Concentration difference for diffusion [M]	0.05 : 0.5
Additional cell modifications	none
Recording frequency [sec/datapoint]	10
Number of measured sample layers	No specification possible
Number of evaluated sample layers	No specification possible

Details, why number of measured and evaluated sample layer cannot be given exactly, is mentioned in chapter "[Results and Discussion](#)".

6.2.2.3 Examinations for improving reproducibility

Described in chapter ["P84 membranes – Reproducibility examination"](#) reproducibility is not achievable for using P84® polyimide membranes. Thus, various optimisation examinations are proceeded. Using exactly the same PET network barrier as for Nafion, mentioned in chapter ["Osmotic impact: method for reducing osmotic deformation"](#), this instrumental setup is used for polyimide. Furthermore, long-time measurement with polyimide layers are made over approximately two months, to determine the potential difference trend curve after a significant long period of time. Also, polyimide layer production method is changed, to produce layers with significant lower thickness, described as "DS" samples, german for "Dünnschicht", to determine the impact of these on potential difference measurements, discussed in chapter ["P84® reproducibility optimisation: "DS" samples"](#).

6.3 Element specific analysis

6.3.1 Element specific quantification

To quantify the number of diffused ions, a calibration must be prepared. For this thesis, matrix supported standard addition is chosen. [37] Contrary to common examination in liquid medium, the used matrix is based on solid polyimide. Consequently, a chemical analyte substance must be found, which is solvable in polyimide N-methyl pyrrolidone mixture. The addition of liquid standard solutions is omitted, as the input of hydrophilic substances into the highly saturated organic matrix ensures immediate polymer solidification. So, an organic salt as standard material is needed. Precursor solution for layers must be spiked with the organic

salt in different concentrations to produce different concentrated layers, which are ablated with the same laser conditions as for sample examinations. Every produced layer, spiked with a specific chemical in certain concentration, represented a level for the calibration line.

For quantifying potassium chosen chemical is trifluoro methane sulfonic acid potassium salt, CH_3SO_3K. Producing spiked sample solutions turns out to be difficult, as on the one hand increasing matrix volume will increase precision and reduce errors due to weighing, but on the other hand polyimide solution is a limited resource for this thesis. As only less millilitres are needed for spinning, remaining spiked solution will be wasted, as it cannot be used for other examinations. 10 to 20 ml polyimide solution is an optimal volume for operation without wasting too much matrix. It must be mentioned that it is a 20 % mixture. As it has to be assumed that the organic solvent evaporated completely during the heating-out phase after spinning, a 1:5 factor must be added. The following table 22 contains the weighted amount of trifluoro methane sulfonic acid potassium salt.

Table 21: List of produced spike solutions for K calibration

Concentration Potassium [μg/g] [ppm]	Weighted mass CH_3SO_3K [mg]	Volume PI / NMP solution [ml]
0 (Blank)	0	10
100	1	20
500	9	20
1000	19	20
2000	38	20
3000	58	20
4000	77	20
5000	96	20
6000	57	10
7000	67	10
8000	77	10
9000	86	10
10000	96	10
11000	106	10

Quantifying chloride is a greater obstacle than potassium. Chloride contamination probability is an ubiquitous issue, as well as chloride ions are generally difficult to detect via LA-ICP-MS. Benzalkonium chloride C14, $C_6H_5CH_2N(CH_3)_2RCl$ (R=$C_{14}H_{29}$), is took for adequate calibration analyte substance. This chemical shows useful characteristics like enough quasi-stability at room temperature and normal laboratory humidity, as well as a high solvability in organic solvents. Advantageously, used benzalkonium chloride has a long alkyl-organic group with 14 chain-bridged carbons. This organic non-functional group increases lipophilicity and molecular weight. Subsequently, to achieve same chloride concentration, more analyte basic chemical has to weighted in. Increased weighted mass reduced standard error of analytical balance and errors induced by the operator. Production of stock solution is analogous to potassium quantification.

Table 22: List of produced spike solutions for Cl calibration

Concentration chloride [μg/g] [ppm]	Weighted mass $C_6H_5CH_2N(CH_3)_2RCl$ (R=$C_{14}H_{29}$) [mg]	Volume PI / NMP solution [ml]
0 (Blank)	0	10
100	4	20
500	20	20
1000	42	20
2000	83	20
2500	104	20
3000	62	10
4000	83	10
5000	103	10
7500	124	10
10000	156	10

All spiking processes are executed using piston-operated pipettes. Due to the high viscosity and the high tendency of the polymer to solidify by humidity, volumetric exact adding using pipettes is difficult. PI NMP mixture shows less adhesive interaction with the material of the pipette tip mantle hull. If suction and unload phase are executed slowly enough, definite volume can be added without generating bubbles or leaving residues of the mixture within the pipette tip, although piston-operated pipette is calibrated for deionised water. All layers for calibration issues are produced according to table 24.

Table 23: Spinning parameters for spiked layers for calibration

Number of produced layers per spike concentration []		3
Number of different spinning modes []		2
Pre-spinning phase	Spinning time [sec]	240
	Rotation number [rpm]	200
Fast-spinning phase	Spinning time [sec]	10
	Rotation number [rpm]	2000
Resting phase [sec]		120
Volume of superimposed sample solution [ml]		0.8
Number of different heating modes []		2
Solidification phase	Temperature [°C]	90
	Heating time [min]	15
Hardening phase	Temperature [°C]	180
	Heating time [h]	15

At last, spiked layers had to be ablated. Contrary to sample ablation, spiked layers should not be removed from their production wafer. Advantageously, layers lied opaque on the silicon surface, which promoted ablation efficiency. Nevertheless, correct ablation is required and must be consistent with the sample measuring mode. The also executed stepwise laser penetration on the spiked layers of every concentration on multiple production batches, eventuated in a high time investment, beside of the former steps.

6.3.2 Examination of ion penetrated samples

After diffusion observation, penetrated layers are removed from the cell, cleaned and fixed on a silicon layer using adhesive strips for elemental analysis. As explained in chapter "Sampling and evaluation", ablation scan lines are formed to a rectangular pattern and are repeated on themselves to achieve depth resolved, elemental analysis. Penetrated Nafion and P84 samples are used for elemental analysis.

Measuring via LA-ICP-MS is a follow-up analysis. So, first samples must be successfully produced, penetrated using diffusion cell and a reproducible or at last comprehensible potential difference change trend must be recorded, then they can be used for element analysis. Consequently, no strict measure pathway can be established, as this examination is limited to the successful penetrated and prepared samples.

7 Results and Discussion

In the following sub-chapters results of all measurements will be discussed, which contribute the most information to the individual task areas. The main issue of this thesis is the focus on corrosive impact by penetrated polymer layers, on important material, like semiconductor surface, so the examination of ionic diffusion within the protection medium, which leads to corrosion. However, this thesis is limited to the measuring methods, which have to be developed, examined and their accuracy confirmed first and to the useable resources, like mass producing polyimide layers of sufficient quality in the first place. So this thesis's discussion focus is changed to the developed methods on the electrochemical, but also on the analytical side.

7.1 Results of layer thickness determination method examination

This chapter presents the reproducibility examination of the "Cratering" method. For this, a polyimide layer production batch was created, containing ten samples. On every sample six laser spot locations were defined. For each position, the necessary number of laser shots was determined first, then the crater for profilometry was made. Every produced crater depth was measured twice by using profilometer, to identify and isolate statistical outliers. If a significant outlier or another error of measurement was detected, the crater scan would be repeated at another position. From two successful scans, the arithmetical mean was calculated. Table 25 contains the results of the profilometry for cratering reproducibility examination.

Table 24: Results of layer thickness reproducibility examination (cratering method). Crater depth results of every sample are arithmetic mean of double determinations

Sample Name	Crater 1 depth [μm]	Crater 2 depth [μm]	Crater 3 depth [μm]	Crater 4 depth [μm]	Crater 5 depth [μm]	Crater 6 depth [μm]	Layer thickness [μm]	Deviation of the thickness [μm]
8	9.6	9.4	9.5	8.2	9.7	10.0	9.4	0.6
9	9.5	9.5	9.3	9.4	9.3	9.5	9.4	0.1
10	7.0	8.3	7.0	5.8	5.9	5.4	6.6	1.1

12	11.0	6.8	7.0	6.2	8.6	8.4	8.0	1.7
13	10.0	10.3	10.6	9.5	9.6	9.2	9.9	0.5
15	7.2	8.3	7.5	9.5	8.9	9.2	8.4	0.9
16	10.9	11.7	10.9	10.6	11.0	10.7	10.9	0.4
18	7.8	7.6	7.3	7.9	8.0	7.4	7.7	0.3
19	8.0	8.5	6.9	8.3	8.2	7.7	7.9	0.6
20	5.8	6.8	5.5	6.2	5.7	5.9	6.0	0.5

If the individual, averaged layer thicknesses were compared, differences became apparent. The average deviation over all samples was 0.667 µm. Consequently, the standard error by using cratering for thickness determination was significant high. The reason for these results is the surface irregularity of the layers. Cratering was an one-point measurement, so total thickness was determined by few measure points. Surface irregularities, like accumulation of polyimide material during spinning process or artefacts, falsified thickness results. In addition to this, the measure process of produced craters contained errors. An ideal crater profile requires an ideal laser beam cross section with an uniformly distributed laser fluence. Nevertheless, the beam had no ideal profile. Additionally, the ablated polymer had different local, physicochemical composition, as it must be assumed, that, during heating process, it comes to local different accumulation of the material, which led to local dependent densities. Consequently, the laser beam impact led to different ablation products. Furthermore, the nonuniform energy transfer in polymer, after laser hit, had an influence on ablation efficiency.

Figure 19 shows crater profiles of various samples to explain analytical profilometric problems using cratering method.
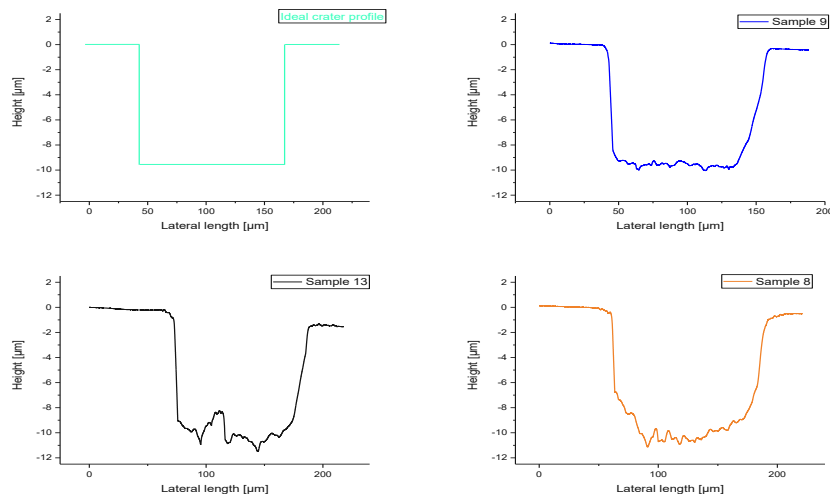

Figure 15. Types of crater profiles

In cyan colour an ideal crater profile is presented, and an abrupt rise and decreasing is visible. The image right from the ideal one, shows sample 9, a real crater with a high analytical potential. The polyimide around the crater was useable for height reference, and the deviation of the crater ground was low. The abrupt trend on the crater edges flattens but was discernible clearly. Sample 13 in black colour shows an example for an artefact in the crater profile. Either a particle, relaxed from the aerosol state, felt into the crater or the laser could not ablate this location with the same energy as other parts. Regardless of the phenomenon that had

occurred, the influence on the profilometry was the same. The increase in height was measured too and was included in calculating the arithmetic crater depth. The fourth image, sample 8 in orange, shows an example for radial dependent laser energy distribution. In this profile a valley type trend is visible. For evaluation this trend must be interpolated as planar surface, so deviation is increased.

To recap, cratering method was too inefficient for measuring layer thicknesses. Thus, for this thesis the "Total profile" method was implemented. Total profile method showed many advantages in comparison to cratering method. First, the amount of used analysis instruments was reduced, as well as the entire analyses time. A complete layer thickness determination took about four to six minutes, depending on the set profilometer scan resolution, instead of one to two hours, excluding LA-ICP-MS preparation time, using "Cratering" method. Secondly, it was a non-destructive method and repeatable. Furthermore, the result of a scan was not only a layer thickness value, but also a 2-D profile of the layer. With this profile different assertions were possible. This method allows a precise analysis of the impact of polyimide layer spinning process and enabled the opportunity to optimate the layer production method. More information about "Total profile" method is located in chapter "Polyimide layer production examinations ".

In summary, if planarity and settable reference points on substrate is achievable, "Cratering" should be replaced by "Total profile" method as default method for thickness determination of layers.

7.2 Observation of potential difference change due to diffusion

The following chapters contain the evaluations and discussions of PDMD examinations concerning Nafion and P84 membranes.

7.2.1 Nafion® membranes

7.2.1.1 Reproducibility determination

Figure 20 shows the arithmetic mean of the recorded potential difference change trend using 0.05 M KCl soaked Nafion NR-211 soaked membranes.
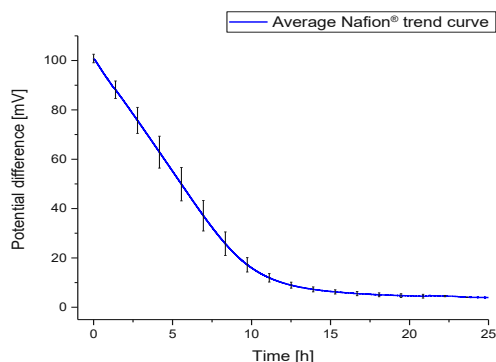

Figure 16: Average trend curve for Nafion reproducibility determination

Figure 21 shows, the expected curve for such membranes. First, a starting potential difference point over 59 mV was recorded. 59 mV was the Nernst voltage obtained by Nernst equation without any diffusion potentials, for this concentration gradient. More detailed information about Nernst equation and diffusion potentials are in chapter "Theoretical basics". By evaluating averaged trend curve, a starting potential of 100.44 mV +/- 1.6912 mV was measured. According to equations in chapter "Nernst potential and diffusion potential" the diffusion potential for using Nafion membranes with a concentration difference of 0.05 to 0.5 M aqueous KCl amounted to -41.287 mV, with consideration of the actual, algebraic signs choice. This increase of voltage had its source in correlation between the transported ions and the charge active sulfonated groups.

In free aqueous medium, that means transporting ions of a KCl solution without any diffusion barrier, K^+ and Cl^- showed nearly the same transport mobility, defined by transference numbers. Table 26 shows the values for transference numbers of KCl in free medium, obtained by literature [4] in comparison to the calculated ones for Nafion.

Table 25: Comparison between transference numbers (Nafion vs. free medium)

Ion	Transference number in Nafion (from measurement) []	Transference number in free medium (from literature [4]) []
K^+	0.849	0.495
Cl^-	0.151	0.505

Nafion led to a significant difference in transference numbers of both ions and consequently had an impact on electric mobility, which was verifiable by the diffusion potential. In Nafion nano channels electric mobility difference occurred by affinity to the acidic position of sulfonated groups. The sulfonacid end balanced between deprotonated and protonated state due to the water molecules, which were able to adduct a proton for creating hydronium due to autoproteolysis equilibrium.

During transport of a cation and the corresponding anionic charge in free aqueous medium, one charge moved forward. As soon as a distance between both charges was created, a potential occurred between both charges, which was directed in opposite direction of migration. That electronic field acted as inhibiting force for the moved charge. As a result, the distance of both charges was reduced again, so that both charges reached migration end without deprivation. [10]

Nafion nano channels showed a high impact on the mobility of the charges. A positively charged potassium ion and a negative charged sulfonated group showed a high attractive force to each other, similar to protons. The natural equilibrium of adduction and abduction still existed even for this resulted carbonic acid salt, as functional group could be hydrolysed due to existing active protons and hydroxides in the surrounding matrix. [17] However, the deprotonated form, the negative charged carboxylate anion is describable with identical, mesomeric structural states, which results in a high resonance energy. The negative charge is

distributed over the sulfur-oxygen complex in the resonance hybrid, which reduces the basicity of the carboxylate anion and so its reactivity. This makes protonation, which is the prerequisite for the back reaction of the dissociation, more difficult. [18] This effect is even stronger due to the electron-withdrawing groups on the α-carbon, the trifluoro substitution, which increases acidity. [18]

Consequently, positive charged potassium ion mobility could be increased due to negative charged sulfonated groups. But potassium ion would not bound irreversibly to one of the sulfonate oxygens due to the high electron resonance. [18] Like simple protons, potassium ions were also enhanced by this active sulfonated groups without generating stabile sulfonic acid salt molecules in the first place. Chloride was not influenced by this negative charged channel mantle and explained the difference in transference numbers and the high diffusion potential.

Used Nafion membrane was not soaked in pure, deionised water, but in potassium chloride solution. So, nano-channels were not fully equipped with azide protonated positions, they were exchanged with potassium ions during soaking process. Soaking was one of the reasons for generating this immense diffusion potential. A more precise examination is discussed in chapter "Soaking impact on diffusion observation".

The previous evaluation referred to the starting potential, obtained from the average potential difference trend curve for Nafion in figure 21. A few data points later a sloping trend was observable. In figure 21 high error bars are shown. Nevertheless, this deviation from averaging occurred due to the time-drifted measurement. Described in chapter "Assembly of the diffusion cell", the filling of the cell chambers with fluids was proceeded sequentially and after filling it took time closing, connecting with PDMD and starting recording, respectively ending and saving a previous one. According to the time axis of the average trend, already few minutes were sufficient to shift the entire curve on the abscission. Only using the average trend curve profile, it was not possible to make more statement about curve trends and what they were influenced by.

Approximately after ten hours, the curvature characteristics changed und flattened. An absolute reduction of less than 15 mV was recordable, and the concentration gradient was very low. Notwithstanding, it was observable, that still potential difference was decreasing, but a point, where a concentration equalisation was definable, was not possible. The reason for this, was that the used electrodes always generate a fluctuation and a baseline voltage of a few mV (in this thesis described as normal electrode voltage), even at experiment end. In the last seven hours of the reproducibility experiment the recorded potential difference was in range of this electrode influenced region. So, an "diffusion end" could only be determined, if two following points were confirmable.

- Reduction of recorded potential difference change was less than 0.1 mV per hour (with exception of membranes with high ionic resistance)

- Fluctuation (continuous, random increasing and decreasing of potential difference as a function of sequential made data points) within an hour was observable (with exception of membranes with high ionic resistance)

Further analysis, concerning more detailed explanation of trend and comparison with simulations, were proceeded by supervisor Dipl. Ing. Lars Varain. For this thesis there was no authorization for the presentation or comparative analysis of these simulations with the measured data, therefore this point was not further elaborated.

7.2.1.2 Osmotic impact: structural impact

The osmotic impact is evidenced by observing the deformations of the Nafion membranes. If the entire diffusion cell was an isolated, self-contained system, ionic diffusion and osmose would still exist. Nevertheless, amount of exchanged water would be decreased over time. The reason for this, was that the osmotic pressure would work against the inner chamber pressure of the higher concentrated solution until the back pressure was so high, osmotic water transport would be reduced to an infinitesimal value. Notwithstanding, the diffusion cell was no isolated, closed system in this way. Although it could be assumed that the cell was sealed in the first approximation, the chambers could be changed in their maximum volume due to the flexibility of the membrane. By transferring water into the higher concentrated solution chamber, to reduce chemical potential, hydrostatic pressure due to the increasing amount of water was compensated by deforming Nafion membrane into lower concentrated region, shown in figure 21.
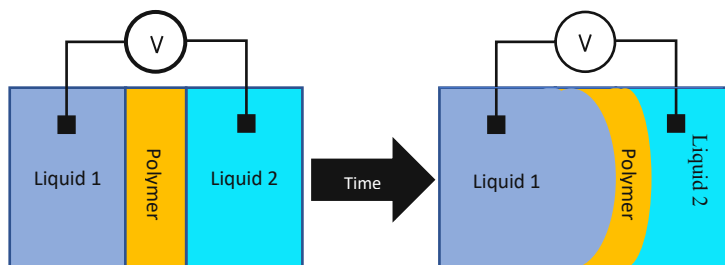

Figure 17: Scheme of osmotic deformation (Concentration of liquid 1 > concentration of liquid 2 in first state)

In figure 22 a scheme for osmotic influenced deformation of a polymer in the diffusion cell is shown. The concentrations of both liquids would equalise while diffusing, but the volume of Liquid 1 would increase. Additionally, this scheme shows reduction in layer thickness. This could be proven both theoretically and practically. On the one hand polymer membrane were fixed due contact pressure by the sealing ring. So, when osmose deformed membrane, no additional material could be delivered for increasing surface and layer thickness must be reduced. On the other hand, this was proved by proceeding LA-ICP-MS measurements when executing layer bombardment and measuring a too fast polymer breakthrough and silicon signals from the wafer, seen in chapter "Examination of ion penetrated samples" Also, this deformation is observable visually, shown in figure 22.

Figure 18: Photographic recording of osmotic deformed Nafion membrane

The osmotic influence was also observable in using polyimide membranes. Nevertheless, the effect was much lower, as polyimide provided less opportunities to transport water due to no existing nano channel. It was difficult to examine the osmotic deformation on polyimide layers, because the lateral extension, as well as the elasticity of this material, was so low, that, when isolating the membrane after executed diffusion measurement, the deformation re-formed to a large extent back to its origin form. The existence of osmotic deformation on polyimide membranes was only visible within the diffusion cell due to light dispersion. By generating a plug type formation, visible light is reflected is more different directions than on a planar surface, discernible by brighter, undirected light reflecting, zones within the diffusion region, shown in figure 23.
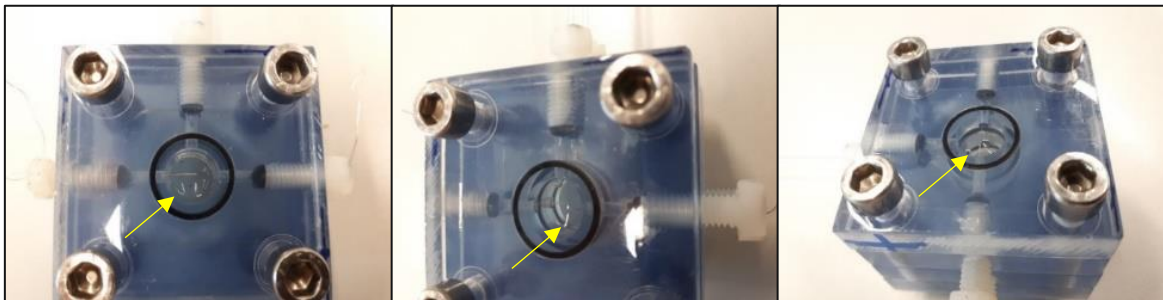

Figure 19: Photographic recordings for polyimide osmotic deformation (yellow arrows point to the undirected light reflexion on deformed polyimide surface within the diffusion region)

Beside of falsifying potential difference change measurements, such deformations complicate any surface related analyses, like using LA-ICP-MS, immensely, as needed planarity was not given. Consequently, eliminating, or at least reducing, the osmotic influence was an objective for this thesis.

7.2.1.3 Osmotic impact: method for reducing osmotic deformation

Figure 24 shows the comparison between the averaged trend of the reproducibility determination of using PET-network for reducing osmotic impact and the reproducibility determination without any cell modification.
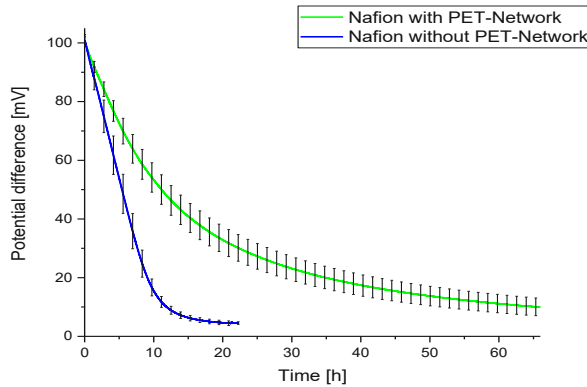

Figure 20: Comparison of averaged PDMD results with / without using osmotic barrier

For every sample, an own PET network was created to eliminate systematic statistical errors due to already deformed and stretched networks. Figure 25 shows a comparison between the average potential difference change trend using unmodified diffusion cell and with PET network. Both reproducibility analyses are executed using a concentration difference between 0.05 and 0.5 M KCl and Nafion membranes were prepared in 0.05 M KCl.

The consequence of using a PET network was an immense increasing in time required for diffusion. Instead of taking about 24 hours, diffusion took over 60 hours to reach background electrode voltage using the osmotic barrier. The reason for this was the reduction of provided interaction surface between ionic active membrane surface and liquid bulk, but also the reduction of exchanged water. The amount of exchanged water was measured by using conductivity determination device, short CMC, which was explained in more detail in chapter "Conductivity measurement cell (CMC)". Table 27 shows the amount of water exchanged with and without using an osmotic barrier.

Table 26: Comparison between exchanged water with / without using osmotic barrier

Parameter	Diffusion without using PET network	Diffusion with using PET network
Averaged amount of exchanged water [ml]	0.54	0.39
Samples for averaging []	7	4

Using PET network reduced the amount of exchanged water slightly, so improvement was given, but not satisfying to reduce osmotic impact on PDMD measurements significantly. Additionally, regarding table, the amount of averaged sample results was much lower than using unmodified diffusion cells. The reason for this was the increased leakiness probability of the cell. In an unmodified diffusion cell, polymer membranes acted as sample, but also as sealing. In a modified cell, the sealing was provided by contact pressure between membrane,

network and between network and sealing ring. As network was an in-house product, quality for essential sealing was much lower. The result was that three of seven executed sample measurement must not be evaluated, as they became leak, observable by a salt crystallization at the bonding sites of the polycarbonate plates. Secondly, the standard deviation between measured samples with using osmotic barrier was higher, regarding to all visible error bars. Indeed, between one- and 8-hours diffusion time, both potential difference observation trend showed error bars with nearly equal size, but instead of decreasing bar size, trend curve with using osmotic barrier showed a consistent error over time. The trends of these samples showed different anomalies, like drifts on the abscissa and on the ordinate, but also deviations in curvature.

So, using a mechanic osmotic barrier did not have a significant improving effect in PDMD analyses. Nevertheless, membranes were examined if this barrier had an impact on reducing deformation while diffusing. Figure 25 shows a photographic recording of an isolated Nafion sample after diffusion process with a PET network. (Rest of PET network is removed for better observation).
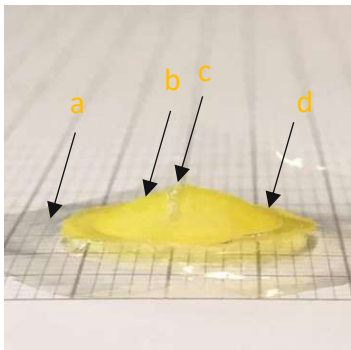

Figure 21: Nafion membrane with osmotic barrier PET network

Table 28 shows the description of the marked sections in figure.

Table 27: Description of marked section in figure 26

Mark	Description
a	Nafion membrane material
b	PET network (deformed by osmose)
c	Fissure site in PET network
d	Hardened PET network with closed lattice for sealing

Comparing Nafion membranes deformed by osmose with and without using a PET network, it turned out, that evagination was reduced due to the osmosis barrier. Nevertheless, osmotic force was so immense over time, that the polymer lattice was also deformed. Contrary to Nafion, PET had a reduced elasticity module, so after isolating the membrane from the cell, PET did not form back into origin shape. Additionally, due to existence of weak points in the lattice area, osmotic pressure was even able to tear the network apart, seen in section "c". Over time, Nafion was pressed trough this fissure site, changing the interaction surface and profile of the layer. Another disadvantage was, that although glue for sealing around diffusion zone, was hardened out completely, the Van der Waals force between polymeric glue and Nafion in combination with consequent high contact pressure was so strong, that it was nearly

impossible to remove the layer from the network without structurally harming it. Consequently, using a network acting as an osmotic barrier reduced deformation, but the disadvantages using such materials prevailed.

7.2.1.4 Examination of soaking impact on potential difference change observations

Another reproducibility determination was executed with pure water soaked Nafion membranes. The reason for this was to observe the effect of offering a Nafion membrane transport matrix with fully protonated sulfonated groups and with potassium contaminated and occupied places. The following figure 26, shows the comparison between the potential difference observation of the reproducibility determination and the trend, obtained by using water-soaked membranes. The curve was averaged after measuring five samples.
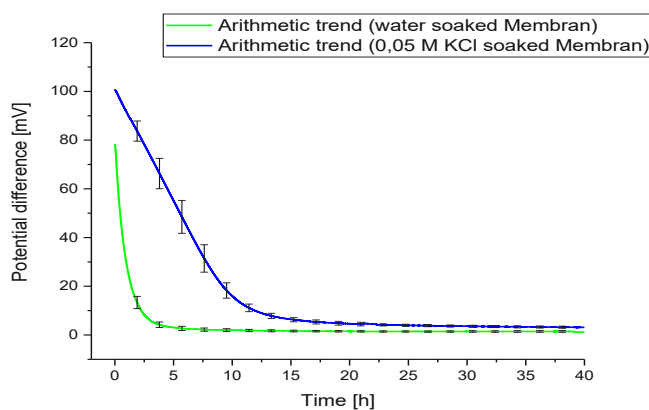

Figure 22: Arithmetic trend of potential difference change using water / 0.05 M KCl soaked membranes

Evaluating figure 26, following results are observable using water-soaked membranes:

- Reduced standard deviation, averaged over entire trend curve
- Less time needed to reach concentration equilibrium
- Reduced starting potential difference

First, a reduced standard deviation of recorded potential difference change was observable. This was because, soaking in 0.05 M KCl and consequently, exchanging protons for potassium ions, was not reproducible. The success of homogeneous ionic input during soaking execution suffered from various parameters. On the one hand, ionic diffusion in the soaking cell was, comparing to the assembly of the diffusion cell, without any strong propulsion. Indeed, ionic exchange operated on every side and edge equally, as Nafion membrane was fully surrounded by solution, but exchange rate was decreasing exponentially with increasing layer penetration. So, after soaking the potassium concentration would be higher on the outer side than in the bulk of the membrane. Additionally, soaking medium was not an infinite proposition of ions. During exchanging, the provided ionic source decreased itself over time, also reducing exchanging rate.

Furthermore, time for reaching concentration equilibrium was reduced significantly using water soaked Nafion membranes. In contrast to KCl soaked membranes, less than 5 hours were needed, instead of 24 hours. Potential difference was not only reduced by transferred ions due to diffusion, but also by ionic loss to the sulfonated groups of the membrane.

Consequently, if this mechanism had this effect, both chambers should show two nearly equal concentrations at the end of the diffusion both this concentration should be lower than the concentration of the diffusion chambers using KCl soaked membrane. After every diffusion conductivity of both solutions were measured and using calibration KCl concentration was calculated. Table 29 shows the results.

Table 28: Comparison of calculated solution concentration using water and KCl soaked membrane

Preparation of Nafion membrane	Water soaked		0.05 M KCl soaked	
Concentration of used solutions before diffusion experiment [M]	0. 500	0.050	0.500	0.050
Averaged measured concentration of used solutions after diffusion experiment [M]	0.302 +/- 0.006	0.307 +/- 0.014	0.227 +/- 0.023	0.224 +/- 0.017

On the basis of fundamental calculation operations, the equalisation concentrations of both chambers should be 0.275 M KCl. Using 0.05 M KCl soaked membrane averaged concentrations were measured slightly under the expected value. This could be explained by input of ions into the layer, not only induced by stabilisation to a carbonic acid salt, but also by simple steric stabilisation as potassium chloride. The difference of 0.003 M was in the ratio of standard deviation. Nevertheless, a higher value in the higher concentrated solution after diffusion was comprehensible, as the propulsion by chemical potential difference was so low, that a complete equilibration would take several hours. Notwithstanding, comparing results of water-soaked membrane, unexpected values were observable. The concentrations of both solutions were even higher than the expected one of an ideal ionic transfer. The reason for this anomaly was not a higher salt concentration in the chamber fluids, but a limitation error in measuring concentration via CMC.

CMC was measuring conductivity in unspecific. The value of measured conductivity was directly dependent on the electric chemical mobility of ions in the sample solution. Using water soaked Nafion membranes, protons of the sulfonated groups were exchanged with potassium ions. These highly mobile hydrogen ions were removed from the solid membrane into both fluid media. After diffusion, when solutions were extracted to measure conductivity, both liquids showed different KCl concentrations, but a higher number of free protons. A final prove for this statement would be a pH-value determination of both solutions. Nevertheless, it was not possible due to the low volumes of the diffusion cell chambers for this determination.

Subsequently, measuring concentration via conductivity was impossible using water soaked Nafion membranes, excluding elemental specific, follow-up measuring methods, for example using high performance liquid chromatography with ionic exchange stationary phases.

The arithmetic trend of potential difference change using water soaked Nafion showed a reduced starting potential difference, comparing to 0.05 M KCl soaked one. Referring to equations, containing the calculation of diffusion potential and the transference numbers, table 30 shows the measured and averaged starting potential differences and the calculated transference numbers of different soaked membranes.

Table 29: Transference numbers, obtained by measuring different soaked Nafion membranes

Preparation of Nafion membrane	Water soaked	0.05 M KCl soaked	Free, aqueous medium (literature values) [4]
Starting potential difference [mV]	78.431 +/- 1.0902	100.44 +/- 1.6912	59.153
Transference number for K^+	0.661	0.849	0.495
Transference number for Cl^-	0.339	0.151	0.505

According to table, the difference in ion specific transference numbers is influenced by the transferring medium. Comparing to the numbers of 0.05 M KCl soaked membranes, the difference was reduced using water soaked Nafion membranes. On the base of theoretical interpretation of transference numbers, this would mean, that the completely protonated sulfonated groups had less impact on transferred ions than using mostly potassium occupied acid groups.

Considering a KCl soaked membrane, protons were exchanged with potassium. So, there would be no change in charge equilibrium. A simple positively charged proton was removed from the sulfonated groups into the soaking medium, increasing pH-value and stabilising negative charges, while simple positive potassium ion was stabilising deprotonated groups. Nevertheless, the size of potassium, as atomic but also as ionic radius, was much higher than of a simple hydrogen. Every "copolymer arm" consisted of a lipophilic, flexible ether Teflon® modification and a sulfonic acid termination. If a potassium occupied the position of the acidic hydrogen, the steric status changed significantly. The electrostatic repulsion was higher now, as the potassium occupied positions takes more space than the hydrogen. Due to the flexibility of the ether links, the copolymer arms had the opportunity to take the steric most simple location and change their original position. This change did not lead to a macroscopic obstacle, as water and transported ions were small enough to still pas those channels, but it had an effect on the charge transport mechanism.

For impacts of the soaking, another transport mechanism must be explained: The Grotthuss mechanism. [16]
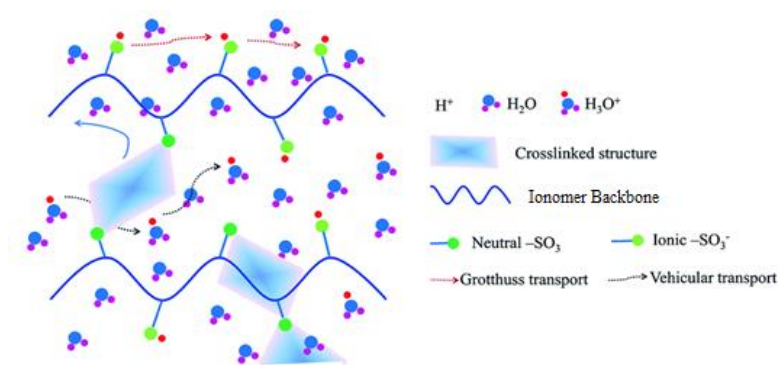

Figure 23: Representation of the transport mechanism in Nafion membrane [16]

49

Figure 27 shows the schematic representation of proton transport mechanism in Nafion, in detail in an exemplary ionomer. [16] Visualised with a black arrow, the known vehicular transport is seen. Hydrogen ion is deprotonated and adducts on a water molecule, hydronium is formed. The hydronium acts as transport molecule and releases the proton when another free position is encountered. That is the fundamental transport mechanism for using Nafion as proton exchange membranes. It can be summarised as a chain like, short distance handing over of protons. Beside of this, another transport mechanism is described, named Grotthuss mechanism. Instead of moving ion via aqueous medium, covalent bonds between hydrogen and oxygen of sulfonic acid is broken and created on the next oxygen location. This transport is possible by providing close located acid groups with weak bonded H atoms. [3] A precise determination of share distribution of absolute membrane conductivity between vehicular and Grotthuss transport is not possible, nevertheless in such materials Grotthuss is the dominating mechanism. [7] [41]

Consequently, proton transfer between close located sulfonated groups is an important mechanism for ionic transfer. In 0.05 M KCl prepared membrane potentials difference change trend was significant slower than prepared with water. By exchanging protons with more steric potassium, Grotthuss mechanism was reduced significantly, as now sulfonated arms had more distance to each other due to electrostatic repulsion, as well as showed no opportunity to act as anchors for incoming protons. That also explained the higher standard deviation of measured 0.05 KCl soaked membrane trends, as input and penetration of potassium was different intense and so the reduction of possible Grotthuss transport opportunities. This effect could explain the measured higher starting potential difference. Proton depositions, hydronium generation was much more chaotic and steric hindered in salt solution soaked medium and this could cause in a different measured transference number. Furthermore, the higher transference number difference using 0.05 M KCl soaking medium could also be explained on macromolecular base. It was possible, that potassium ions could also be transported like protons using Grotthuss mechanism. Indeed, atomic diameter of potassium ion is much higher than of proton and they do not even show approximately the same electro mobility, however it would be possible that entire current could be transported more by potassium using salt solution soaked membranes, as already potassium particles are within the Nafion bulk. If concentration dependent diffusion begins, potassium and chloride ions penetrate the bulk. However, potassium dependent conductivity is higher as already stored and bounded potassium to sulfonated groups can leave the membrane to the other, lower concentrated chamber side. But, to keep charge equalisation, chloride must generate a much higher inhibiting back-force. So, transference number difference increases significantly, promoting potassium movement. But this is only an assumption, as no literature was found during execution, which could proof this for this instrumental setup.

Already mentioned, after potential difference change measurement, the remaining solutions of each chamber were extracted and used for conductivity examination, which could also be used for determining exchanged water between the chambers. Table 31 shows a comparison between the amount of measured chamber liquids of different soaked membranes.

Table 30: Comparison of amount of exchanged liquid using water / 0.05 M KCl soaked membrane

Preparation of Nafion membrane	Water soaked	0.05 M KCl soaked
Average exchanged amount of liquid [ml]	0.06 +/- 0.04	0.54 +/- 0.06
Consequences for membrane shape due to ascending osmotic pressure	Marginal / no deformation visible	Heavy deformation visible

According to table 31, soaking had an immense impact on the efficacy of ascending osmose. Using a water-soaked membrane, amount of exchanged was reduced over 89%. As a result, no deformation or at most a slight one was observable. Evaluation of this was problematic, as neither electrochemical, nor elemental analytic offered the opportunity to examine directly this different osmotic influence. Nevertheless, for this thesis, following assertion was made: Osmotic pressure is calculated according to equation (16).

$$\Pi = i * c * R * T \tag{16}$$

In equation (16) i is a factor, which respects the dissociation of salt molecules in water. For this thesis only KCl is used, so it dissociates into two ions, the factor i = 2. As temperature T is kept constant during diffusion, only the time dependent concentration of both solutions in the diffusion chambers controls the osmotic pressure. According to the recorded potential difference change trends of both soaking, 0.05 M KCl soaked membrane took more time for completing diffusion. That means, concentration difference was reduced more slowly than using a water-soaked membrane and impact of osmotic pressure was higher over time. The osmotic impact averaged over diffusion time was higher, so the force for transferring water and the force for deformation the membrane too.

To achieve a more precise examination of this, multiple Nafion membranes had to be analysed with different soaking times. Notwithstanding, due to limited time and Nafion material resources, further examination concerning soaking medium impact were not able to establish. Without any reproducibility determination, a comparison between normally soaked membranes and a Nafion sample with another soaking time was still made. While Nafion samples were soaked in normal conditions for 24 hours, this sample was soaked for two months. The figure 28 shows this comparison.
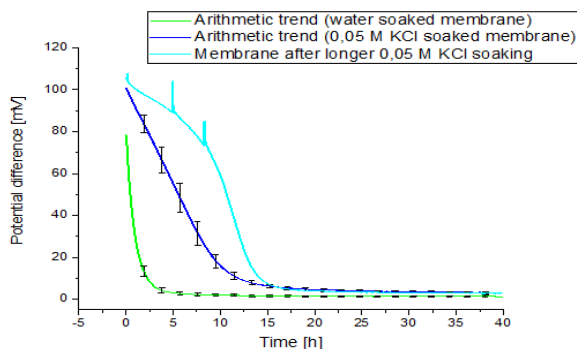

Figure 24: Comparison of potential difference change between membranes with different soaking times

In figure 29 three trends are shown. The start potential difference change observation using water and 0.05 M KCl soaked membranes, but also using a Nafion membrane, soaked in 0.05 M KCl for two months, instead over 24 hours, was nearly the same. Referring the soaking mechanism, it could be claimed, that a higher number of protons was exchanged for potassium of this membrane. This resulted in a deformed trend curve with a different curvature behaviour. The two potential difference "jumps" were common voltage measuring errors during observation. Further results are listed in table 32.

Table 31: Results after diffusion examination of long soaked membrane

Consequence for membrane shape due to ascending osmotic pressure	Heavy deformation visible
Measured concentration in chamber with "low" concentrated liquid after diffusion [M]	0.207
Measured concentration in chamber with "high" concentrated solution after diffusion [M]	0.221
Amount of exchanged water [ml]	0.56

These results showed that number of not-exchanged protons in Nafion membrane bulk had an impact on the measured chamber concentration via conductivity, on the amount of exchanged water via osmosis and on the resulting potential difference trend. Furthermore, bulk containing water amount had an influence on ionic interaction and transport referring Grotthuss and vehicular mechanism [16]:

> "*When a hydrogen atom separates from the sulfonic acid group, the group will carry a negative charge. Because of the negative charge, the hydrated ion with the positive charge is more attracted to the sulfonate group when compared to the free water molecule. As a result, the hydrogen atom in the hydrated ion forms a weak bond with the oxygen atom in the sulfonate group. Therefore, the hydrated ion is closer to the sulfonic acid group than the free water molecule. [...] when the water content in Nafion 117 is low, H_3O^+ is the main transfer ion among the different hydrated ions. However, at higher water content, the hydrated ion in the form of $H^+(H_2O)_2$ is the main transfer ion.*"[7]

Consequently, these results showed that the preparation with ionic solution, if medium led to proton exchange was not a possible option for analytical issues if a further surface examination was required. Additionally, to combine this examination with theoretical base of Grotthuss and vehicular transport, ionic and water transport could not be simply divided into carrier and jumping mechanism. Due to the hydrogen bridge binding opportunity and hydration cell cages of cations and anions in aqueous media several intermediates of covalent and bridge were formable. As a result, to determine the real influence of soaking on Nafion membranes, a new examination must be established, consisting of an adequate, reproducible soaking system.

---

[7] [16] Hong Sun, Mingfu Yu, Zhijie Li, and Saif Almheiri: "A Molecular Dynamic Simulation of Hydrated Proton Transfer in Perfluorosulfonate Ionomer Membranes (Nafion 117)"

7.2.1.1 Examination of Nafion N-117 membranes

For reproducibility determination, four samples were cut out into layer shape, soaked in 0.05 M KCl for 24 h and diffused with a concentration difference like reproducibility determination of NR-211, which is shown in figure 29.
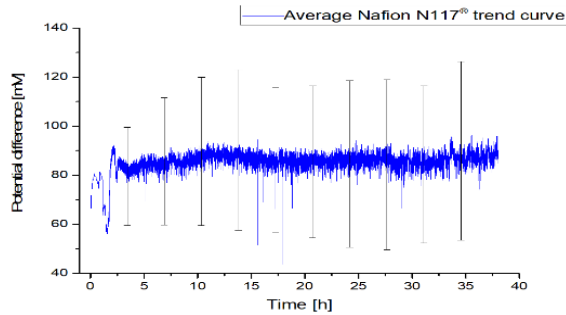

Figure 25: Reproducibility determination using N-117 Nafion membranes, averaged over four samples

If the potential difference trend using NR-211 and N-117 were compared, several differences were observable. The average trend of N-117 showed no expected potential difference reduction over time. In averaged representation the starting potential difference was over 59mV, but lower than NR-211. An explanation about this could not be given on the base of nano channel depending ionic movement, as fundamental material information about both Nafion types were not obtainable. In dependence of increasing time, the trend showed no expected behaviour, was increasing and decreasing without any expected curvature. The error bars showed that the individual trends of the samples were highly different from each other. This high deviation was the consequence from the summation of various parameters, but which were all based on the high thickness of the samples, referring different osmotic deformation, soaking quality, and other variables. Furthermore, after about two hours diffusion process, resulting trend started fluctuating heavily. Neither it could be explained why this fluctuation occurred, nor why the fluctuation only occurred after one to two hours. The following figure 30 showed the individual N-117 trends for comparing reasons and figure 31 shows a magnification of time referring the first hours, to identify the starting fluctuation.
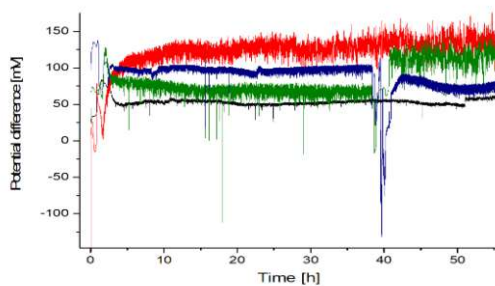

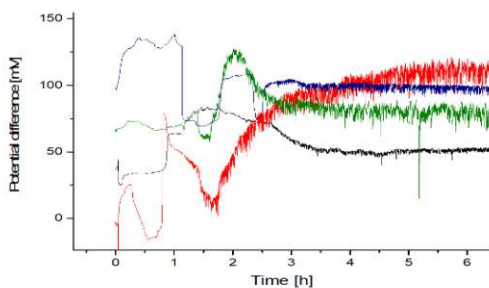*Figure 26: Individual trend curves of N-117 membranes*

Figure 27: Individual trend curves of N-117 membrane for the first hours

Approximately after 1.2 to 1.5 hours the fluctuation start was observed. Also, it was discernible, that fluctuation was getting stronger with increasing time, up to a maximum of three to four hours. This fluctuation was different intensive, depending on the sample. While N-117 samples, presented as blue and black line, had a fluctuation size of about 5 mV, intensity of other samples pf the same material, marked in red and green, was about 20 to 25 mV. Nevertheless, already the lower deviation was high enough to make N-117 membranes impossible for achieving reproducibility. Additionally, no sample reached normal electrode voltage, consequently it was also not possible to define, when concentration equalisation would be reached. To summon up, reproducibility determination of N-117 membranes turned out to be a failure, however it could be claimed that there was a limitation to the thickness of the used membranes.

7.2.1.2 Proton exchange between Nafion and soaking medium

Table 33 shows the evaluation of pH- value examination of Nafion membranes.

Table 32: Results of pH-value examination

Soaking medium	Number sequence of soaking medium []	Amount of soaked 3x3 cm Nafion NR-211 layers []	pH-value []	Soaking time [h]
0.05 M KCl (Reference)	0	0	5.65	0
0.05 M KCl #1	1	8	4.66	24
0.05 M KCl #1	2	8	4.78	24
0.05 M KCl #1	3	8	4.85	24
0.05 M KCl #2	1	4	4.81	24
0.05 M KCl #2	2	4	5.07	24
0.05 M KCl #2	3	4	5.12	24
0.05 M KCl #3	1	4	4.78	72

The column "Number sequence of soaking medium" describes, if the soaking process was divided into multiple, isolated steps, realised by different soaking chambers. The reason for this, was to examine the impact of providing uncontaminated soaking liquid after proceeded proton exchange. By bringing already soaked membranes in contact with new salt solution, the surrounded chemical potential for potassium was higher, so that the proton exchange ran faster. The column "Amount of soaked ~3x3 cm Nafion membranes" described the amount of used individual membrane pieces. Membranes were not soaked individually, as proton

exchange would be too low to detect via pH-value. Secondly, "~3x3 cm" is the approximated size of cut Nafion membranes from the sheet. Actually, membranes neither showed exact quadratic shape, nor showed exact 3 x 3 cm size, as they were cut out using a simple scissor. It was assumed, that Nafion layer had the same size as polyimide layers, which were produced on a 3x3 cm silicon wafer.

According to table 33, pH value was decreasing by bringing soaking medium in contact with Nafion membranes. Referring to first, three step soaking procedure, the pH-value was lowest, with 4.66, as membranes were soaked the first time. When changing soaking medium with a new one, number sequence from 1 to 2, the measured pH-value was not so low, as already protons were exchanged from the membrane with the former solution. The same was realisable concerning number sequence 3. This experiment was also executed using only four instead of eight membranes. As expected, the results showed, that pH-value was higher than using more Nafion membranes, as less absolute proton exchange area was brought in contact with aqueous potassium chloride. Also, four Nafion membranes were exposed three times longer in one solution, marked as "0.05 M KCl #3", without switching the liquid. Indeed, pH-value was lower with 4.78, but it would be much more efficient to switch solutions to achieve better soaking efficiency.

Consequently, to achieve best and most reproducible soaking efficiency with ionic liquids, a low number of membranes should be added into large as possible soaking flask. Temperature increase should be avoided, as this do not match with diffusion conditions, which can have an influence on channel size when membrane bulk adapts to cell temperature. Furthermore, additional mixing by magnetic stirring would improve homogeneity. At last, multiple change of soaking medium with fresh solution will improve consistence of soaking rate.

7.2.2 P84® membranes

7.2.2.1 "Jump " examination

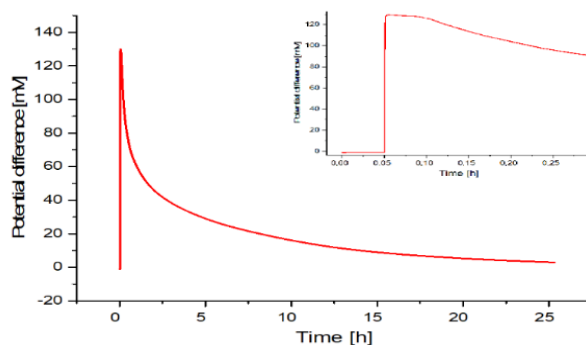Figure 32 shows the trend of sample "1A", a polyimide membrane for "Jump" examination.

Figure 28: "Jump" experiment on sample "1A", entire potential difference change trend and included zoom presentation

As expected, measured start voltage lied in range of normal electrode voltage, fluctuating between -/+ 800µV, shown in zoom presentation as parallel trend to the abscissa, as no concentration gradient was given After putting through the other concentrated solution, the

"Jump" phase was visible, observable as an intensive increase in potential difference. After closing diffusion cell system by clamps and generation of hydrostatic equilibrium, the impact of diffusion was recorded. To achieve reproducibility, this experiment was proceeded several times. Nevertheless, three of them were not evaluable, as immense measuring errors corrupted the results. The figure 33 show the potential difference trends and the zoomed in one.
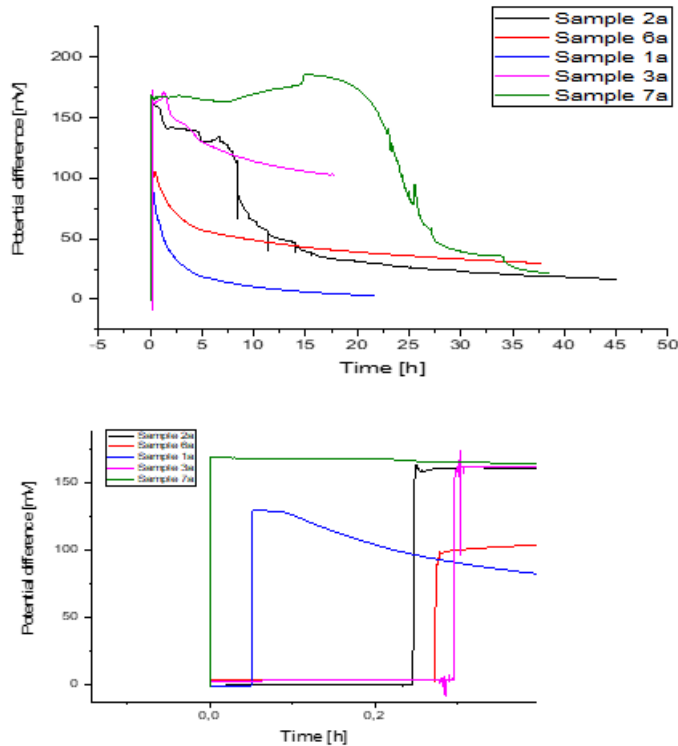

Figure 29: Potential difference change observation for five samples using "Jump" cell modification

First, it must be mentioned, that these experiments were executed, using a chamber concentration difference between 0.01 and 3 M KCl. These concentrations were proposed by the supervisor, as this should provide a high starting potential, as well as high diffusive interaction. According to equations for Nernst voltage and diffusion potential, the resulting measured voltage should be about 146 mV. Comparing the individual trend curves, the "Jump" phases were initiated after different times, but within ten minutes. Every, evaluable sample showed the same starting trend. This fact confirmed the concentration depending function of the electrodes in cooperation with the entire PDMD. Nevertheless, reproducibility was not achievable using this cell modification. The starting potential differences showed different values between 100 and 160 mV.

The reason for these immense differences could be concentration matching problems. As diffusion chamber must be filled with another concentrated solution completely and ideally, errors could occur like dead bands in the cell chamber, which would hinder a complete exchange. Furthermore, anomalies in recorded trend were observable, for example changing

in curvature behaviour, sudden voltage increases during diffusion process, or beginning parallelisation to the abscissa, although normal electrode voltage was not reached.

7.2.2.2 Reproducibility examination

Table 34 shows the parameter for spinning and potential difference observation, as well as a used sample description. It must be mentioned that for reproducibility determination 107 P84 samples were produced. From this, only about 40% were useable for PDMD measurements and from this, only about 20% to 30% brought useable results. Additionally, samples, which were produced with unoptimised production method were not used for evaluation, as they did not bring relevant information for solving reproducibility issue. Consequently, only a certain amount of polyimide samples, which fulfilled production criteria, could be fully prepared and diffusion could be observed completely. In table 34 parameters of optimised and used spinning process method and parameters of used potential difference change observation method is shown.

Table 33: Spinning and diffusion observation parameters for polyimide reproducibility determination

| Spinning parameters		
Number of different spinning modes []		2
Pre-spinning phase	Spinning time [sec]	240
	Rotation number [rpm]	200
Fast-spinning phase	Spinning time [sec]	10
	Rotation number [rpm]	2000
Resting-phase [sec]		120
Volume of superimposed sample solution [ml]		0.8
Number of different heating modes []		2
Solidification phase	Temperature [°C]	90
	Heating time [min]	15
Hardening phase	Temperature [°C]	180
	Heating time [h]	15
PDMD parameters		
Used samples for evaluative presentation []		7
Type of membrane		P84®
Soaking medium		Deionised water
Soaking medium concentration [M]		-
Soaking medium volume [ml]		250
Salt solution for diffusion chambers		$KCl_{aqu.}$ solution
Concentration difference for diffusion [M]		0.05 : 0.5
Additional cell modifications		none
Recording frequency [sec/data point]		10
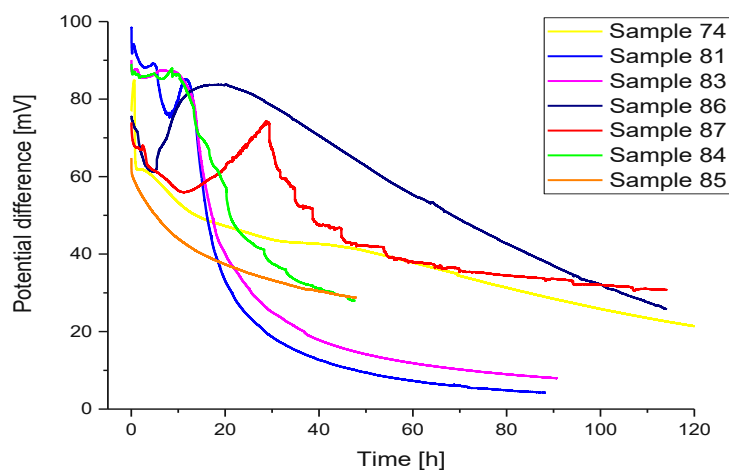
Figure 30: Potential difference trends of P84 reproducibility determination

In figure 34 potential difference trends of P84 samples are observable. The production process of every sample was the same, as well as the diffusion conditions. Nevertheless, resulting trend curves showed different monotonies and curvature behaviours. Sample "81" and "83" showed an expected trend, beginning at a starting potential over 59 mV with a following decreasing curve, ending close to the normal electrode voltage. However, even these trends showed anomalies. First, the starting potential differences lied approximately at 90 mV. This would mean that using polyimide membranes a high diffusion potential would be generated. Nevertheless, comparing to Nafion membranes, polyimide showed no active ionic substituted, which could enhance individually or simply change equal ionic electric mobility. Cations and Anions should move through the layer, more slowly comparing to a free, aqueous liquid, but not with such different motilities. On the other hand, in sample "81" a local minimum was observable between 5 and 15 hours. This time interval was too ample, to reduce this anomaly to a measure error. Probably this error was ascribable to the static solution status. The chamber liquids were only internal mixed by chemical potential equalisations, not by mechanical mixing. So, this local minimum could be a local concentration reduction in the higher concentrated chamber close to the electrode.

Furthermore, it was observable that sample "83" started at 20 hours setting apart of sample "81", so that at measure abort, at 90 hours, sample "83" did not reach the area of normal electrode voltage, which was the potential difference, measured without any concentration gradient. Approximately, about 15 to 25 hours would be needed to reach the same potential difference. This trend was explainable by layer thicknesses. While sample "81" showed an average thickness of 9.242 µm in the diffusion region, sample "83" had a thickness of 9.512 µm. Ions needed more time to pass layer area of sample "83".

Another anomaly was seen comparing sample "86" and "87". Both trends started at 75 mV approximately decreasing along the ordinate. Nevertheless, at different times, sample "86" after 5 hours and sample "87" after 10 hours change his behaviour and an increasing potential difference was shown. Thereby, the potential difference of both trends reached a value over the starting potential, then a local maximum and continued with a decreasing trend without reaching the normal electrode voltage. This anomaly was difficult to explain, but at least an

58

approximate interpretation was possible. A recorded increase of potential difference was on the one hand influenced by different measured concentrations, on the other hand by actual electric base. If an electrostatic voltage would be built up, PDMD would be influenced by this. On chemical base, this potential difference increase could be occurred by eventual ionic surplus concentration. Disadvantageously, the used diffusion cell showed no opportunity to add an internal system to mix the chamber liquids. Every convection was based on diffusive movements. If an ion penetrated the layer, it would enter the lower concentrated region. However, already mentioned in chapter "Polyimide layer production examinations", the interaction surface, provided by the layer "diffusion region", was not planar. Consequently, it was possible, that induced by inhomogeneous invaginations and evagination regions of different sizes on the layer surface and in the bulk ions could lead to temporal surplus concentration zones, which would not have an significant effect, if the opportunity of rotation in the chamber was given. On the side of the electric and electronic base, it was difficult to create assumptions and hypothesis about the influences of external voltage sources, as neither the operator of this thesis had the required electrochemical education, nor there were recordings of assembling the PDMD.

Sample "85" and "87" were examples for trends with unexpected potential difference changes during the last hours. On the one hand, those curves started flatting, along the abscissa, but on the other hand, without reaching the normal electrode voltage. The reason for this anomaly was also difficult to identify. On the chemical base, this would mean, that with continued diffusion process the transport mechanism rate was decreasing while both chambers contained liquids with different concentrations. So, a physicochemical process must happen to decrease the number of transported ions over time. The first assumption based on an influence by the layer. It was improbable, that ion transport was hindered by increasing amount of input salt particles during diffusion, as polyimide layer did not show high abilities to storage these. Furthermore, Nafion membranes highly incorporated potassium and chloride ions, without showing such an anomaly. Another theory would be a unique layer profile which could cause this. Nevertheless, profilometer results showed no significant change in layer surface form, concerning diffusion region. On the electrostatic base, this trend was only explainable, if diffusion kept on transporting ions, but during this process a potential was built up, which was increasing while concentrations were still equalising. However, the probability of this effect occurring was low, as it would happen more often, if the problem origin was the PDMD itself or an external source. To summon up, this anomaly was difficult or even not possible to explain with direct influences.

Another hypothesis is, that diffusion was not complete. This anormal trend was only a step in the entire diffusion process, but recording was aborted too early. Referring the time axe of the trends, it was obvious, that these examinations took exceedingly much time. This fact in combination of the low number of simultaneously running measure places, namely two, led to the problem, that every measurement was time limited. However, it was tried to observe at last one sample over a long diffusion time. Figure 36 shows the potential difference recording of sample "96", a polyimide layer sample, which was inserted into the diffusion cell for over two months. The concentration differences were 0.05 to 0.5 M potassium chloride solution.
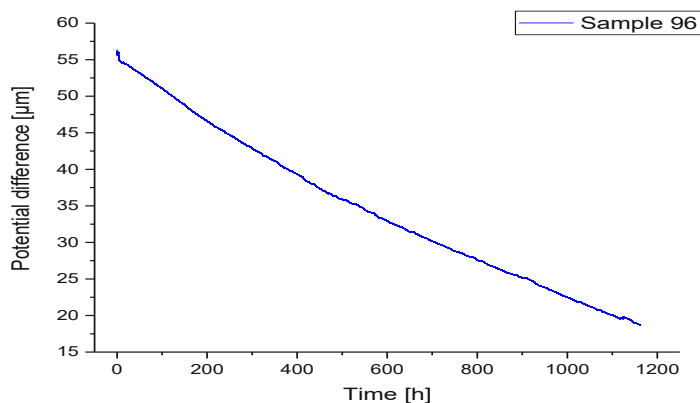
Figure 31: Potential difference observation of sample "96"; long time diffusion recording

Shown in figure 35, it was obvious, that diffusion was not complete, even after 1200 hours diffusing. This was also confirmed by the results of conductivity determination, seen in table 35.

Table 34: Results of conductivity examination of sample "96"

Initial chamber concentration [M]	Measured conductivity after diffusion [$\mu S/cm^2$]	Calculated concentration after diffusion [M]	Measured chamber volume [ml]
0.05	6110	0,1255	0,85
0.50	12870	0,2825	0,8

According to table 35, in comparison with figure 36, the diffusion was not complete even after this long-time interval. Taking the trend into account, it could be assumed that if the curvature behaviour had continued, diffusion would have taken many more weeks to reach the expected course approximating the abscissa. Furthermore, the measured starting potential, 56.4 mV, was beneath the expected 59 mV, which could be due to lower concentration difference of the sample solutions. Indeed, this is possible, as this difference would be caused by less than 0.003 M deviated concentration. In combination with the extreme low chamber solutions, such deviations were possible. Nevertheless, it must be mentioned, that diffusion potential must not increase measured potential difference from Nernst voltage. It would only had an increasing influence, if, according to the equations, cation had a higher transference number as the anion. But if chloride would be faster than the cation, diffusion potential would change the algebraic sign of diffusion potential and would change measured potential into the other direction. According to literature data, in free aqueous system chloride would have slightly a higher transference number [13]. This would be reflected in polyimide matrix, as this bulk had no charge active substituents. No significant influence by diffusion potential was seen, which was expected by using polyimide membranes. Nevertheless, more samples were not analysed, as experimental and instrumental conditions were not provided.

Comparing sample "96" with other samples, like "81" or "83", diffusion times differed from each other significantly. DekTak layer profiles of these samples were compared, shown in figure 36.
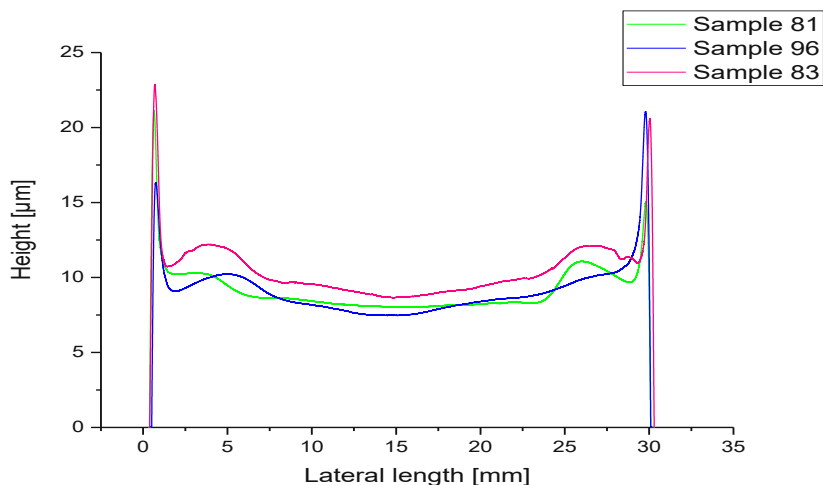
Figure 32: Comparison of layer profiles of samples "81", "83", and "96"

Layer thickness of sample "83" was slightly higher than sample "81". This corresponded with the potential difference observations, as sample "83" diffusion needed more time to reach approximate concentration equalisation. Nevertheless, comparing with DekTak result of sample "96", no significant difference was observable. Neither a distinction in thickness, nor an existing local anomaly or deformation on the surface. Total-profile analysis did not support identifying the reason for these different diffusion times. It could be assumed, that neither layer thickness, nor any structural, local deformations on the layer surface led to this high time difference during diffusion. Furthermore, assembly of the diffusion cell and diffusion parameter, like concentration difference were also the same. Another possibility, which could cause this difference, but also deviations in potential difference trends of various polyimide samples, was based on the polyimide material itself.

Polyimide layer samples had to be heated out after spinning process. So, an indefinite volume of air humidity could react with the layer surface. Subsequently, it was possible, that the slightest accumulation of water on the still liquid surface would lead to local, preterm or to local, temporally varying polymer precipitation. These in turn could lead to macroscopic inversions on the surface or even to ruptures or channel-like cracks in the material. Furthermore, as sample layer were heated out on a heating plate, the heating source lied beneath the wafer. So, solidification occurred first in the lower part of the complete layer in relation to the effectiveness of the thermal effect. Furthermore, it was also possible that the solidification in the upper area is favoured by the fact that organic solvent molecules are more easily released into the gas phase. These effects led to the high possibility of inhomogeneous hardening, which also could cause the generation of bulk defects. Using DekTak profilometry, several statements about the impact of the surface formation on diffusion observation but measuring the bulk structure was not possible. For this thesis, no additional instrumentation was available to determine the impact of inhomogeneous solidification.

7.2.2.1 P84® reproducibility optimisation: PET network

Using Nafion membranes, reproducibility examination was also executed using an osmotic barrier PET network. This network had an interpretable impact on diffusion, so it was tried to use such networks with polyimide membranes. The diffusion parameters were the same as in

reproducibility determination of P84 layers, only a PET network was added, which assembling is explained also in chapter "Osmotic impact: method for reducing osmotic deformation". In figure 37 the diffusion observation using PDMD is shown for seven samples.
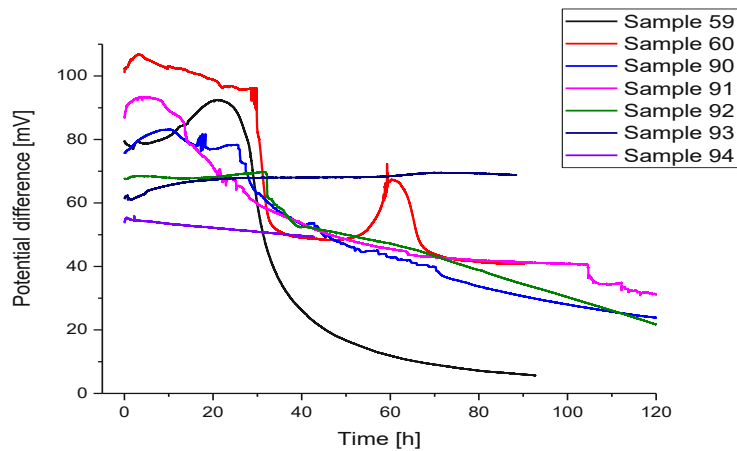

Figure 33: Potential difference observation reproducibility examination of polyimide samples using PET network

Comparing reproducibility determination of polyimide samples with and without using a PET network, several conformities were visible, shown in figure 38.
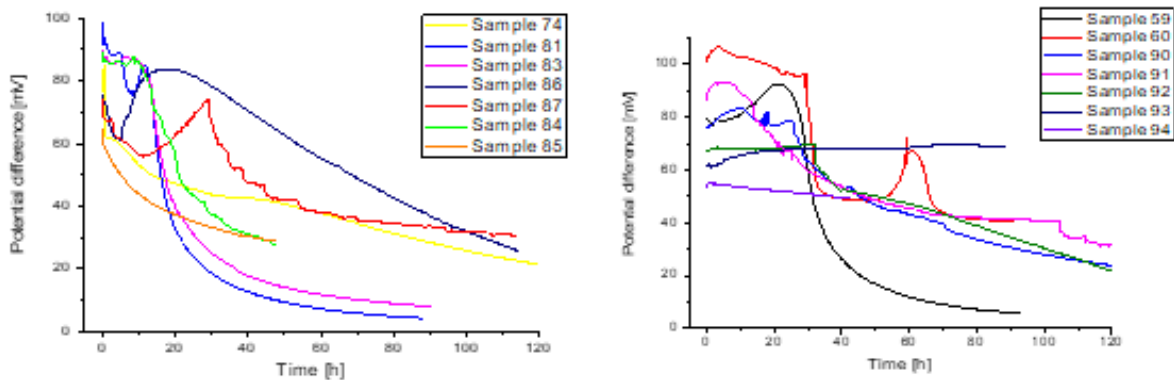

Figure 34: Comparison of reproducibility determination for polyimide membranes with and without using PET membrane

First, despite diffusion experiment parameters were kept constant, recordings showed different starting potentials. Furthermore, already mentioned and identified anomalies were visible, like suddenly appearing potential difference increases, showed in sample "60". Samples showed various trend behaviours with different expected, approximated concentration equalisations. While conductivity examination showed that concentrations of sample "59" were nearly matching, diffusion trend recording sample "93" showed no significant decreasing behaviour. In comparison with reproducibility determination without using PET network, it could be assumed, that by reducing ionic exchange cross section due to the mesh size in combination with the increased transport path due to the penetration thickness of the network, diffusion would take more time to reach concentration equalisation. Nevertheless, no significant, coherent increasement in diffusion time was observable comparing both figures. Consequently, this could substantiate the assertion, that the fastest reached concentration equalisation, in figure 38 sample "59" and sample "81" and "83", were

accelerated by leakiness in the layer. Such leaks could be located within the membrane, as already mentioned, but could also induced by insufficient closure on the fringes. Polyimide layers had a lower elasticity than Nafion membranes, so after assembling diffusion cell, Nafion could easily adapt to the sealing formation. But polyimide surface was much more inhomogeneous, so it was assumable, that sealing was not always completely given in polyimide examinations. If liquid was able to leave the chamber and flew through the polycarbonate walls or even out of the cell on small scale, where it could evaporate, different impacts on diffusion observation would be possible. The volumes of the liquids would not be the same, which would shift the interacting diffusion force. This assumption can be explained in detail with an example.

Imaging a diffusion cell with polyimide layer and common diffusion parameters, as in reproducibility determination. Furthermore, it was assumed, that the polyimide on the lower concentrated side was not sealed completely or is at least not stable enough. With increasing time, ionic diffusion as well as osmotic effects happen. The slightest change in the shape of the layer, structural conditions in the bulk material and the contact pressure of the cell, resulted in a slight leakage in the system. Few μl of ionic liquid was released from the chamber to the cell walls and sealing fringes. One side had lost ions and liquid volume. Consequently, diffusion flow was influenced by different chamber pressures and volumes. Indeed, impact on chamber concentration could be classified as minor, comparing the loss of few μl liquid to the 1.1 ml chamber solution, primarily (homogeneous concentration distribution was given). Nevertheless, by reduced backpressure in the lower concentrated side, diffusion flow was enhanced from the higher concentrated side. As volume was reduced on one side, less quantity of ions will be needed to achieve concentration equalisation. Subsequently, concentration on lower side will be increased faster, than concentration on higher side will be reduced. After several hours diffusion rate will be reduced significantly, without reaching equalisation due to different liquid volumes and hydrostatic chamber pressures.

Using PET network, reproducibility for PI layers was not achieved.

7.2.2.2 P84® reproducibility optimisation: "DS" samples

Mentioned in chapter "Polyimide layer production: "DS" samples" in appendix, it was demanded by supervisor to examine the impacts on voltage change observation during diffusion using layer with significant different effective thicknesses. Disadvantageously the practical execution of this thesis chapter was limited to approximately one month, as PDMD must be returned for other experimental issues. Nevertheless three "DS" samples were able to be observed. Figure 39 shows the potential difference change of these "DS" samples, table 36 the average thicknesses of these samples within diffusion region.
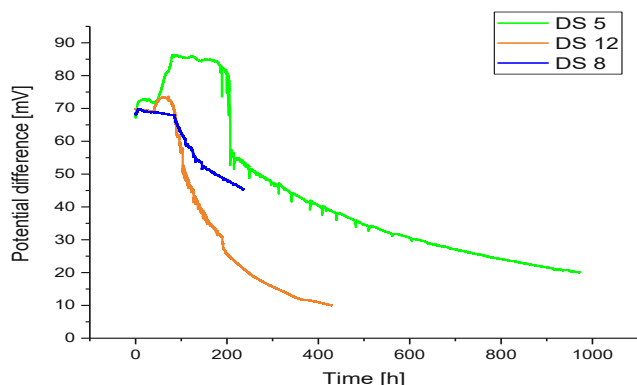
Figure 35: Potential difference change observation using "DS" samples

Table 35: Average layer thicknesses within diffusion region of "DS" samples

Sample	DS 5	DS 8	DS 12
Average layer thickness (diffusion region) [μm]	6.2	6.3	6.2

In figure 40 the starting potential difference and difference change within the first 100 hours were of high interest, especial the starting potential difference, shown in table 37.

Table 36: Starting potential difference of "DS" samples

Sample	DS 5	DS 8	DS 12
Starting potential difference [mV]	65.68	66.45	69.93

In contrast to samples with thicknesses about 9.6 μm, produced by optimised method and used for reproducibility determination, deviation of starting potentials of "DS" samples was much smaller, when figure 40 was compared with figure 39. Furthermore, values of starting potential of "DS" samples were more expectable and more comprehensible with the theoretical basics. According to Nernst equation, expected starting potential without diffusion barrier would be 59 mV. The averaged value of 67.35 mV of "DS" samples was more expected than starting potentials of thicker PI membranes between 70 and 100 mV. This showed, that more reproducible values were obtained by using thinner PI samples as diffusion barrier than the original ones. However, this issue could not be discussed more in detail, as no entire reproducibility determination measurement could not be proceeded.

After approximately 100 hours, "DS 12" and "DS 5" began increasing with different intensity. Comparing diffusion time of "DS" samples, with normal produced samples in figure 39 of reproducibility determination it was noticeable, that although "DS" sample layers were much thinner than all other sample layers, all three measured "DS" need more time for reducing potential difference. This observation did not support the attenuation, that layer thickness would increase needed time for penetrating, although this theory based on a fundamental physical chemistry. Nevertheless, it confirmed the hypothesis, that using these polyimide-based layers for PDMD had not the required psychically and materialistic quality for such high resolved measurements. Other parameters, especially defects and imperfections in the bulk

medium of the sample, which had a higher possibility to occur when producing thicker layer, had too heavy impacts on diffusion observation too achieve expected results. This was also seen by reproducibility determination, when it was not possible, to achieve equal potential difference trends.

7.2.3 Diffusion and diffusion coefficient determination

In the introduction of this thesis mentioned, the main goal of this thesis would be a direct determination of a diffusion coefficient by using PDMD for several kinds of high-resistant polymer layer. Nevertheless, while executing the practical part, it turned out that observation of a correct diffusion trend and so the evaluation on this basis was a complex task. Even if all samples would achieve enough reproducibility, like Nafion, the calculation of a main diffusion coefficient would be complicated. This chapter shows the superposition of main laws for diffusion processes with the instrumental setting.

One of the most fundamental equations for explaining diffusion flows and resistances is Fick's first law. Fick's first diffusion law can be used, when several conditions are fulfilled [11]:

- Homogeneous Amorphy
  Polymeric matrix must have a homogeneous amorphous bulk, without any crystalline structures within the bulk to guarantee homogenous micro-structure for diffusion. The entire polymeric volume can be separated into two parts, the interstitial free volume and the free volume of the empty space. The interstitial free volume is required by the polymer chains for their anharmonic oscillations. It is evenly distributed over the polymer chains. A redistribution is associated with large energy conversions. The free volume of empty space is distributed over the polymer discontinuously. This volume can redistribute itself without changing the total energy and guarantees temporal intercalation processes and transport of small particles trough the polymer. As industrial product, Nafion fulfilled that criterium, however it was not possible to make assumptions about P84 layers, as no information was given about macroscopic changes when powdery raw material was solved and re-solidified in layer shape. Secondly, P84 layer could contain inhomogeneous sized and number of cavities and invagination within the bulk which could disturb diffusion reproducibility.
- Sufficient concentration gradient
  The concentration gradient between both solutions must be so high, that diffusion is only hindered by structural obstacles within the bulk. Most of the examinations were executed using a concentration difference of 0.5 and 0.05 aqueous KCl solution, so this criterium was fulfilled for every used polymer.
- Uninfluenceability by non-diffusion parameters
  Executing this thesis, it turned out osmosis was an important factor for determining diffusion process. By transporting water from one chamber to another, a common equation for diffusion flow could be used, as another, multiple parameters were added, for example amount of exchanged water within the diffusion cell, the influence of different interacting liquid volumes, the influence of existence of multiple, different concentrated liquid layers close to the polymer due to not sufficient mixing within the chamber solution where water is transported in. Additionally, hydrostatic pressure due

to osmosis deformed cross section. So, ideal planar surface changed to a centre focussed, but still inhomogeneous shaped, one-sided evagination. Not only all of these exemplary parameters must be summarised into equation for calculating the right diffusion coefficient of the material, all of them are co-dependent to each other and time dependent. Nevertheless, common diffusion laws must be optimised for this. For example, the Fick's first diffusion law cannot be used, as system is not stationary. Fick's second diffusion law must be considered, which is mathematically much more complex and contains different solution approaches.

- Reproducible data set
  As already mentioned, Nafion layers, soaked in 0.05M KCl, but also in pure deionised water, were the only useable samples for determining diffusion coefficient due to the achieved reproducibility. Furthermore, Nafion layers were penetrated in less than one day, instead of polyimide layers. Due to the long diffusion time probability of mis-observations, artifacts and several interferences was much higher.

- Unlimited ion source
  Diffusion equations, such as Fick's first law, determine diffusion coefficient and diffusion flow by evaluating the increase of concentration in the absorber phase over time. During this process, absorber phase, in the diffusion cell the lower concentrated KCl solution, must be provided with a constant, unlimited source of diffusing particles or ions. So, penetration through polymer bulk is only a function of diffusion resistance and concentration difference, simplified. However, higher concentrated solution is a limited resource, and the reduction of ion amount must be considered.

- Ideal penetration
  Also, Fick's laws base on mass equalisation. That means, that all particles which enters polymer bulk will leave it on the other side to realise complete diffusing. But, all used polymers had the ability to intercalate particles and ions, so they will not appear in the absorber phase, the lower concentrated solution.

- Uninfluenceability of distribution factors
  Stationary system conditions also require that the resting, liquid layers at the interfaces have no significant influence on the permeation of the substance through the barrier. Furthermore, the contact resistances are small. Therefore, the concentrations of the donator phase and of the acceptor phase within the membrane can be replaced by the product of the distribution coefficient and the concentrations in the donor and acceptor phase, so from the chamber solutions. Using the generalised distribution coefficient, the diffusion coefficient and the layer thickness, the permeation coefficient of the membrane is calculatable. However, in contrast to common diffusion laws, charged ions are penetrating due to diffusion, so layer close to the membrane could have an influence due to possible electrostatic charging. Furthermore, indeed Nafion shows great ionic up-take characteristics due to charge-active sulfonated groups in polymer chains, the first-layer-penetration resistance of P84 is not definable, but much higher contact resistance is predictable. So, an exact distribution coefficient could not be defined without detailed and precise examination about penetration of the membrane-solution interface.

- Requirement for determination of the diffusion-coefficient and imbrication with used instrumental setup

On the base of Fick's first law, there are several methods to determine diffusion coefficient, by determining mass flow and distribution coefficient or by determining amount of absorbed or desorbed substances, however, all tw methods require over time measured absorber concentration and further conditions. [12] Used instrumental setup only give information about the potential difference. Indeed, by using Nernst equation, it would be possible to calculate potential difference into concentration ratio, but the result would be mole fraction, not the direct concentration of a solution.

To summarise all mentioned criteria, it was only possible by approximation to calculate diffusion coefficients from obtained data. However, at least to determine this coefficient a determination method was used and modified, the lag-time method.

> *"For this purpose, the diffusion of a substance through a membrane is considered. From the moment the diffusing substance arrives on one side of the membrane and before the equilibrium is established, the flow rate and concentration at any point of the membrane varies over time"[8]*

Although this method also bases on Fick's first and second laws, several simplifications and adjustments can be adapted. Lag-time method separated the recorded diffusion concentration into instationary and stationary part. [12]. In common measuring conditions instationary phase would be influenced by self-adjustment of the system to the diffusion system, like stable interaction with liquid or gaseous diffusion source stable or stable continuous desorption from the barrier material on the permeate side. In contrast to this, stationary part continuous input into barrier and other sided output of referred substance was given. These phases were also given for this instrumental setup. However, the instationary phase was defined by different factors like the growing osmotic deformation and increased concentration equalisation and so reduced diffusion force. Such problematic occasions were eliminated by simply using the stationary part for calculation. As this method was a linear one, the stationary part would be determined by analysing average trend profile of potential difference change observation. This phase was set on the most linear part of the recorded trend at the beginning. In figure 40 the averaged trend of 0.05 M KCl soaked Nafion membrane is shown.
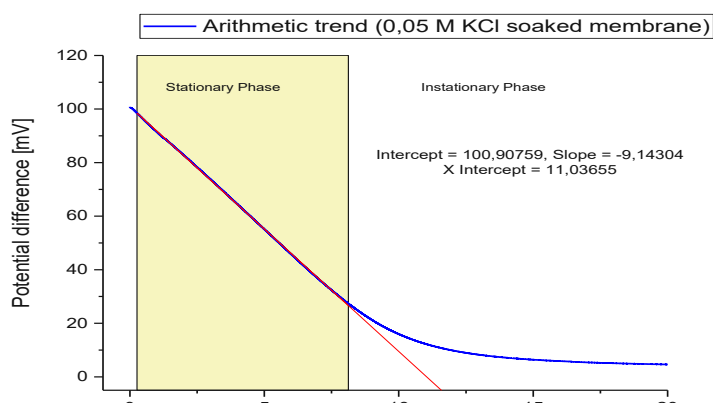

Figure 36: Averaged potential difference change trend of 0.05 M KCl soaked Nafion with stationary and instationary phase

---

[8] [11] Barbara Weh: „Permeationseigenschaften von Polydimethylsiloxan-Membranen in Abhängigkeit von der Netzbogenlänge" (S.: 20)

Using software "Origin2016" a linear fit method was used to identify the most linear part of the first hours during diffusion. Then linear extrapolation was used to determine cross section with the time axis. This point characterised the lag-time t_{lag}. Using lag-time the diffusion coefficient can be determined. (17)
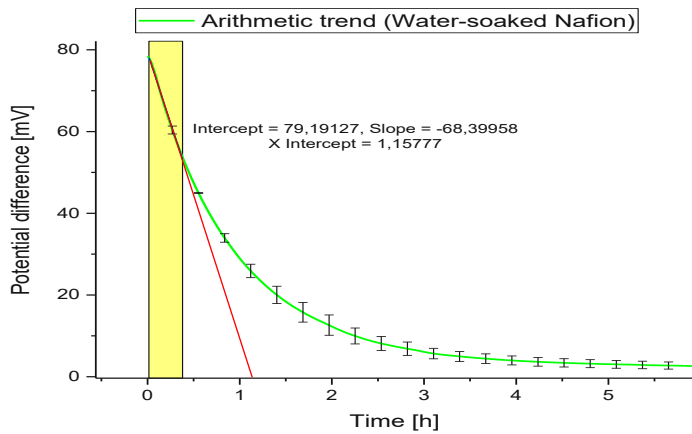
$$D = \frac{d^2}{6 * t_{lag}} \tag{17}$$

Figure 37: Averaged potential difference change trend of water soaked Nafion with stationary and instationary phase

Using given Nafion layer thickness for d, 25.4 µm, and 11.0 h for t_{lag}, resulted in a diffusion coefficient of $1.623 * 10^{-9}$ cm^2/s. Using this method for water soaked Nafion profile was more problematic. The reason for this was the curvature profile, which impaired the quality of correct setting of the stationary phase. Nevertheless, it was plotted. A diffusion coefficient of $1.548 * 10^{-8}$ cm^2/s was calculated, much higher than the coefficient of 0.05 M KCl soaked membrane.

Comparing these results with literature data is complicated, as the experimental setup, the diffusion cell and the PDMD, is an unique, in-house measurement setup, while various literature diffusion coefficient were obtained by using different technics. Table 38 shows a summarisation of three different literature diffusion coefficients and their determination technic, concerning diffusion trough Nafion matrix.

Table 37: Comparison between different determination and calculation methods for one-particle diffusion coefficients

Determination technic	Diffusion coefficient [cm^2 * s^{-1}]	Diffused particle	Literature indication
AC-Electrogravimetry	$0.97 * 10^{-6}$	H$^+$	[26]
Impedance Spectroscopy	$1.1 * 10^{-6}$	H$^+$	[27]
Kinetic model (theoretical base)	$18.0 * 10^{-7}$	K$^+$	[25]

The literature data shows that proton has got a higher diffusion coefficient as potassium ion, which was already expected due to the Grotthuss mechanism and steric effect in chapter "Examination of soaking impact on potential difference change observations". Nevertheless, compared to water soaked Nafion membrane, diffusion coefficient, $1.548 * 10^{-8}$ cm^2/s, was

smaller by two orders of magnitude. The main reason of this difference was complicated to define, as various impacts were presents, not only proton-potassium exchange within the matrix, but also two different ion sources with inconstant concentration gradient and electrostatic and steric blockades for particles and ions within hydrostatic diffusion fluids.

To summarise this sub-chapter, using high quality simulation software and correct mathematical background for each experiment conditions would be the fundamental base to calculate correct diffusion coefficient. Furthermore, diffusion cell must be adapted and optimised to establish correct model systems for diffusion to calculate diffusion coefficients.

7.3 Element specific analyses of penetrated samples

7.3.1 Element specific quantification

Many standards with different concentrations were produced for the calibration in order to cover a large dynamic working range. Following level were defined: 100, 500, 1000, 2000, 3000, 4000, 5000, 6000, 7000, 8000, 9000, 10000, 11000 [µg Potassium /g] (=[ppm])

However, some standard level could not be integrated into calibration due to several reasons. Spike level "100 µg/g" and "6000 µg/g" were too low as expected in comparison with the trend generated by the other calibration points. Spike level "7000 µg/g" was not useable for ablation, as all produced layers showed uncharacteristic surface deformations. Spike level "9000 µg/g" was also classified as outliner.

Table 40 shows the used laser and mass spectrometer parameter for potassium calibration.

Table 38: Parameters for potassium calibration

Analyte (Ion)	^{39}K
Used substance	CF_3SO_3K
Matrix	P84®
Laser energy [%]	35
Pulse rate [Hz]	10
Spot size [µm]	80
Plasma power [W]	1400
Scan speed [µm/sec]	240
Overlap [µm]	5
Average number of set scan lines []	8
Average number of evaluated scan lines []	6
Average lateral line length [mm]	3.0 +/- 0.3
Average evaluated line length	2.4 +/- 0.3
Average number of proceeded penetration steps (patterns) []	30
Average number of evaluated penetration steps (patterns) []	22 +/-2

The parameter "Overlap" describes the reduction of the distance between two contiguous laser scan lines. As already mentioned in chapter "Sampling and evaluation", depending on spot size, and chosen instrument focus mode ablated region is slightly smaller than set spot

size. For potassium quantification, the distance between the centres of both lines were not 80 µm, but 75µm for correct ablation. Figure 42 shows the calibration line for potassium.
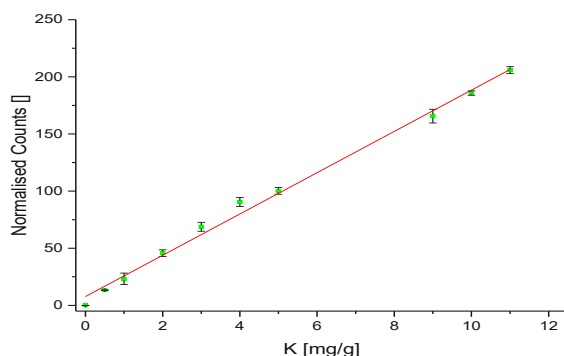

Figure 38: Calibration line for potassium

Seen in figure 43, ordinate is called "Normalised Counts". Executing normalisation on this and every other examination is explained in sub-chapter "Normalisation procedure". Data was normalised on 13C counts, which was measured simultaneously. In table 41 calibration data is given.

Table 39: Summary of statistical data of potassium calibration (all values dimensionless)

Intersection with the ordinate		Gradient		Statistic
Value []	Standard deviation []	Value []	Standard deviation []	Corrected R^2 []
7.7	2.8	18.1	0.47	0.9938

Results of chloride calibration is listed below.

For chloride calibration following standard level were produced: 100, 500, 1000, 2000, 2500, 3000, 4000, 5000, 7500, 10000 [µg Chloride /g] (=[ppm]). Spike level "2000" and "3000" were identified as statistical outliner, so they were eliminated from calibration. During layer production process, it turned out that concentrations over 5000 µg/g were not possible using benzalkonium chloride. During heating-out phase dark, blackish, crystal-like particles were observable on all layer of spike level "7500" and "10000". Using LA-ICP-MS local one-point measurement it turned out, that these particles contained a high amount of chloride. Either such high concentrations would need a more intensive mixing before layer spinning, or solution is so close to saturation limit, that slightest heating resulted in sequential, substance specific solidification. Layer production parameters was analogous to potassium quantification. Table 43 contains chloride ablation parameters.

Table 40: Parameters for chloride ablation

Analyte (Ion)	$35Cl$
Used substance	$C_6H_5CH_2N(CH_3)_2RCl$ $(R=C_{14}H_{29})$
Matrix	P84®
Laser energy [%]	60

Pulse rate [Hz]	20
Spot size [µm]	200
Plasma power [W]	1550
Scan speed [µm/sec]	400
Average number of set scan lines []	5
Average number of evaluated scan lines []	3
Average lateral line length [mm]	3.6 +/- 0.3
Average evaluated line length	2.8 +/- 0.3
Average number of proceeded penetration steps (patterns) []	15
Average number of evaluated penetration steps (patterns) []	9 +/-2

By comparing ablation parameters for potassium and chloride, it could be concluded that the total ablation mass rate for chloride had to be increased significantly. It was tried to obtain calibration using potassium parameters, but signal to noise ratio of expected chloride peaks was too low to use it for quantifying. By increasing spot size, laser output and pulse rate enough sample mass was ablated to identify incoming chloride atoms. To balance ablated mass and intensity of laser impact scan speed was increased to better distribute laser pulse over set line scan. Furthermore, it turned out increasing plasma power from default setting, 1400 W, to 1550 W increased S/N.

A disadvantageous consequence of increasing the amount of ablated material per time unit was reduced depth resolution. While average pattern depth, so depth of produced cavity due to laser impact after one executed line scan, of potassium calibration laser setting was about 0.5 µm, chloride laser settings resulted in depth about 2.2 µm. So, depth resolution was reduced to less than a quarter. Another disadvantage was the fact, that calibrations of both ions were not executable simultaneously. Due to other required laser parameters, determination of potassium and chloride had to be executed on different locations, so a complete local independence of measured concentration could not be excluded. Furthermore, this increased time investment and, as diffusion region on samples was limited, reduced number of sampling positions and repetition possibility.

As can be deduced from figure 44 the obtained calibration function for chloride shows a linear behaviour over the whole investigated concentration range. Statistical parameters to this calibration function are presented in table 43.
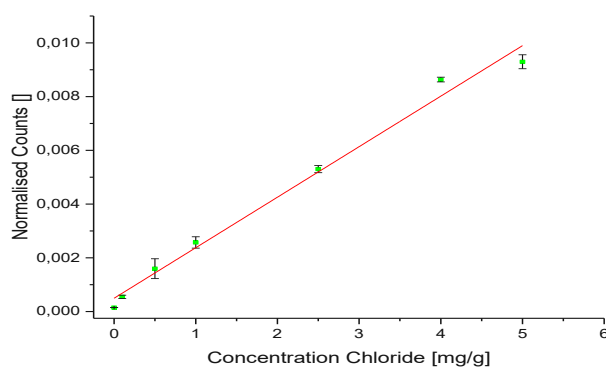

Figure 39: Calibration line for chloride quantification

71

Table 41: Summary of statistical data of chloride calibration (all values dimensionless)

Intersection with the ordinate		Gradient		Statistic
Value []	Standard deviation []	Value []	Standard deviation []	Corrected R^2 []
$4.9 * 10^{-4}$	$2.3 * 10^{-4}$	$1.9* 10^{-3}$	$8.9* 10^{-5}$	0.9866

By establishing calibration lines for potassium and chloride quantification of diffused ions was possible. As no other salts were used during this thesis, further element specific calibrations were not proceeded.

7.3.2 Examination of ion penetrated samples

After diffusion observation, penetrated layers were removed from the cell, cleaned and fixed on a silicon layer for elemental analysis. Following chapters contain element specific examinations of diffusion penetrates samples.

7.3.2.1 Examinations of polyimide layers

It must be mentioned, that in this chapter only samples with definite, high potential information content were presented in this thesis, considering potential difference change observation and element analyses. Furthermore, only a percentage of diffusive penetrated samples were also used for elemental analysis. Producing useable sample layers for LA-ICP-MS was the main limitation for elemental analysis. Only samples with evaluateable information from the diffusion process and sufficient physical condition, regarding planarity were used for laser ablation experiment. Not fulfilling these criteria would impair sampling using the laser and to analytical inconsistency, as evaluated data would not be matchable with PDMD data.

To mention examination mode again, within ablation cell a pattern, consisting of a certain amount of laser scans, was set on sample surface. From this rectangular measure zone, a lateral reduction for evaluation was executed. To reduce amount of presented data within one graph for depth resolved presentation, data within one line was averaged and averaged line data was averaged again. Consequently, for every pattern penetration step, which described a certain penetration in µm, one point for measured and evaluated concentration for a certain element within a penetration step was made.

The following figure 44 show the depth resolved potassium concentration within two polyimide samples "81" and "84"and their potential difference change trends.
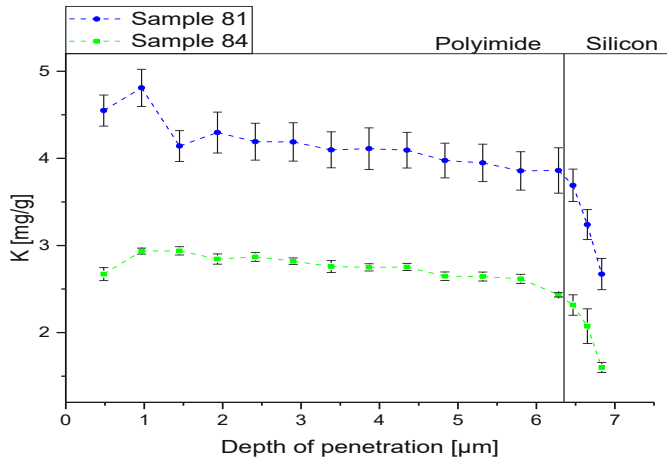

Figure 40: Potassium concentration within sample "81" and "84"
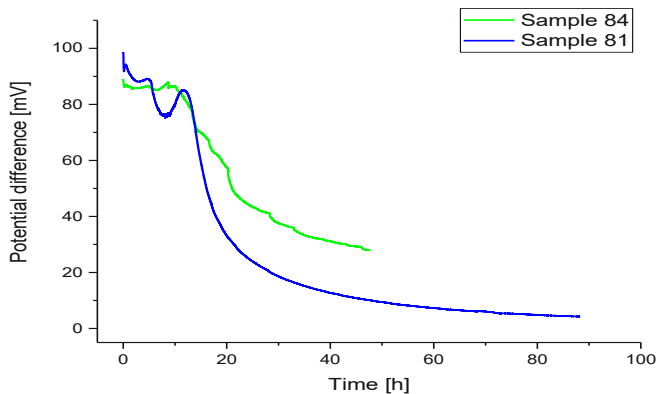

Figure 41: Potential difference change trend of sample "81" and "84"

In the graph in figure 44, and in following depth resolved images, the material limitation is given. For these samples, laser fired trough polyimide surface into polyimide bulk. This was repeated until polyimide was fully penetrated and silicon substrate of the wafer was measured. So, in penetration diagrams a schematic boundary between polymer and silicon is given. It must be mentioned that this material specific limitation was approximated. The layer thickness was determined by one line using profilometry with "Total profile" method, but before diffusion. After diffusion, the polyimide layer thickness could not be measured again via profilometry due to lacking planarity and not settable reference points. Layer thickness after diffusion could only be determined by laser penetration and silicon signal detection. When silicon signal increased significantly, polyimide was penetrated completely, and silicon wafer was ablated. For graphic representation, a vertical line was drawn. Advantageously, sample "84" and "81" showed nearly the same layer thickness, considering used depth resolution. Comparing with determined layer thickness of these samples before diffusion, a reduction in thickness was clearly visible, shown in table 45.

Table 42: Comparing layer thicknesses of sample "84" and "81" before and after diffusion

Sample	Average layer thickness before diffusion (diffusion region) [µm] (Total profile method)	Average layer thickness after diffusion (diffusion region) [µm] (Cratering method)
81	9.072	6.283
84	9.255	6.771

According to results of table, layers lost nearly 2.8 µm bulk thickness after diffusion. This reduction was observed in several samples in different intensities. Examining process between profilometric measurement and laser ablation, this thickness reduction must be caused by diffusion cell and osmosis. When layer was inserted into diffusion cell, it was fixed and sealed by two sealing rings on each side. Using M6 screws the cell was closed. By increasing contact pressure, sealing rings were compressed and stretched the layer within diffusion region. Due to stretching layer lost thickness. An additional reason for reduced layer thickness was the impact of osmose. Indeed, osmotic influence was lower than with Nafion membranes, but still existed. Furthermore, deformative effect due to osmosis was increased by much longer dwell time within diffusion cell. Osmotic deformation was visible at both samples.

For interpreting and evaluating depth penetration graph of sample "84" and "81" in figure 45, the correct sampling in laser ablation cell must be mentioned. To reduce evaluation errors, layers, whether Nafion or polyimide, were always fixed on the wafer, so that the side, which was directed to the higher concentrated side in the diffusion cell, was directed upwards in every experiment. Consequently, if chamber concentrations did not reach equalisation by diffusion, a concentration trend for penetrated ions should be detectable. Penetrating first patterns potassium and chloride signal should significantly high. With increasing penetration, a reducing concentration trend should be observable, as less ions could penetrate entire polymer bulk. After breaking through the polymer layer, the concentration should decrease immensely, as no penetrated polymer was ablated, but silicon wafer.

Sample "81" and "84" showed nearly the same trend. In the first penetrations steps concentration of potassium increased until it reached a maximum. For sample "84" maximal potassium concentration was already reached after 0.966 µm, while sample "81" concentration maximum was detected after 1.933 µm. As expected, a low, but existing reducing trend after this maximum was detectable in both samples. This corresponded to the potential difference change observations, as for both samples nearly concentration equalisation was reached. After breaking through polymer layer, potassium concentration decreased significantly, as silicon layer was ablated. Nevertheless, even after several ablation patterns, detected potassium was still high, referring to background signal. The reason for that is, that laser still ablated polymeric material, not only at the ground, but also on the side walls of the material. Another coherent result between potential difference change observation and elemental analysis was influence of diffusive penetration. Sample "81" nearly reached normal electrode voltage, so background potential difference of the PDMD, while diffusion of sample "84" was aborted before it could reach equalisation. Conductivity determination of diffusion cell chamber liquids confirmed this attenuation. This different experiment modes were also identifiable in elemental analysis. The longer penetrated sample "81" layer had a

higher average Potassium concentration within the bulk, as a higher number of ions could be embedded into bulk and surface.

Figure 46 shows three depth resolved concentration trends of the sample "58". All results originated from three individual laser patterns, executed on diffusion region of sample "58".
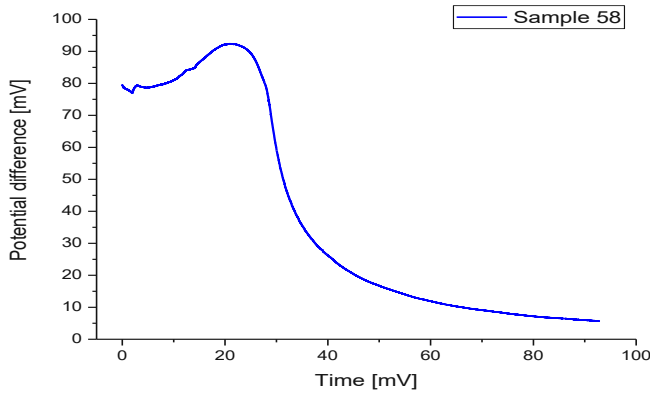

Figure 43: Potential difference change observation of sample "58"
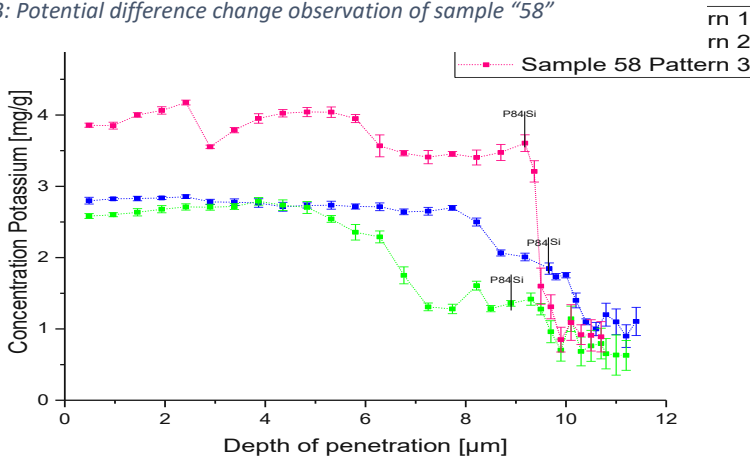

Figure 42: Depth resolved potassium concentration of sample "58" for three patterns

Three laser patterns on sample "58" with Potassium laser parameters were executed to determine depth dependent potassium concentration and to determine reproducibility of diffused potassium when varying lateral position. While penetrating first 6 µm polyimide bulk approximately equal average potassium concentration was measured for pattern 1 and 2. But, pattern 3 showed a significant higher average concentration in the bulk. As the same normalisation and sampling conditions were applied, the concentration of pattern 3 was higher indeed and not due to an evaluation difference. It must be mentioned that pattern 1 was positioned in the upper left area of the diffusion region, while pattern 2 was located further down on the right. Pattern 3 was performed exactly in the centre of the diffusion region. So, the assumption was made, that the concentration of diffused ions decreased with increasing radius of the measurement position referenced to the centre of the diffusion region.

After about 5µm penetration, concentration of pattern 2 decreased significantly compared with pattern 1. The assumption was made, that due to inhomogeneous density or simply material condition in this bulk region a smaller number of ions could fully penetrate here.

Pattern 2 also showed a reducing trend after about 8 µm penetration, which was expected due to non-complete ionic diffusion as this side was directed to lower concentrated chamber solution. Comparing pattern 3, the trend obtained by penetrating bulk showed various local concentration maxima and minima, explainable by inner agglomeration effects within the material. For every concentration trend, the silicon signal dependent distinction between polyimide layer and silicon wafer was marked. Indeed, border determination was difficult to determine, as depth resolution was reduced to single pattern penetration depth, about 0.4 µm, and due to silicon signal increase detection, as determination was averaged over each individual line and increase was not clearly abrupt jump-like. Nevertheless, different borders were determined for each pattern, which was caused by inhomogeneous local layer thickness and by osmotic pressure deformation.

Figure 48 shows potassium and chloride concentration of sample "101" and the potential difference observation trend.
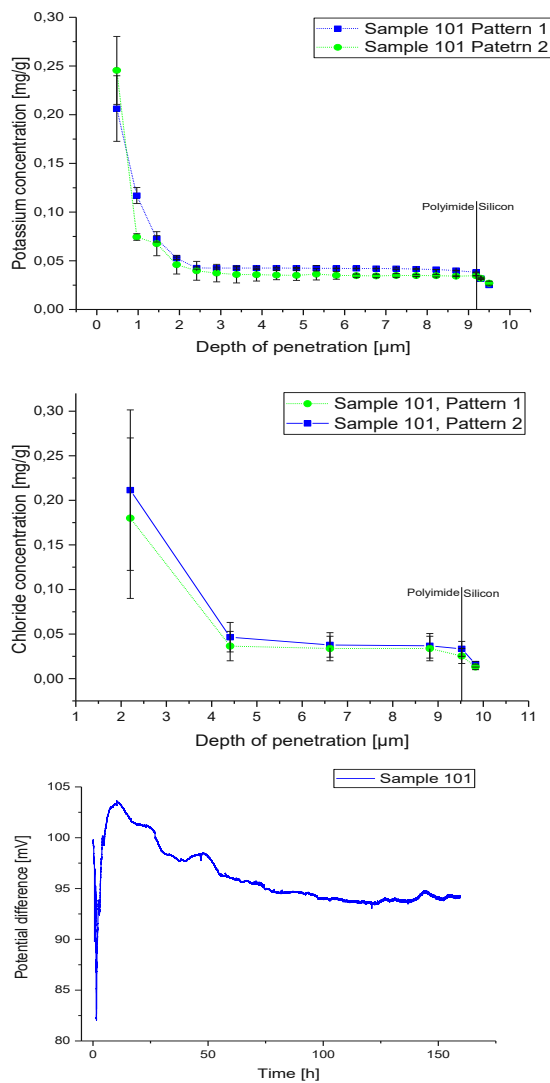

Figure 44: Depth resolved potassium and chloride concentration of sample "101" for two patterns with potential difference change observation

This sample was measured, because of its unexpected voltage trend during diffusion. Although sample was brought into contact with chamber solutions for over 150 h, potential difference decreased only for less than 10 mV and after 125 h no significant reduction was observable. So, without any expectations, neither due to inhomogeneous layer profile, nor by layer deformations, nor any other changed diffusion parameters (0.05M KCl vs. 0.5 M KCl), it was tried to determine potassium and chloride concentration trend within the bulk via two laser patterns. The laser and mass spectrometer conditions were the same as for quantification issues.

To reduce influence of measure position depending concentration locations, patterns for each measure were positioned equidistant from diffusion zone centre. All concentration trends, potassium as well as chloride, show an expected concentration trend. Despite long diffusion time, potential difference observation showed, that no significant ionic diffusion was observable. In depth resolved potassium concentration graph, left above, a high Potassium concentration was recorded the first patterns, so within the first 2µm of the polyimide bulk. It can be assumed, that this resulted from a high contaminated surface and/or from imported potassium ions due to diffusion. After about 2µm penetration, measured potassium concentration acquired a value of about 0.04 mg/g without changing it significantly while further penetration, until polyimide / silicon border was breached, and concentration was reduced further. To mention it again, polyimide layer was adjusted for elemental analysis insofar, as side, which was directed to higher concentrated solution chamber within diffusion cell, was penetrated first, which explains high concentration at the beginning. Comparing with potential difference observation, by interpreting elemental distribution this assumption as made:

As diffusion assembly, physicochemical active parameters like temperature or hydrostatic pressure or chamber solutions for diffusion were not changed from the default setup, the only reason for this type of diffusion trend was located in the polyimide layer. Indeed, diffusive input of ions into polyimide layer was not obstructed, nevertheless it seemed as further ionic transport was prohibited within the polyimide bulk. As outer conditions were kept constant, the reason for this phenomenon was material specific. Also, as P84 showed no great water uptake characteristics or any type of charge functional ligands, it was most likely that the origin of this ion blocker was physical bulk density. Density and density homogeneity were one of the only parameters, which could not be checked for quality determination, neither with profilometry, nor by other useable instruments. It was possible, that due to heating out phase, which efficiency was depending on position on the heating plate, combined with too much

Figure 45: Depth resolved potassium and chloride concentration of sample
"101" for two patterns with potential difference change observation

PI/NMP solution remaining on the wafer after spinning, polyimide particles were agglomerating at the bottom of the layer, which results in higher, one-sided density, or at least higher dense bulk comparing with other samples. This evaluation should emphasise the fact, that this high precise examination was not possible using self-made P84 layers due to their low quality.

For reproducibility issues, the same pattern was proceeded on the mirrored position within diffusion region. Furthermore, these examinations were also proceeded with 35Cl laser

parameters to determine chloride concentration in the sample. Despite of lower depth resolution due to higher needed material ablation rate, the same trend as expected from potassium determination was recordable. Nevertheless, an analytical obstacle was observable by comparing both elemental distribution analyses. Both depths resolved graphs showed the highest deviation at the first data points, where concentration was highest. This was reasonable as here highest elemental input was expected and the highest deviation in storing and particle agglomeration. But chloride deviation was much higher as potassium. The deviation is based on the absolute chloride concentration corresponding to given analytical sensitivity. Signal response by measuring 35Cl is less intense compared with Potassium signals. Therefore measuring concentration close to limit of detection resulted in higher standard deviation regarding the individual lines.

Next discussed sample represents the elemental analysis of a polyimide film, which was penetrated with ions for a much longer time. Figure 50 shows the elemental analysis result and potential difference observation from sample "96".
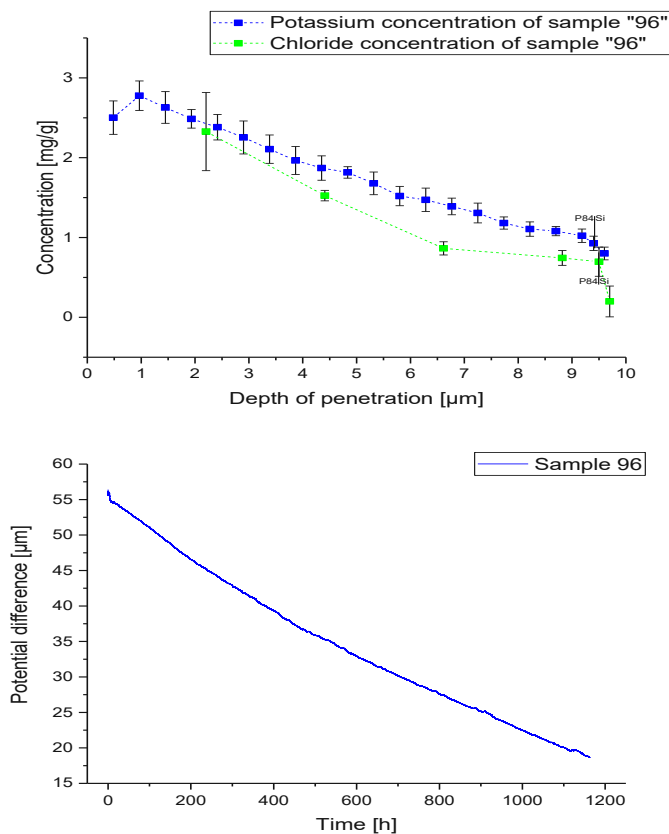

Figure 46: Depth resolved potassium and chloride concentration of sample "96"
for two patterns with potential difference change observation

Sample "96" was already evaluated in chapter "P84® membranes - reproducibility examination", presented as a polyimide layer, which was brought in contact with diffusion chamber solutions for a very long lapse of time. However, it was not possible to reach concentration equalisation, even after 1200 hours. Now, also elemental analytical results are given. The highest, depth dependent concentration points were comparable with other

samples like "58", although sample "58" was already aborted after 100 hours. Furthermore, the assumption could be established, that increasing diffusion time did not increase diffusive ionic particle input and storage into the layer bulk significantly, but membrane diffusion resistance had the greatest impact.

To establish a recapitulating statement for the entire polyimide elemental analysis, it was possible to determine elemental distributions within the layer bulk and identify several effects and matches with diffusion observation. However, without achieving reproducible sample recordings and definite diffusion trends with polyimide layers, no definite elemental analysis was possible to calculate diffusion coefficients or other diffusion resistance related parameters. Nevertheless, quantification and sampling ablation showed, that established method is multifunctional and useful for further analytical issues.

7.3.2.2 Examination of Nafion membranes

Examining of Nafion membranes showed various problems. First, fixing Nafion membranes on silicon layer for ablation cell to provide a planar sampling surface was more difficult than using polyimide layers. The reason for that, was inhomogeneous drying of the intensively soaked membrane after diffusion and cleaning. By fixing layer on the wafer adding low tension stress, it was tried to reduce exvaginated and invaginated areas. However, this was only efficient at a low percentage, as deformations were undirected and had various intensities on the entire layer surface. Consequently, it was necessary to search for location, which were planar enough to provide sufficient ablation at the entire pattern, or at least within an individual line of a pattern. Due to the enormous spot size using chloride ablation conditions it was nearly impossible to definite sampling positions with guaranteed qualitative ablation success.

One of the greatest problems comparing polyimide and Nafion membranes was the thickness to be penetrated. Averagely, about 20 to 22 patterns with potassium laser conditions were needed to break through polyimide bulk and reach silicon substrate with an expected layer thickness of 9.2 to 9.5 µm. However, Nafion membranes had a layer thickness of 25µm, so number of executed patterns must be greater than 50 to 55. That resulted in a significant increase in measuring time and argon consumption. First, it must be determined, if using the same laser ablation parameters, the same penetration depth per laser line was produced by changing sample polymer. It turned out, that Nafion showed a higher resistance to laser pulse impact. Using potassium laser parameters average pattern depth for Nafion membranes were determined and calculated to 0.2996 µm. So, more patterns were needed to reach the same depth comparing with P84 samples.

To visualize the effect of penetrating different polymeric materials, figure 51 shows the line average silicon signal of a Nafion and P84 sample. This graph shows that only number of proceeded patterns must be increased for penetrating Nafion film completely.
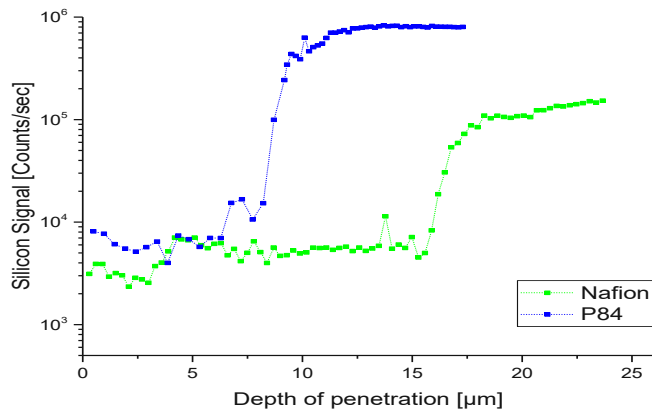
Figure 47: Comparison between measured silicon counts per second during layer bulk penetration of polyimide sample "58" and a penetrated Nafion layer

Indeed, both silicon signal trends began with different average, absolute values, this was only a result of different blanks due to sequential ablations, each of them with different plasma torch and ablation cell conditions. After about 8 µm silicon signal of polyimide trend was visible and reached upper curve region between 9 and 10 µm penetration. Within this region, additionally setting silicon signal with carbon and potassium in relation, a breakthrough point was definable. After breaking through polyimide bulk and ablation silicon wafer, silicon signal increased slightly, because remaining parts of polyimide were ablated, until it reached a quasi-stable region. Now, only silicon was ablated within spot range.

As expected Nafion needed more patterns to reach breakthrough, not only because of the lower amount of ablated material per line, but also because of the higher thickness. Nafion original thickness was 25.4 µm, however silicon signal jump was detected already at 16 µm. This immense reduction in layer thickness came from the osmotic deformation, as already mentioned in chapter "Osmotic impact", which had an immense impact on this material, due to its water-uptake characteristics and high elasticity. After deforming by water pressure, it was not possible to bring back diffusion region to original shape, deformation zones were generated due to the expended material surface. The resulted layer thickness, recorded by silicon signal, was depending on measure position and osmotic deformation impact. In figure 51 an example is given for the result of osmotic deformation. Determined by interpreting silicon signal increase, the average thickness within this set pattern of this Nafion membrane sample was reduced to 16.2 – 16.4 µm from 25 µm.

Another effect was also observable by plotting silicon signal. In contrast to this polyimide sample, and other samples, increasement of silicon signal was nearly zero after break-through point. But after laser broke through Nafion bulk, silicon signal showed an increasing trend, despite of continuous ablation. The reason for this led to another problem using Nafion samples for LA-ICP-MS, the interaction between laser focus spot and polymer material in different depths. As already mentioned, before starting laser pulse bombardment, laser instrument x, y, but also z- position must be set. Lateral position was easy to define, as macroscopic artifacts on the surface like deformations or particles could be identified. Also,

laser pattern was reduceable in its size or expendable to optimise ablation success. However, setting z-position, and so laser focus point was another issue. Focus point was set with microscope camera, integrated into laser ablation system, to guarantee efficient ablation. However, patterns were copied on each other without changing this focus point. Technically, by completing one entire pattern, laser focus point must be readjusted for new focus. But as only examination tool for focus related ablation efficiency was visual analysis with integrated microscope, it was not possible to determine factor for z-position change per pattern depth. This effect will be discussed again in chapter "Examination of inhomogeneous penetration: "Imaging" method".

Now back to silicon signal presentation. Discussed in chapter "5.4.3 Sampling and evaluation" samples were attached to the silicon wafer after diffusion using adhesive strips. Neither planarity is given on the surface on the layer, nor between layer and silicon. So, laser beam could be impaired after leaving polymer matrix, as layer ground was not planar and between silicon and polymer air space was probable. Furthermore, increasing penetration depth impaired ablation efficiency due to fixed focussing, resulting laser spot, or to be more precisely, resulted laser crater profile deviated from expected one. Instead of homogeneous spot or line type ablation, Nafion bulk was broken through fragmentally. Follow-up examinations, using analytical microscope "Keyence VHX-500" with various magnification optics, showed, that diameter of laser line craters was getting reduced with increasing depth. Using visual calculation methods by referring crater diameter of the first patterns as 80μm, using potassium laser conditions, after 40 to 50 patterns crater diameter was reduced to 20μm approximately. So, after breaking through, laser kept removing remaining Nafion material from silicon surface at the border point and bared more and more silicon, which would be ablated and detected. Consequently, due to marginal ablation by poor focussing at this depth, silicon signal would still increase until maximal polymeric ablation was completed, and silicon signal would stabilise. To summarise this examination, it was possible to penetrate Nafion complete, however ablation efficiency and amount of ablated material changed with increased depth, which had an influence on calculated pattern depth and therefore on measured and evaluated concentration distribution within the bulk.

The figure 52 shows the potential difference trends of four, in 0.05M aqueous KCl solution soaked Nafion samples. Additionally, depth resolved potassium concentration determination was proceeded on each of these samples. To simplify interpretation, identical samples was plotted in the same colours.
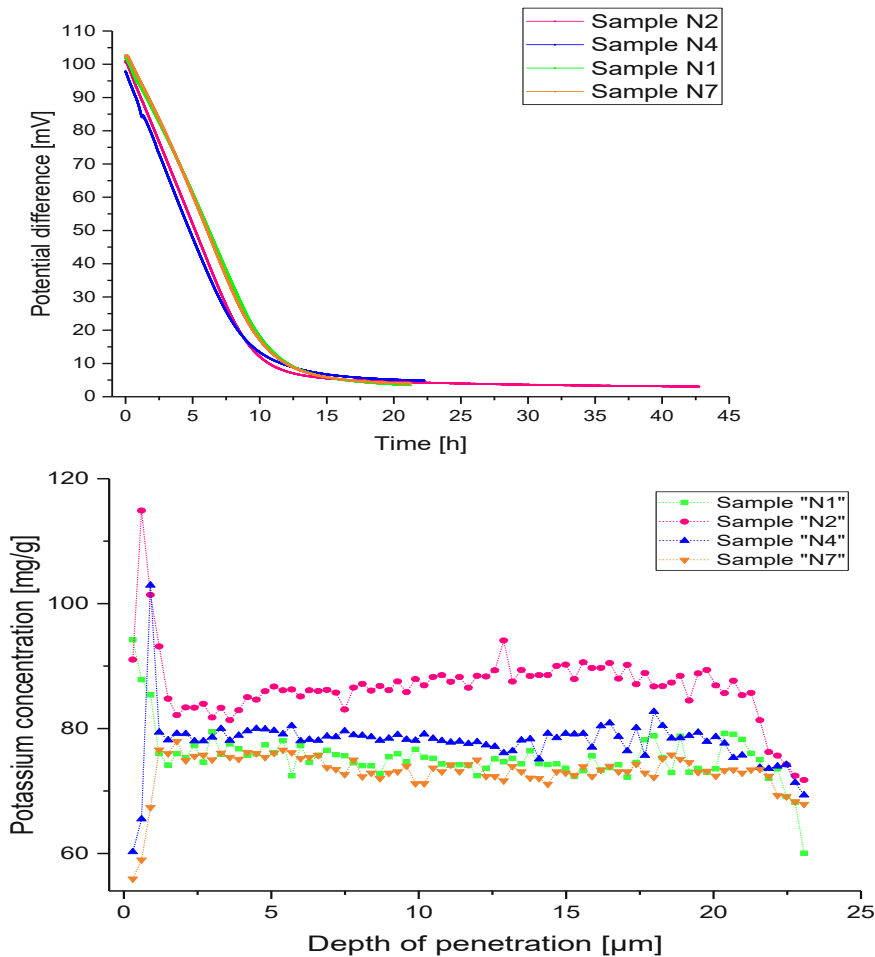

Figure 48: Potential difference change observation and potassium concentration for four Nafion samples

The potential difference observation compares four individual Nafion layers. Each of these were soaked in 0.05 M KCl and were inserted into the diffusion cell with chamber concentrations of 0.05 and 0.5 M KCl. Three of these samples were isolated and cleaned after 24 hours, one sample was penetrated for nearly two days. All of them showed reproducible trends, as expected, with low drifts along abscissa and ordinate due to time dependent difference in procedure. However, all of them reached normal electrode voltage range, which was the criterium for concentration equalisation. The figure 52 shows also the potassium concentration within the bulk of these samples. As for polyimide examinations, Nafion were fixed on the wafer insofar, as side directed to higher concentrated chamber solution, was above and measured first. All samples showed several important regions.

All samples started with a maximum concentration localisation in the first few patterns. This local increase in detected potassium was attributable to the higher ionic diffusion and penetration probability on this layer side. Figure 53 shows a zoomed in presentation of the regarding depth.
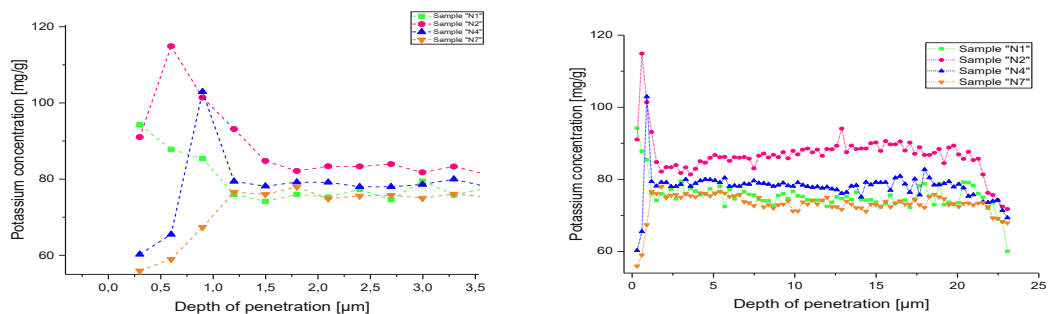

Figure 49: Zoomed in presentation of Nafion potassium concentration determination (left) and complete depth profile (right)

Despite of the intensive signal, which was recorded ablating the second to third pattern, the first pattern showed lower concentration concerning maximum and average bulk concentration. It must be mentioned that depth resolution in this pattern was not absolute correct. Laser penetration of the first pattern was highly conditional to laser focus adjustment. Indeed, normalisation compensated reduced ablation by carbon reference, but this reduced penetration could not be integrated into pattern-depth calculation, as this was a separate technic. So, rightly the distance between first and second pattern would be smaller than to other patterns depending on correct laser focus success. Furthermore, reproducibility along the lines would be low due to insignificant ablation. On various lines laser impact was so low, that 13C amount was comparable to blank value. Such errors would be integrated into evaluation without the opportunity to identification.

After the maximum, an average bulk concentration was detectable. Such homogeneous distribution was expected due to the already measured concentration equalisation with the PDMD. This bulk concentration was quasi-stable as standard deviation of individual data points, which was not presented as it would overload the graph and showed no local maxima and minima concentrations. Following statements However, after 20µm and further penetration, silicon signal increased and potassium concentration was decreased slightly. The potassium concentration did not reach any concentration limit under 50 mg/g. 29Si and 39K signal of this examination was compared with them from polyimide. After breaking through point measuring polyimide, the silicon signal intensity increased by over two decimal powers. That this point it must be re-mentioned the effect of reduced laser focus and ablation efficiency with penetration depth. Indeed, it was possible to break through Nafion layer, however no complete set laser spot size was given due to laser focus. This point must be further discussed.

Ablating line-type patterns were evaluated as averaged data points. Nevertheless, lines represented a 3-D crater formation with information resulting from ablated material from the lateral side as well as from the ground. These various origins of information were summarised

as data points per time unit. So, this assumption could only be established by evaluating all silicon, carbon and potassium counts per second for each line, pattern and sample. The exact locality of a materialistic border between Nafion and silicon wafer could not be definite, as "silicon signal jump" was heavily dependent on lines. As example, while some lines already showed abrupt silicon signal increase, other lines of the same sample showed this increase much later. Especially lines, which were located on the peripheral zones of the pattern were the most affected. If polymer layer would had been attached to the silicon in a more reproducible way to guarantee planarity, silicon signal detection would had been such an importance, as material ablation rate could had been used for depth profiling.

Furthermore, the effect of higher intensive ablating at the end of a line, which was explained in chapter "Sampling and evaluation", did have even greater influence on results using Nafion. For repetition, due to slow communication between software and laser instrument, more laser pulses were fired at last part of each line, exactly the size of set spot, which let to faster penetration and so faster to the break-through point. Due to immense increase of numbers of measured patterns using Nafion, this effect was intensified and must be corrected by reducing evaluated line length. Comparing polyimide samples, like "96", "81", "84", "58", with Nafion samples, an enormous concentration difference was detectable. While polyimide samples had maximal concentration localisation of about 4 to 5 mg/g, Nafion layer showed average concentrations between 70 and 90 mg/g. This immense particle input and storage into the layer bulk was predicted due to the charge active, polymeric molecules and the water-filled nanochannels. In sub-chapter "Examination of soaking impact on potential difference change observations" the influence of different soaking media on resulted diffusion observation was examined, insofar, as Nafion layers were soaked in pure, deionised water.

Two of the penetrated samples were measured via LA-ICP-MS, to determine potassium concentration, which is presented in figure 54.
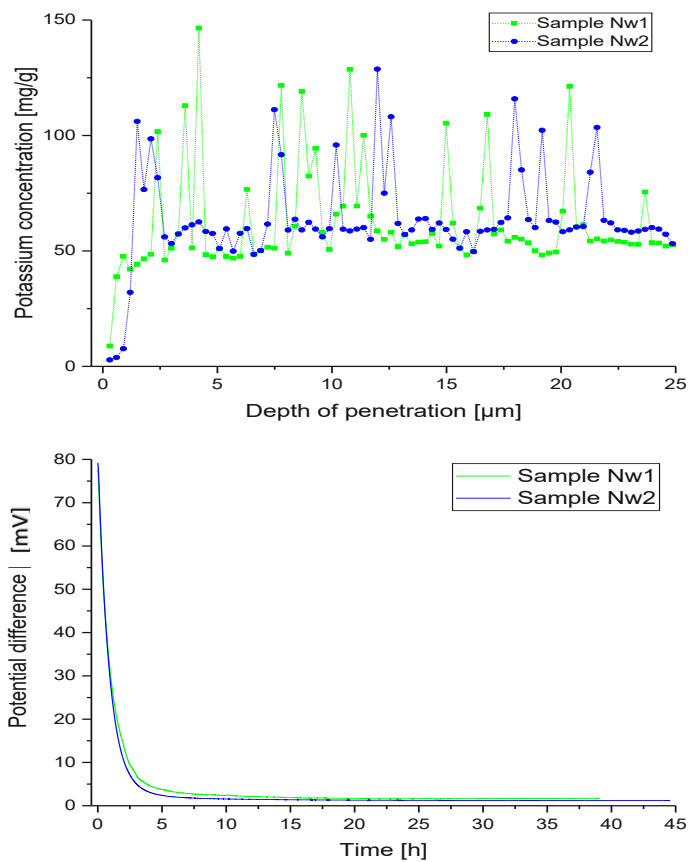

Figure 50: Potassium concentration and diffusion observation of water soaked Nafion samples (Charge "Nw")

The difference of voltage change trends between deionised water soaked and 0.05M KCl solution-soaked layers was clearly observable. Membranes, which were soaked in pure water, were penetrated faster and with higher reproducibility. They reached normal electrode voltage already after less than 10-15 hours. Additionally, their starting potential difference was lower compared with KCl soaked membranes, a lower diffusion potential was assumable and calculatable.

If potassium concentration determination between those two soaking type samples was compared, also differences were identifiable. First, average concentration of the bulk was lower than measuring KCl soaked sample, which were described as "N"- samples. This was expectable due to enough soaking time and due to chemical and physicochemical surrounding of the 0.05 M aqueous KCl solution. Additionally, potassium concentration of first patterns were also much lower compared with bulk concentration like in "N" samples. But "Nw" samples also showed another interesting anomaly. Comparing with KCl soaked membranes, during laser penetration several data points were recordable with much higher concentration. Analysing the raw data, it turned out that these concentration increases were highly depending on localisation. To be more precisely, these were attributable to individual lines. For better understanding, a normalised data segment of sample "Nw1" is shown.

Table 43: Presentation of segment of normalised counts 39K/13C [] (sample Nw1)

Line 1 []	Line 2 []	Line 3 []
714.751181	575.986815	585.60315
1130.0912	735.670578	688.519653
1198.5849	801.866731	659.879151
1406.18057	1194.83278	2944.84444
1147.43597	987.974172	931.773335
658.011859	969.754701	1175.09566
1079.05347	822.076987	1236.49206
3803.78692	1298.2995	1055.11935
1022.18847	792.084371	994.309658
4044.27721	2951.07184	985.912309
648.422295	665.936821	794.940161
557.024611	993.935393	1053.92859
583.038497	586.10261	538.77064
709.695524	951.965941	1487.43302
580.37177	760.876483	683.361812
813.532304	723.000068	1613.23057
1368.12538	1059.48862	1758.64632
738.047084	764.728493	611.392844
456.698509	814.815946	1476.75121

Increasing penetration depth

Table 46 shows a part of measured counts after normalisation procedure and reductive evaluation, like line-lateral reduction and line-number reduction. In the presented columns, which stands for individual laser lines, single data points were recorded with significant higher concentration, about two to three times higher than averaged bulk concentration, which were coloured to identify these data points better. Such spikes were not detected by measuring "N" samples, which let to following assumption: Already mentioned, soaking Nafion membrane in 0.05M KCl solution caused to replace protons, which were located in the sulfonated groups in the copolymeric chains, with potassium and chloride. So, diffusion penetration in the diffusion cell let to further storage of potassium and chloride into the polymeric matrix by completing replacing process and intercalation and inclusion.

However, "Nw" samples were soaked in pure water, so active chains were still protonated. During diffusion, common intercalation in polymeric structure was much less promoted than replacing process, which was confirmed by conductivity measurements as follow-up examination method. Therefore, the mainly insertion of potassium was located at the ends of the side chains. Macroscopically considered, within soaked Nafion bulk charge active chain sides were directed together to form nanochannels due to polarity. So, the potassium-proton exchange will be most intensive at such nano-channels inner side walls, where sulfonated groups are located. At this point, this fact was combined with the individual line concentrations, establishing another assumption. Ionic transport is enhanced greatly due to this nanochannels, which are intervening the bulk. The high concentration of this local area could be explained by ablating a great agglomeration of such nano-paths or cross-sections between multiple paths. This would explain why in one pattern line concentration was increased intensively but decreased to smaller value even in the next penetration step,

comparing red marked values with surrounding data in the table. Nafion bulk contain a network of different shaped and linked nano-channels, which could be examined via specialised technics, for example electrostatic force microscopy in combination with phase drift modes and imaging evaluation.[9] In literature [9] following conclusion could be established:

> *"Using EFM, we have shown that the pore structure in Nafion can be characterized by long connected channels that conduct protons from one side of the membrane to the other, short dead-end channels that are open to one side of the membrane but do not connect to the opposite side of the membrane, and branched channels that have multiple paths from one side of the membrane to the other."[9]*

Consequently, the origin of high concentrated data points could be explained by high interconnected nano-channels with low number of dead-end channels, as in this ionic transport would not be expected and so less ionic intercalation.

To summarise, it was possible to determine potassium concentration distribution within Nafion bulk, but with several limitations like laser focus issues, measurement time and immense signal intensity. Chloride quantification adjusted laser conditions could lead to a detector overload, so this was not executed.

7.3.3 Examination of inhomogeneous penetration: "Great line" method

"Great line" method was executed on polyimide layer sample called "84". Spinning and laser ablation parameters are not mentioned, as they were the same as used in reproducibility determination and quantification calibration. The following figures 55 - 58 show the photographic presentation of polyimide layer with marked scan lines and the resulting potassium and chloride concentrations over vertically and horizontally set lines.
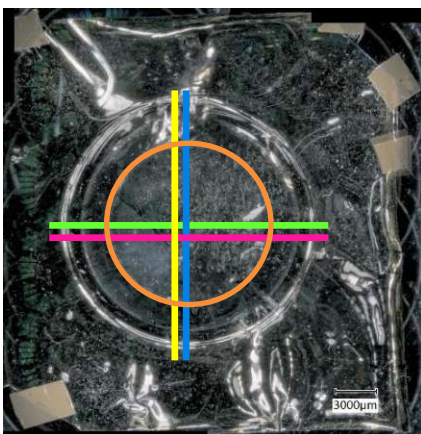

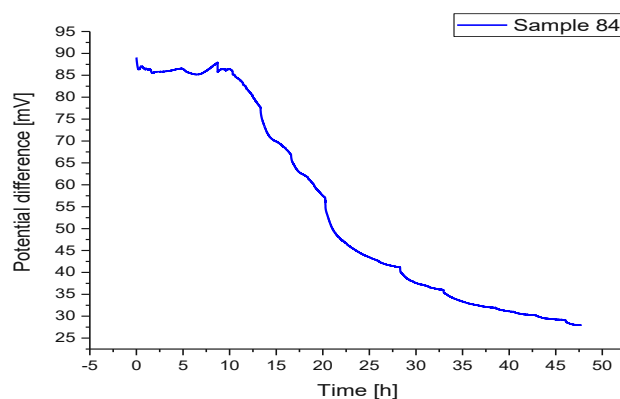*Figure 52: Photographic presentation of sample "84" with marked lines for Great line method*

Figure 51: Potential difference observation of sample "84"

[9] [9] Austin M. Barnes and Steven K. Buratto: "Imaging Channel Connectivity in Nafion Using Electrostatic Force Microscopy" S.: 1294
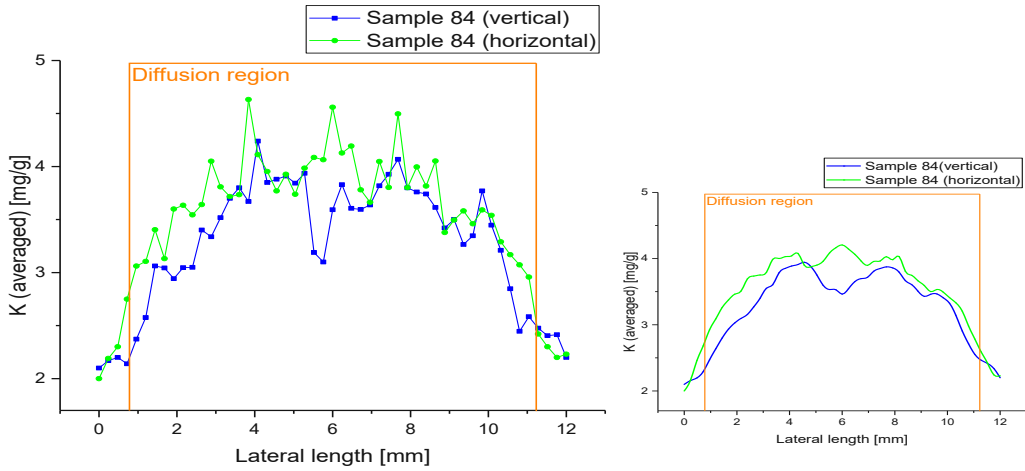
*Figure 54: Average Potassium distribution over scan lines (in centre of diffusion region) of sample "84",
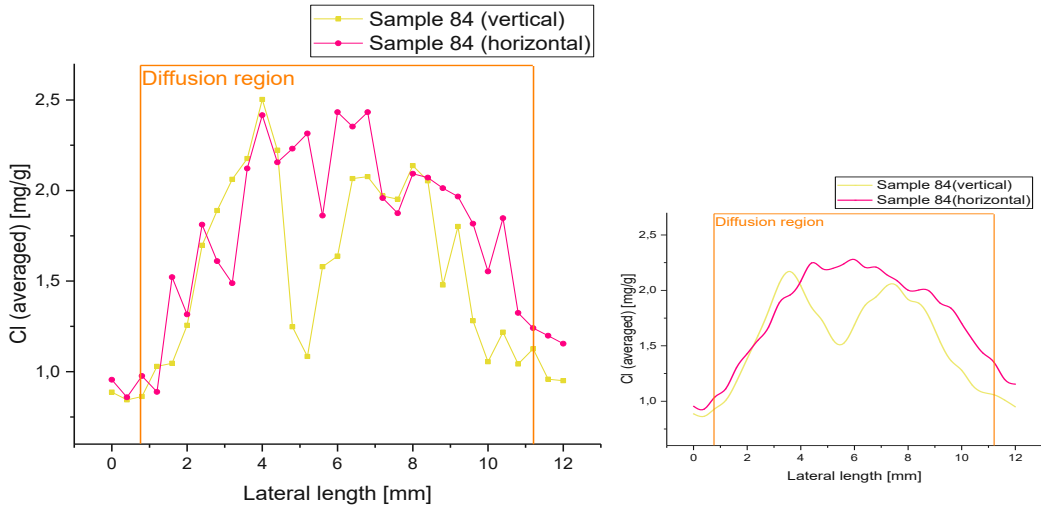with smoothed visualisation (calculated using moved arithmetic mean)*

*Figure 53: Average Chloride distribution over scan lines lines (in centre of diffusion region) of sample "84",
with smoothed visualisation (calculated using moved arithmetic mean)*

Theoretically, if detected counts per second versus lateral length of set laser scan line according to figure 12 and 56 is plotted, different areas are definable. Ablating polymer which is deformed by sealing ring and area between sealing ring and diffusion zone shall show no significant increased chlorine and potassium as no diffusion is proceeded here. Once diffusion region is reached, an abrupt increase in ionic concentration should be detected. If diffusion process run homogeneously over entire lateral surface, a nearly constant signal trend in mass spectrum will be recorded.

It must be mentioned that it was averaged over all measured patterns to achieve an average lateral concentration. The reason for this, is that main task of "Great line" method was to examine concentration inhomogeneity over sample surface. Adding depth resolved axis would generate a diagram which would show measured concentration versus lateral length versus depth penetration, as 3D distribution pattern, which would increase complicity of visualisation for this objective. Furthermore, to explain figure 55 and 58 better, colour of marked scan lines

88

in photographic representation and one of data points are the same. Even limited diffusion region and its peripheral zone is marked in all figures.

First executed ablations were these with potassium settings. The reason for this was that these parameters were less harmful to absolute layer surface. It was start with horizontal line. Here assumption of existing inhomogeneous input potassium was confirmed. Within the diffusion region a trend into centre of the interaction area was visible. Potassium concentration was higher in the centre then close to the peripheral zones. Consequently, during diffusion ions did not penetrate layer surface with the same intensity over entire region. Indeed, as expected, after leaving diffusion region concentration was reduced immensely. Nevertheless, although this surface, distance between sealing ring and diffusion zone, was not connected to diffusion chamber solution, a significant high concentration comparing with reduced background signal was measured. Additionally, it was observable, that a cursive character before and after peripheral zone of diffusion region existed. This could be caused by two effects. Either in infinitesimal scale solution was pressed into this limitation zone by osmosis or simply contact pressure and diffusion could occur or within the layer diffusion flow was not directed ideally from one side to another as polyimide layer represented an extreme wide penetration path with inhomogeneous distributed preferential pathways for ionic transport. Both effects would be possible for this observation. The vertical line showed nearly the same trend, but with an immense concentration reduction within the layer centre. In this location laser line crossed horizontal line, which was ablated previously. So, at this position less potassium and carbon were detected due to examination method and not due to diffusion.

The same trend characteristics were visible in chloride distribution like centre directed concentration increasement, as well as interstratification after leaving diffusion region. The sharp decline in centre was bigger than in potassium determination as chloride sampling settings contained higher intensive ablation rate over time. Additionally, chloride examination was proceeded after potassium one, so lines had to cross more pre-ablated sections. Also, amount of evaluateable chloride data points was less than using other ablation method, as by using higher scan speed and spot size lateral resolution was reduced. Comparing figures 55 and 58 with each other, it was noticeable, that average concentration of potassium was higher absolutely as chloride ones. Already shown in sample pattern measurements, the reason for this was not definable.

7.3.4 Examination of inhomogeneous penetration: "Imaging" method

For "Imaging" polyimide layer samples and Nafion samples were used, shown in table 47. Detailed information about "Imaging" is provided in chapter ""Imaging" method". Following samples are listed up in table 47 and results are shown in figure 59 to 62. (Coloured scale was created by "ImageLab"-Software using measured, 13C-normalised Potassium signal. So, in every figure description coloured scale range is explained as normalised counts per second)

Table 44: List of used samples for "Imaging" analysis

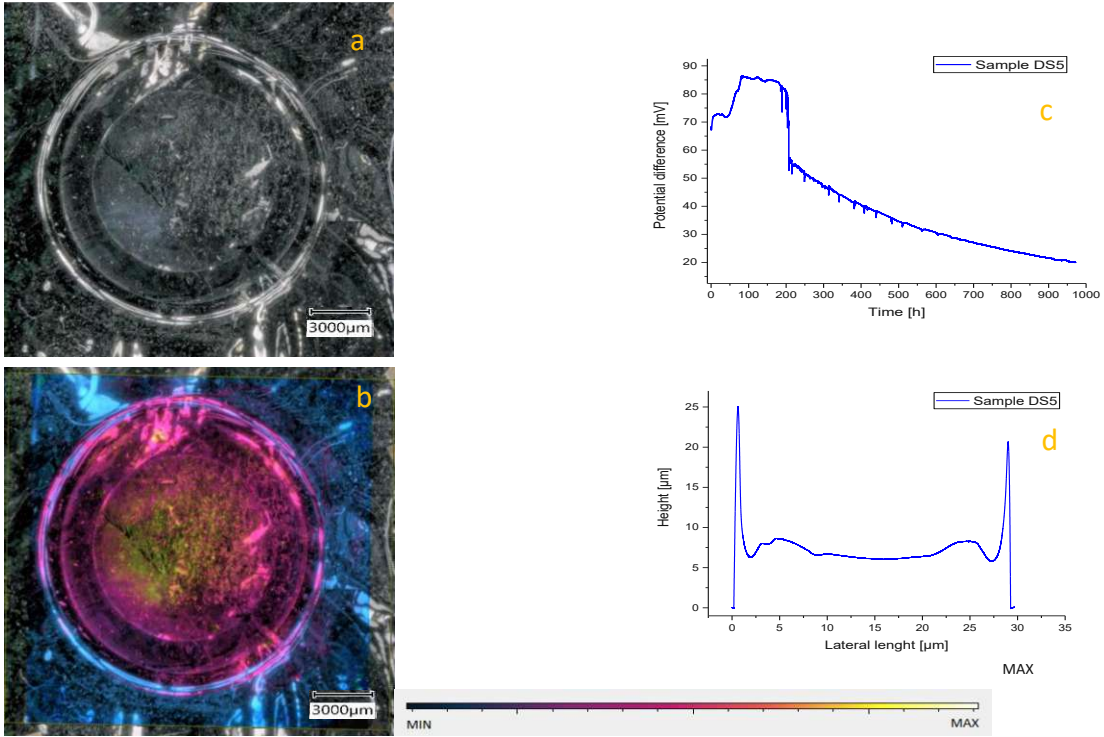| Sample name []	94	99	DS2	DS5	DS12	N5	Nw3
Material	P84®	P84®	P84®	P84®	P84®	Nafion®	Nafion®

Figure 55: Sample "DS5": Microscopic recording (a), Potassium distribution via "Imaging" (b), potentials difference observation (c), layer profile (d).

Coloured scale: MIN (≈ 15 Counts $^{39K}/_{13C}$ per sec)); MAX (≈ 95 Counts $^{39K}/_{13C}$ per sec)
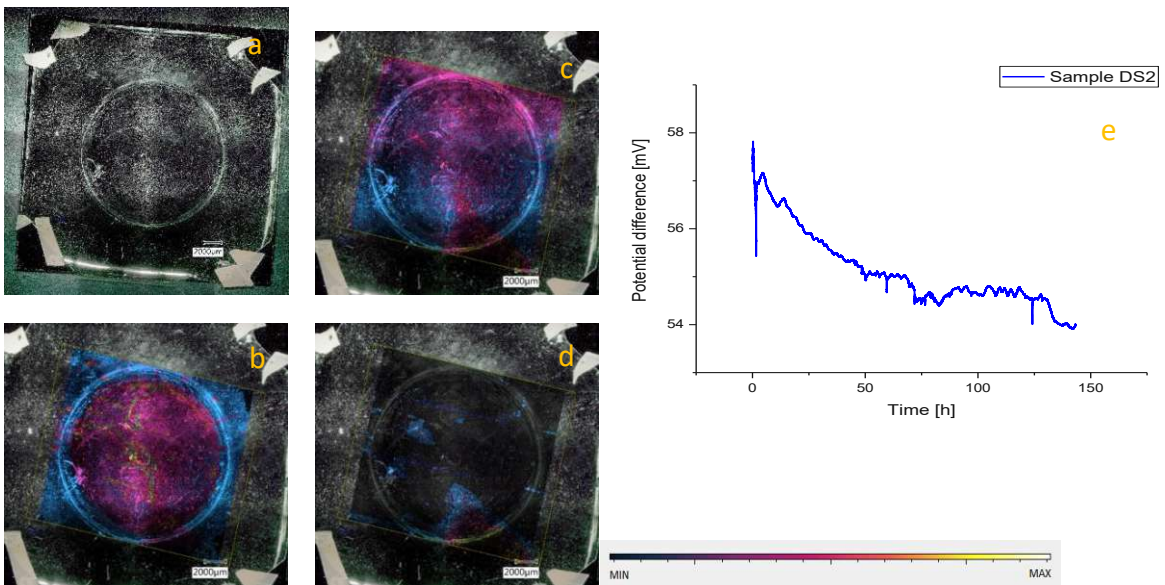

Figure 56: Sample "DS2": Microscopic recording (a), Potassium distribution via "Imaging" (b), Chloride distribution via "Imaging" (c), Silicon distribution via "Imaging" (d), potentials difference observation (e)

Coloured scale: MIN (≈ 2 Counts $^{39K}/_{13C}$ per sec)); MAX (≈ 40 Counts $^{39K}/_{13C}$ per sec)
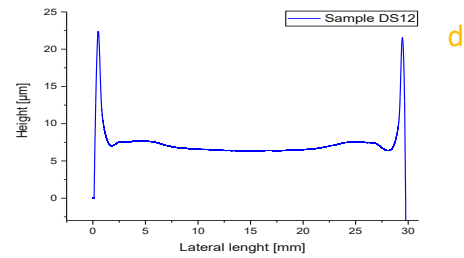
Figure 57: Sample "DS12": Microscopic recording (a), Potassium distribution via "Imaging" (b), potentials difference observation (c), layer profile (d)

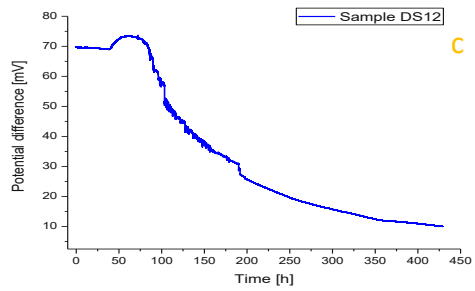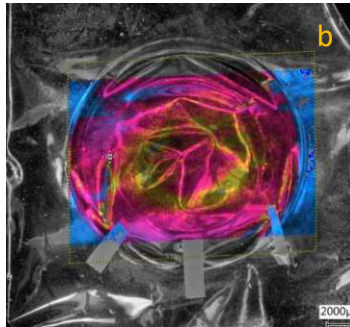*Coloured scale: MIN (≈ 5 Counts $^{39K}/_{13C}$ per sec)); MAX (≈ 145 Counts $^{39K}/_{13C}$ per sec)*
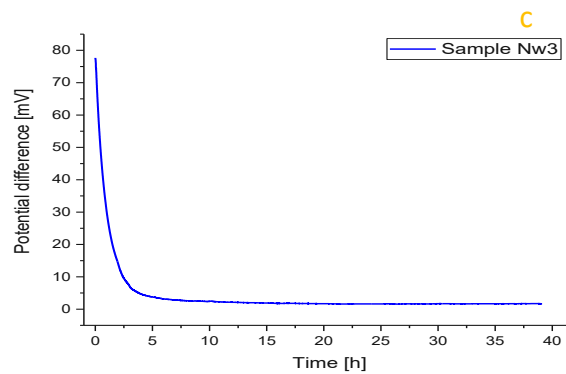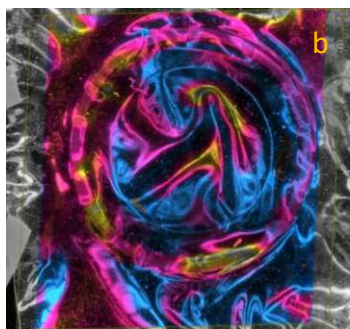

Figure 58: Sample "Nw3 Nafion": Microscopic recording (a), Potassium distribution via "Imaging" (b), potentials difference observation (c)

Coloured scale: MIN (≈ 280 Counts $^{39K}/_{13C}$ per sec)); MAX (≈ 9050 Counts $^{39K}/_{13C}$ per sec)

91

First shown sample in figure 59 is polyimide layer "DS5". Polyimide samples from "DS" batches were characterised by more homogeneous layer profile and less average thickness within the diffusion region, but also advantageously by less osmotic deformation. These properties were expedient for "Imaging", as they guaranteed that layer was ablated completely after one line scan. In "a" the result of microscopy examination is shown. For this issue, the analytical microscope "Keyence VHX-500" was used. It benefited from multiple photo catching in combination with fast instrument movement and photo assemblage programmes. Due to resolution of the used microscope and its manipulating contrast and brightness technic it was possible to identify different functional regions on the sample layer. In "a" following sections are visible: In the centre the diffusion region is located. Clearly zoned the following section is the distance between sealing ring and diffusion region, where ideally no ion input should be expected. After this zone a deformed ring-like area is shown where sealing ring was adjusted. The remaining layer is outer zone which only existed due to structural stability reasons. These sections were important for identification and alignment for "Imaging". In "b" the result after ablation, detection and evaluation by "ImageLab" is shown. This image shows the distribution of detected potassium within the set ablation rectangle. On the right side of the element specific distribution image a scale is located to interpret shown colour schemes.

Within the diffusion region the inhomogeneity, already mentioned in chapter "Examination of inhomogeneous penetration: "Great line" method", was clearly observable due to the colour contrast and alternation of yellow, red and their intermediate compositions. Also, the concentration increasing trend directed into the centre of this region was visible. After leaving diffusion region, the intersection showed a mixed contrast (approximately 50 [Counts $^{39K}/_{13C}$ per second]). The concentration of potassium within this section was lower than in the diffusion region, but higher than expected. Until sealing ring was reached a significant amount of potassium can be detected, so although this area did not take a part in diffusion process, ionic penetration was still provable there. The sealing ring section had more dark areas with pink parts until remaining sample surface was reached.

In figure 60 sample DS2 is shown. In potassium distribution a nearly cursive, contrastless segue between diffusion region and intermediate section was observable. Within the diffusion region line-type concentration maxima were also identifiable. Comparing with microscopic figure, in "a", these maxima were coextensive to whitish, brighter regions in the real photo. So, it was possible, that amount of embedded potassium ions during diffusion was higher than in other area parts within this region. This preferential input could be caused by different effect. The most possible reason was a local depending weak point within the bulk structure of this layer sample. Due to inhomogeneous polymer particle distribution during spinning and heating out an inner cavity with another density could be generated. Such a structural idiosyncrasy, magnified by ascending osmosis during diffusion, could be a one-sided enhancement for ionic transport, which resulted in magnified input of particles in this region. The distributions of chloride 35Cl in "b" and the one of silicon 29Si in "c" are shown. These element specific images are presented to show the induced limitation for elemental analysis due to the sample preparation, regarding the attachment on the silicon wafer. The distribution of chloride was not even approximately congruent to the one of potassium. Over the already mentioned sub-regions of the sample surface within set laser scan rectangle no significant region-related concentration maxima and minima were observable. The chosen ablation

parameters did not correspond to the laser conditions for chloride determination. Additionally, it appeared as if the concentration decreased more as the position was shifted downward. This could be caused due to a slight shift in z-axis of the sample surface within the ablation cell due to non-ideal planarity of the layer. Silicon distribution image in "d" showed, after manually controlled, manipulated signal suppression, where layer breakthrough was reached earlier than on other locations, which gave information about structural bulk layer inhomogeneity.

It must be mentioned, that "Imaging" ablation parameters could not be changed as easily as common pattern ablation sampling. First, laser scan speed had to be three times the set spot size to guarantee correct evaluation in "ImageLab". Secondly, spot size and laser output had to be set to guarantee complete ablation of chosen area without losing to much image resolution. Examinations showed that laser output of 70% and higher led to cracks close to ablated line, which resulted in shearing off sample material before scan on this line was complete. Laser output of 60% and under this value led to an insufficient penetration of the laser.

To summon up, no setting was best for chosen elements, however at last potassium was detectable sufficiently for "Imaging" to identify particle accumulation.

Figure 61 shows sample "DS12". Referring to "c" and "d" layer production and diffusion observation generated satisfying results. However, "Imaging" analysis led to an unexpected potassium distribution. Although an absolute potassium increase was observable within the diffusion region, most maxima and minima were not located at diffusion related regions. The sample was evaluated to present one of the greatest limitations and obstacle for laser ablated mass spectrometry for this thesis, working with non-planar surfaces. Already mentioned, after diffusion polyimide and Nafion layer must be put on and fixed on silicon wafer for further surface related examinations. The planarity of the layer was a decisive factor for correct ablation. Low differences in depth can be corrected by normalisation. However, the soaking in fluid and the osmosis during diffusion deformed Nafion membranes to immense for correct abaltion

Before experiment start, not only horizontal and vertical position and movement lines must be set, but also focus point of the laser instrument. The importance of correct set laser focus will be explained by figure 63.
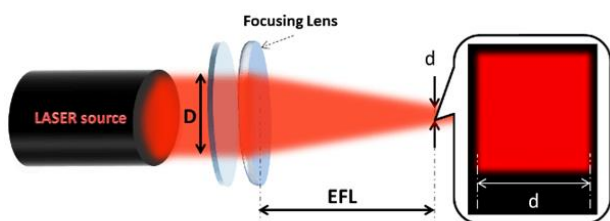

Figure 59: Scheme of laser focus instrumentation

Generated laser beam with input beam size D comes to focus lenses. After pacing a certain effective focal length EFL on sample surface a spot size d is adjusted. However, if laser instrument is moving laterally, the same ablation rate and produced crater depth and wide is

only guaranteed if no artifacts or changes in EFL occur. For this thesis movement paths for ablating entire sample surface were extreme long. As within the sample surface, especially within the diffusion region, various invaginations and evaginations of different diameters and heights were detectable. Ablation efficiency suffered severely if EFL shift within a laser line was too high. This could be observed during ablation process, when produced crater line showed various thicknesses and depths although laser parameters were not changed. Such evaginations and invaginations could even lead to a miss focussing and although laser instrument fire laser pulses at this area, no ablation was observable. Indeed, such errors could be compensated by normalisation, as reduced carbon sampling was integrated, but only for a small error scale. If ablation efficiency was so low, that carbon signal was approximate comparable with background signal intensity, normalisation was unable for correction. However, laser beam focus is even more affected by non-planarity, especially in "Imaging". It is possible to correct focus using an integrated ablation rate parameter, but such non-planar surfaces is not correctable by the instrument itself.

Mis-ablation let to serious problems for determining elemental content and distribution as shown in sample "DS12". Here, in the centre of diffusion region, reduced potassium concentration was detected. Comparing with microscopic image, a heavy deformation was identifiable. So, the probability was very high, that this concentration decrease came from mis-focussing of the laser instrument due to non-planar target surface resulting in insufficient sampling. Such localisation were multiple times detectable by comparing the potassium distribution image with the photo in "a" always at special deformed areas.

Figure 62 shows the microscopic recording (a), the potassium distribution via "Imaging" (b) and the potential difference observation (c) of a water-soaked Nafion layer sample, called Nw3. For elemental imaging analysis it was sufficient to present only one Nafion based sample, as they all show the same problem. Nafion layers were more elastic and had greater water uptake ability than polyimide based layers. Consequently osmotic pressure had great impacts on such layers, which was already discussed and explained in chapter "Nafion®: osmotic influence". Furthermore, after diffsuion process and berfore fixing sample on silicon wafer, sample layer must be dried to remove water on the surace from cleaning process and remove water molecules from the inner nanochannels. Nevertheless, complete water removement from absolute, entire area, reffering surface moisture and inner storaged water, was dependent on local segments. These segments described localisations within the sample surface and bulk, which had different sizes and were formed when dried. While drying, sample surface began showing folds with different directions. Such deformations were observable, when using microscope for surface recording. Due to high water up taking such segments had high change to be formed, which is shown in figure 62. The absolute deformation was so intensive, that "Imaging" was not executable, without generating presentation errors due to mis-focusing of the laser instrument. Parts of the region, which did not come in contact with ionic chamber solution and where no diffusion was proceeded, shows areas with higher potassium concentrations, than within diffusion region, which should not be possible. Nevertheless, such results were obtained by every Nafion sample, as most of regions showed higher concentrations, only because laser was able to sample surface. Additionally, setting correct laser focus was difficult, because of using transparent material. At last, using this laser

parameters for Nafion were insufficient, as layer was too thick for complete laser penetration ablation.

To summon up, "Imaging" was a great method for determining potassium distribution within the layer to identify inhomogeneous diffusive penetration. Nevertheless, this method was not useable for other elements without using other laser parameters and for Nafion membranes. Furthermore, as laser conditions had to be changed, no quantification was possible, even for potassium. To achieve quantification, an external calibration with laser parameters for "Imaging" must be created. However, for this thesis a compromise between sensitivity supporting and imaging-related laser parameters was important.

8 Summary

The main goal of this thesis was on the one hand to record the diffusion process for polyimide and Nafion by PDMD and on the other hand to create quantitative – resolved, elemental specific, depth profiles vie LA-ISP-MS. During the procedure, several sub-tasks arose, like establishing a reproducible method for polyimide layer production, determining homogeneity on the sample surface, and dealing with physical side-effects during diffusion, like osmosis.

From this thesis various results and scientific attainment were obtainable. A optimised production method was established successfully. Layer, produced with this method, showed a higher, desirable thickness, less artifacts on the surface and higher homogeneous surface profile, especially within diffusion region. Additionally, production batches had a higher sample output, as amount of not useable layers due to manufacturing errors was reduced. Also, an own method for creating much thinner layers were established.

Considering potential difference change observation to record diffusion process, different result groups were obtained. Using Nafion membranes, the effectiveness and functionality of used PDMD was confirmed. The reproducibility using these membranes were determined and transference numbers of penetrating ions were calculatable. Reproducibility determination was successful. On the base of mathematical background of the diffusion potential by individual ionic current contribution and chemical properties of the acting molecules and functionalities, several assumptions and hypothesis were established to describe ionic transport. Additionally, it was possible to make different examinations referring osmotic influences, soaking impact and membrane thicknesses. Due to these experiments, more assumptions and theories about ionic mechanism and interaction with the charge active nano channels of Nafion membranes were makeable. It was possible to determine impacts of various parameters, like soaking time and soaking material, but also layer thickness and additional diffusion barrier on the diffusion process. These results are also useable for other research issues, when working with such ionic active membranes and for simulations to anticipate diffusion trends.

Using in-house produced polyimide layers for diffusion examinations let to unexpected obstacles. Despite of several proceeded optimisation methods, it was not possible to achieve reproducibility for potential difference change observation. Without reaching this point, no

further experiments were possible to make. However, after detailed optimisation measures, the cohesive origin of the problems was identifiable, namely the basic material.

First, PI/NMP mixtures had an indefinite affinity to humidity, which could have led to an indefinite high input in water within the resulting layer. Secondly, confirmed by observation studies using microscopes, solid polyimide layer shows various inhomogeneities on the surface and in the bulk. Defects, cavities, agglomerations and densifications during heating out process were possible, which were not recordable by profilometry. These macroscopic structural defects had an immense influence on ion penetration, as these could let to partial leaks, accumulation locations, or transport rate changes. In summary, even after optimising layer profile for measurement, absolute quality of polyimide layers was too low to achieve reproducible results, in contrast to Nafion. Furthermore, PI showed no charge enhancing structural functionalities like Nafion, so an average layer thickness of about 9.5 µm was difficult to penetrate only by concentration depending diffusion.

The lack of reproducibility in potential difference change examinations had also an influence on elemental analysis. Theoretically, if reproducibility determination using polyimide membranes had been successful, elemental distribution reproducibility examinations could had been established. On the base of this, much more assumptions referring distribution, agglomerations and depth resolved concentration trend effects could be established.

However, by evaluating concentration of certain samples with meaningful potential difference change trends much information was obtainable. Coherences between diffusion time, diffusion trends, impact of different soaking media and measured potassium and chloride concentration distribution was determined. Certain elemental trends were observable measuring penetrated P84 and Nafion membranes. Aspirations and goals for the elemental analytical part was fulfilled completely. It was possible to establish high depth resolved sampling methods without overloading the detector and realising break through points by evaluating substrate element signal. Additionally, it was possible to establish quantification methods with successful calibration for required element, despite of losing concurrent detection of all elements with the theoretical fundament to establish a complete multi-element quantification for other analytical issues. Disadvantageously, a limitation was layer thickness, as increased penetration depth reduced laser focus stability. Furthermore, required depth resolution increases time of ablation immensely.

9 Outlook

The proceeding area of this thesis bases is wide ranged, so various optimising methods could be established and consequently a summarising outlook formed.

Already mentioned, the quality of the polyimide layer was not sufficient to obtain reproducible diffusion observation trends. To solve this problem in the first place, several optimisation operations would be realisable. Entire PI/NMP solution production and spinning and heating out process should be executed in a cleanroom to reduce the effect of air humidity and from particles in the air, like dust particles. Also, used spin coater should be able to be programmed for automatic ramp mode to guarantee more reproductive spin processes. In

this thesis extra thin layer production method was established, which showed that most of the structural bulk issues and problems could be solved by reducing mass concentration of polyimide in the stock mixture. Consequently, if spinning method for production was continued, it would be advisable, to change original stock solution to a more diluted version with lower dynamic viscosity. Nevertheless, the easiest way to solve the polyimide layer related problems is to buy commercial available polyimide layer from industrial processes. So, quality could be guaranteed by certificates and by scientific certified and audited examination methods for exact properties and layer thickness. By eliminating these problems, which were caused due to in-house production, operators working on similar topics could concentrate on the main goals, to determine their diffusion permeability.

Now, we come to the diffusion cell itself. Indeed, the cell is a robust system, however optimisations were also possible there. First, the possibility of mechanical mixing should be provided. Due to hydrostatic and quasi-isothermal conditions, where the hydrodynamics is only determined by osmosis, generation of electrostatic field due to ionic membrane transport and agglomeration on the interfaces close to the layer surface could affect recorded potential difference change trend. To avoid such electrostatic charging focused on the diffusion region every chamber could be equipped with a polymeric, for example isotactic polypropylene, stirrer for mixing at with rotation rate. As diffusion cell has got a top opening, the stirrer turning axis could be placed here. Propulsion device, as well as the energy source must be isolated to avoid electromagnetic influence on the PDMD. Another problem to solve is the time exposure for measuring materials with high diffusion resistance. This point is an important topic, as this thesis should be the fundament for measuring industrial used, ultra-high resistant layers for production processes. Nevertheless, the used PDMD and diffusion cells were unable to measure such layers in an adequate time. A possibility to enhance transport rate would be adding a voltage source. By activating an electromagnetic field into diffusion direction, ionic transport would be magnified intensively. Such an instrument add-on would require on the one hand a complete new diffusion cell assemble for guaranteeing enough space for added electrodes and voltage source and on the other hand the PDMD hardware and software must suppress and eliminate the electric enhancing effect and recorded voltage.

Also, used electrodes should be optimised too. Indeed, it was possible to increase quality and measure stability of the Ag/AgCl electrodes, but production, chemical equilibrium and quality check process did take much time. Furthermore, Ag/AgCl electrodes are only able to interact with chloride ions, so chemical composition of used diffusion solution was limited. It would be possible to produce electrodes with other chemical properties, however this would also be limited and would not improve the single-element dependence or time exposure. Another possibility would be to change it with conductivity electrodes. If membranes were measured, which did not interact with chamber solutions like Nafion, calibrated or certified capillary conductivity electrodes would be an option, if only one ion type controls transport rate and diffusion potential could be neglected. Another important issue was the ionic distribution focussed on the centre of the diffusion region, which could be caused by the electrode. Consequently, this effect could be reduced by change the insertion bore hole of the electrode for 90°. As a result, electrode axis would be perpendicular to the diffusion cross-section and only the electrode wire top would be close to the layer surface, instead of the entire wire

structure. The PDMD could also be optimised by separating the multiple measuring stations into individual, isolated chambers with own detection systems. Indeed, use of space would be increased, but measuring systems could be controlled individually without affecting the other stations, as well as chance that individual diffusion cells and detection systems would disturb each other would be reduced.

Referring elemental analysis, LA-ICP-MS is a stable system with multiple possible applications. However, this thesis shows, that ablation efficiency suffers from layer thickness dependent laser focus errors, especially by using such non-planar samples. Software of the laser ablation system could be optimised, by previous evaluation of correct penetration depth of individual patterns and integrating a proportional factor to the z-axis change. This would correct laser focus before starting new pattern and improve laser ablation. Another issue considers measuring preparation. After isolation and cleaning of the sample layer it must be fixed on a silicon wafer. This process includes high chances of contamination and not-eliminable in-layer surface invagination and evagination zones. Contamination can be reduced by drying sample layer in sterile, low-temperature air circulation oven and further working in glove boxes to reduce dust and other particle deposition. Guaranteeing planarity of sampled surface is a problematic issue, as osmosis induced deformations are not re-formable without changing original elemental distribution by diffusion. First further research must be proceeded to eliminate deformative impacts on diffusion region to achieve better planarity and so better homogeneous sampling surface.

10 Appendix

10.1 Polyimide layer production

It should be noted that every experiment and every produced layer was made with the same polyimide P84 powder, which is mentioned in chapter "P84® membranes". So, the main opportunities of improvement concerned spinning and heating process. Additionally, as the result of profilometry was an entire layer profile, a main statement about layer quality was hard to give. So, the spectrum of layer quality is reduced to the planarity of the diffusion region

and to the absolute value and constancy of the layer thickness. In addition to this, it was pre-set, that a layer thickness of approximately 10 μm was striven.

Optimising the polyimide layer production methods took several months. However, any examinations concerning this issue is reduced to the final used and developed method, which will be explained in the following chapter.

10.1.1 Established layer production method and reproducibility examination

The following table 54 contains the parameters for the optimised layer production.

Table 45: Parameters for optimised layer production

Number of different spinning modes []		2
Pre-spinning phase	Spinning time [sec]	240
	Rotation number [rpm]	200
Fast-spinning phase	Spinning time [sec]	10
	Rotation number [rpm]	2000
Resting-phase [sec]		120
Volume of superimposed sample solution [ml]		0.8
Number of different heating modes []		2
Solidification phase	Temperature [°C]	90
	Heating time [min]	15
Hardening phase	Temperature [°C]	180
	Heating time [h]	15

According to table 54, reproducibility determination was executed. "Charge K" with seven samples was produced. Figure 68 shows a comparison between the averaged layer profiles of the pre-set method, and of the optimised, current one.
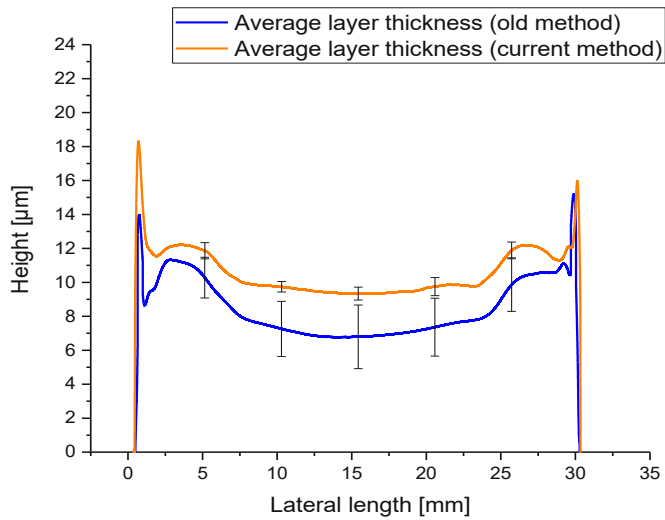

Figure 60: Reproducibility determination and comparison of old and new layer production method

Table 46: Results for layer quality with and without outliers

Method	Old (pre-set)	Current (optimised)
Average layer thickness (diffusion region) with outliers [μm]	7.4	9.3
Standard deviation (diffusion region) with outliers [μm]	2.6	0.8
Depth of the sink with outlier [μm]	0.9	0.5
Deviation of sink depth with outlier [μm]	0.2	0.1
Amount of outlier []	3 of 8	1 of 7
Average layer thickness (diffusion region) without outliers [μm]	6.9	9.6
Standard deviation (diffusion region) without outliers [μm]	1.7	0.4
Depth of the sink without outlier [μm]	0.9	0.3
Deviation of sink depth without outlier [μm]	0.1	0.1

Table 55 shows the most important results for layer quality of both profiles.

To fully understand the results of reproducibility examination, it was necessary to elucidate the outliers. Outliers were described as layer profiles, which showed at least one of these points:

- Layer thickness far above or below the desired or expected (permitted fluctuations interval [8.5; 10.5] for 9.5 µm thick expected layers)
- Diffusion region sink too immense (difference in height at least 1 µm between local minimum and maxima at the borders in lateral distance 0.51 µm)
- Existence of anomalies (existence of invagination, evagination or other distinct deviation of ideal profile in diffusion region, which could cause an influence on diffusion)
- Visible change in layer physiognomy (distinct damage on layer surface due to mechanical impact, for example error in spinning, or due to chemical impact, for example acetone contamination)

If a sample layer showed one of these errors by observation and by profilometry, this layer was not evaluated for any analyses or evaluations in reproducibility examination, as this layer would lead to unpredictable errors in potential difference measurements.

10.1.2 Polyimide layer production: "DS" samples

Entire polyimide layer production was designed to create layer thicknesses about 10µm. Nevertheless, after achieving sufficient reproducibility in layer thickness and homogeneity, it was demanded by supervisor to establish a method for producing layers with thicknesses about 5 to 6 µm to examine difference in potential difference observation when that layers were integrated into diffusion cell. For this, spinning parameters were changed like spinning time, spinning frequency, spinning modes and volume of superimposed material, but without achieving sufficient layer thickness. A limitation of about 8 µm were not deceedable without changing planar profile of diffusion region intensively. However, for thin layer production another method was established. Instead of changing spinning parameters, P84 N-methyl pyrrolidone stock solution was optimised.

It turned out, that thin film layers were not manufacturable with normally used stock solution due to mixture viscosity. Even, when increasing immensely spinning rate over normal conditions, liquid viscosity was so high, that surface tension was too strong to be vaulted from the wafer edge. As surface tension and viscosity were in direct proportion to each other, during executed spinning it was observable, that after certain time no liquid material was catapulted from the wafer and was hold back due to surface tension and the force between silicon wafer edge and liquid phase. [8] So, stock solution was diluted with pure N-methyl pyrrolidone. 20 % PI/NMP stock solution was made normally and mixed until reaching homogeneity. After that 18 g of that solution was weighted into another 50 ml PP screw eprouvette and 2 g NMP was added. The new produced mixture was mixed for over 24 hours using a horizontal shaker. Using this mixture, a polyimide layer batch was produced using the same spinning parameters from final layer reproducibility determination mentioned in chapter "Established layer production method and reproducibility examination". Layers from this batch were called "DS" samples, a German abbreviation for "Dünnschicht". Following figure 69 shows the average layer profile of reproducibility determination for "DS samples".

For reproducibility determination 12 samples were made, while 9 were used for evaluation. Additionally, this layer profile was set into comparison with layer profile of normal produced polyimide layers, so with undiluted stock solution.
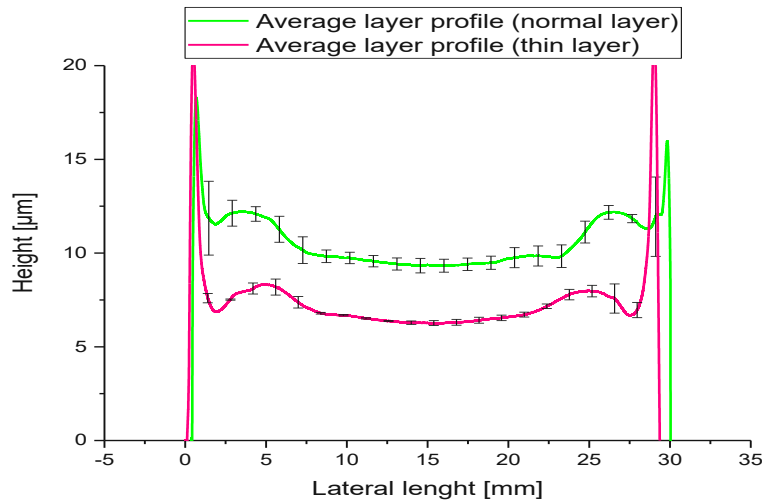

Figure 61: Comparison of layer profiles using methods for normal and thin layers (reproducibility determination of final production method and "DS" method)

Using a 1:10 mixture of pure NMP and PI/NMP stock solution reduced successfully average layer thickness from 9.311 µm to 5.937 µm. So, simply by reducing amount of dissolved polyimide material in NMP matrix, viscosity of mixture was reduced, and average layer thickness could be reduced without increasing layer profile inhomogeneity within diffusion region. Additionally, using diluted stock solution standard deviation of diffusion region was reduced from 0.886 to 0.416 µm which was a significant improvement in layer homogeneity. Furthermore, for this production batch only 3 of 12 were not evaluated. Of this 3, two were destroyed by the operator due to mishandling and only one sample was manufacturing defect. So, the amount of not useable and evaluateable samples using diluted stock solution was also reduced.

11 List of used chemicals and materials

- Ag (Silver Wire Spool)
  - Manufacturer's name: Goodfellow
  - LOT: AG005130/14
  - Diameter: 0,25 mm
  - Purity: 99,99 %
- PET net
  - Manufacturer's name: Separ
  - LOT: unknown
  - Mesh size: 7 µm
  - Colour: Yellow
- Hydrochloric acid 37%

- o Manufacturer's name: Merck
- o Product Nr.: 1003170510
- Hydrofluoric acid 40%
  - o Manufacturer's name: Merck
  - o Product Nr.: 1003350250
- N-Methyl- 2-pyrolidone (NMP)
  - o Manufacturer's name: PanReal AppliChem
  - o LOT: 0001375062
- Trifluoro methane sulfonic acid potassium salt
  - o Manufacturer's name: Sigma Aldrich / Merck
  - o Product Nr.: 83000-25G-F
- Potassium chloride (KCl)
  - o Manufacturer's name: VWR
  - o LOT: 183024107
- Benzalkonium chloride ($C_6H_5CH_2N(CH_3)_2RCl$ (R=$C_{14}H_{29}$))
  - o Manufacturer's name: Sigma Aldrich
  - o Product Nr.: 83000-25G-F
- Polyimide powder P84
  - o Manufacturer's name: HP Polymers GmbH
  - o LOT: 12060-5G
- Silicon Wafer
  - o LOT: VE 830855.X
- Nafion® NR-211®
  - o Manufacturer's name: DuPont™
  - o Product Code: 1600001
- Nafion® N-177®
  - o Manufacturer's name: DuPont™
  - o Product Code: 591239
- Polycarbonate Plates (diffusion cell)
  - o Haberkorn
  - o Product Code: 134969
- Adhesive Strips
  - o Manufactor's name: tesa
  - o Thickness: 60µm

Chemicals and Materials without certain LOT or Product Code or Manufacturer's name, such as acetone, deionised water, screws, syringes etc. will not be listed.

12 Directory of used symbols and indices

- E_0 Electromotive force of a galvanic element [V]
- n   Molar number [g / mol]
- ΔG Free reaction enthalpy [J]
- F   Faraday constant [C / mol]
- z   number of exchanged electrons []
- ΔG_{diff} free reaction enthalpy by diffusion [J]
- $\Delta G_{Cell\ reaction}$ free reaction enthalpy by electrochemical reaction within the cell [J]
- μ_i Chemical potential of substance i [J / mol]
- μ^0_i Standard chemical potential of substance i [J / mol]
- v_i Coefficient for molecular transfer of substance i []
- $\Delta\varphi_{diff}$ Diffusion potential [V]
- a_i Activity of substance I []
- $t^{+/-}$ Transference number of cation / anion []
- m_a Mass within the absorber system [g]
- m_d Mass within the donator system [g]
- c   Concentration [mol / L]
- D   Diffusion coefficient [m^2 / sec]
- x   Distance [m]
- d   Layer thickness [m]
- t_{lag} Lag-time [sec]
- U_{ges} Measured, total potential difference[V]
- U_{Nernst} Potential difference, calculated by Nernst equation, for system I [V]
- Π Osmotic pressure [bar]
- I   Van't-Hoff-Factor []
- R   Gas constant [J / (mol * K)]
- T   Temperature [K]

13 Indication of source

13.1 Explanation of used source indication characters

In this thesis several characters are used to describe the link to the inherent literature. Table 59 shows the explanation of all used characters.

Table 47: Explanation for used characters for literature references

Character (e.g. for "1")	Explanation
[1]	Indicates source, given in chapter "References from books and papers"
(1)	Allocated number for given equation, not referring to any literature
[I]	Indicates source, given in chapter "References from web pages"
1	Allocated number for given footnote for certain quotation, not referring to any literature

13.2 References from books and papers

[1] Karl Cammann, Helmuth Galster: „Das Arbeiten mit ionenselektiven Elektroden: Eine Einführung für Praktiker"

[2] Dr Bengt Åkesson: Department of Occupational & Environmental Health, "Concise International Chemical Assessment Document 35N-METHYL-2-PYRROLIDONE"

[3] Michael Kellner: „Entwicklung neuer Materialien für protonenleitende Membranen in Brennstoffzellen"

[4] W. Köhler: „Physikalische Chemie für Techniker und Ingenieure. K.-H. Näser. 3. verbess. u. erweit. Auflage. 428 S. mit 92 Abb. u. zahlr. Tab. Deutscher Verlag für Grundstoffindustrie"

[5] A. V. Raghunathan, N. R. Aluru: "Molecular Understanding of Osmosis in Semipermeable Membranes"

[6] Luduena, Ga ; Kuhne, Td ; Sebastiani, D: "Mixed Grotthuss and Vehicle Transport Mechanism in Proton Conducting Polymers from Ab initio Molecular Dynamics Simulations"

[7] S.H. Tan and G. Horlick: "Back-ground spectral features in induc-tively coupled plasma/massspectrometry" Appl. Spectrosc. 40,445–460 (1986)

[8] P. Moritz: „Über einen Zusammenhang zwischen Viskosität und Oberflächenspannung der Flüssigkeiten"

[9] Austin M. Barnes and Steven K. Buratto: "Imaging Channel Connectivity in Nafion Using Electrostatic Force Microscopy"

[10] Carl H.Hartmann, Wolf Vielstich: „Elektrochemie", 4., vollständig überarbeitete und aktualisierte Auflage

[11] Barbara Weh: „Permeationseigenschaften von Polydimethylsiloxan-Membranen in Abhängigkeit von der Netzbogenlänge"

[12] Gernot Voitic: „Gasabtrennung mit Polymermembranen"

[13] Bakr Mostafa, Abdalla: "Measurements of transference number of ions in reacting systems"

[14] Thomas W. May and Ray H. Wiedmeyer: "A Table of Polyatomic Interferences in ICP-MS"

[15] Dipl.-Ing. Lars Varain, Dr. Silvia Larisegger, Dr. Michael Nelhiebel, Ao. Univ. Prof. Dipl.-Ing. Dr. techn. Günter Fafilek: "Diffusion and migration measurement in a minimized migration cell with electrochemical methods"

[16] Hong Sun, Mingfu Yu, Zhijie Li, and Saif Almheiri: "A Molecular Dynamic Simulation of Hydrated Proton Transfer in Perfluorosulfonate Ionomer Membranes (Nafion 117)"

[17] Hans Peter Latscha, Uli Kazmaier, Helmut Alfons Klein: „Organische Chemie Chemie-Basiswissen II, 7. Auflage"

[18] Adalbert Wollrab: „Organische Chemie"

[19] Top Seiko Co.,LTD. "Guide to Materials "

[20] Bruker Nano Surfaces Division: „B516-RevB2-DektakXT_Stylus_Profiler-Brochure"

[21] LLE Review, Volume 92: „The Properties of Polyimide Targets"

[22] Jörg Kärger, Douglas M.Ruthven, and Doros N. Theodorou: "Diffusion in Nanoporous MaterialsVolume 1"

[23] John Osenbach, Semiconductor Science and Technology · January 1999 "Corrosion-induced degradation of microelectronic devices"

[24] Yizhak Marcus: "Ions In solution and their solvation"

[25] Z. Samec et al 1997 J. Electrochem. Soc. 144 4236: "Diffusion Coefficients of Alkali Metal Cations in Nafion® from Ion-Exchange Measurements: An Advanced Kinetic Model"

[26] I. Ressam& M. Lahcini & A. Belen Jorge & H. Perrot & O. Sel : "Correlation between the proton conductivity and diffusion coefficient of sulfonic acid functionalized chitosan and Nafion composites via impedance spectroscopy measurements

[27] Ozlem Sel, L. To Thi Kim, Catherine Debiemme-Chouvy, Claude Gabrielli, Christel Laberty-Robert, and Hubert Perrot: "Determination of the Diffusion Coefficient of Protons in Nafion Thin Films by ac-Electrogravimetry"

[28] Sergei Boulya. Jens Heilmann, Thomas Prohaska, klaus Heumann: „Development of an accurate, sensitive and robust isotope dilution laser ablation ICP-MS method for simultaneous multi emement analysis (chlorine, sulfur and heavy metals) in coal samples"

[29] Maximilian Bonta: "Quantification strategies for elemental imaging of biological samples using Laser Ablation Inductively Coupled Plasma Mass Spectrometry"

[30] Fanny Claverie, Julien Malherbe, Naomi Bier, John Molloy: "Putting a spin on LA-ICP-MS analysis combined to isotope dilution"

[31] Phillip Claude: "Laser ablation and its applications"

[32] Tulej, Marek ; Neubeck, Anna ; Riedo, Andreas ; Lukmanov, Rustam ; Grimaudo, Valentine ; Ligterink, Niels F.W ; Ivarsson, Magnus ; Bach, Wolfgang ; Koning, Coenraad ; Wurz, Peter: "Isotope abundance ratio measurements using femtosecond laser ablation ionization mass spectrometry"

[33] Grimaudo, Valentine ; Moreno-García, Pavel ; López, Alena Cedeño ; Riedo, Andreas ; Wiesendanger, Reto ; Tulej, Marek ; Gruber, Cynthia ; Lörtscher, Emanuel ; Wurz, Peter ; Broekmann, Peter: "Combining Anisotropic Etching and PDMS Casting for Three-Dimensional Analysis of Laser Ablation Processes"

[34] Miller, J. C. ;Haglund, R. F.: "Laser ablation and desorption"

[35] Detlef Günther, Bodo Hattendorf: "Solid sample analysis using laser ablation inductively coupled plasma mass spectrometry"

[36] Steven Durrant: "Laser ablation inductively coupled plasma mass spectrometry: achievements, problems, prospects"

[37] Christian Agatemor, Diane Beauchemin: "Matrix effects in inductively coupled plasma mass spectrometry: A review"

[38] Christine Austin, Dominic Hare, Tristan Rawling, Andrew M. McDonagh and Philip Doble: "Quantification method for elemental bio-imaging by LA-ICP-MS using metal spiked PMMA films"

[39] Henry P. Longerich, Simon E. Jackson and Detlef Günther: "Laser ablation inductively coupled plasma mass spectrometric transient signal data acquisition and analyte concentration calculation "

[40] Anderl Thomas: "Entwicklung einer LA_ICP_MS Methode zur Quantifizierung von Natrium in Polymerdünnfilmen"

[41] Roswitha Zeis: "Materials and characterization techniques for high-temperature polymer electrolyte membrane fuel cells"

13.3 References from web pages

[I] https://nafionstore-us.americommerce.com/Shared/P11_C10610_Nafion_NR-211__NR-212_P11.pdf

[II] https://www.fuelcellstore.com/nafion-211